catalysts

MDPI

Review

An Overview of Environmental Catalysis Mediated by Hydrogen Peroxide

Monica Rigoletto [1], Enzo Laurenti [1,*] and Maria Laura Tummino [2,*]

[1] Department of Chemistry, University of Torino, Via P. Giuria 7, 10125 Torino, Italy; monica.rigoletto@unito.it
[2] Institute of Intelligent Industrial Technologies and Systems for Advanced Manufacturing, National Research Council of Italy (CNR-STIIMA), Corso G. Pella 16, 13900 Biella, Italy
* Correspondence: enzo.laurenti@unito.it (E.L.); marialaura.tummino@cnr.it (M.L.T.)

Abstract: The use of hydrogen peroxide (produced in situ or ex situ) as the main agent in oxidative processes of environmental pollutant removal is widely studied. The degradation of water pollutants, such as dyes, pharmaceuticals, cosmetics, petroleum derivatives, and even pathogens, has been successfully obtained by different techniques. This review gives an overview of the more recent methods developed to apply oxidative processes mediated by H_2O_2 and other reactive oxygen species (ROS) in environmental catalysis, with particular attention to the strategies (Fenton-like and Bio-Fenton, photo- and electro-catalysis) and the materials employed. A wide discussion about the characteristics of the materials specifically studied for hydrogen peroxide activation, as well as about their chemical composition and morphology, was carried out. Moreover, recent interesting methods for the generation and use of hydrogen peroxide by enzymes were also presented and their efficiency and applicability compared with the Fenton and electro-Fenton methods discussed above. The use of Bio-Fenton and bi-enzymatic methods for the in situ generation of ROS seems to be attractive and scalable, although not yet applied in full-scale plants. A critical discussion about the feasibility, criticalities, and perspectives of all the methods considered completes this review.

Keywords: Bio-Fenton; electro-catalysis; Fenton; H_2O_2 detection; hydrogen peroxide; photo-catalysis; water remediation

check for updates

Citation: Rigoletto, M.; Laurenti, E.; Tummino, M.L. An Overview of Environmental Catalysis Mediated by Hydrogen Peroxide. *Catalysts* **2024**, *14*, 267. https://doi.org/10.3390/catal14040267

Academic Editors: Ying Zhang and Fangke Yu

Received: 19 March 2024
Revised: 11 April 2024
Accepted: 15 April 2024
Published: 17 April 2024

1. Introduction

The depletion of water resources is a theme of global concern and it is more and more exacerbated by increasing water consumption (especially connected to certain agricultural and industrial activities [1,2]), contamination sources and climate changes that bring about aridity/desertification issues [3,4]. As a consequence, access to clean water is progressively more limited and the need for the reuse of wastewater is mandatory worldwide [3,4]. Wastewater has to be treated to fulfill the quality requirements before the reintroduction in specific systems (e.g., agricultural, industrial, potable, etc.) [5].

Wastewater depuration is typically a multi-step procedure in which most of the chemical and pathogenic contaminants are successfully removed [4]. Nevertheless, recalcitrant and new kinds of not commonly monitored pollutants (Contaminants of Emerging Concern, such as pharmaceuticals and personal care products), detected at trace/sub-trace levels in water bodies and often not removed by traditional depuration processes, represent a further hurdle to the achievement of high-quality water standards [4,6,7]. For this reason, advanced methods should support these processes, among which the most studied ones since the 1980s are the so-called Advanced Oxidation Processes (AOPs) [8]. The methods involving the presence of Reactive Oxygen Species (ROS) with strong oxidizing properties underlie AOPs' definition and are aimed at bringing about the partial/total mineralization of chemical pollutants to carbon dioxide, water and inorganic ions up to disinfection from pathogens [7,9,10]. The main ROS are non-radical species such as H_2O_2 and singlet oxygen ($^1O_2$), and highly reactive free radicals, such as hydroxyl ($^{\bullet}OH$), hydroperoxide

(HOO•), superoxide ($O_2^{\bullet-}$), carbonate anion ($CO_3^{\bullet-}$), and sulfate ($SO_4^{\bullet-}$) radical, deriving from the activation of precursors (hydrogen peroxide, persulfate/peroxydisulfate, peroxymonosulfate and sodium percarbonate) via oxidation/reduction reactions [7,11–14].

The oxidation processes exploiting H_2O_2 and the derived ROS are the focus of the present review. Many different treatments have been proposed [11,15–18], also in a variety of combinations and with different triggering sources (ultrasounds, UV/vis light, heat and electrochemical energy) [7,15,19–24], as summarized in Figure 1.

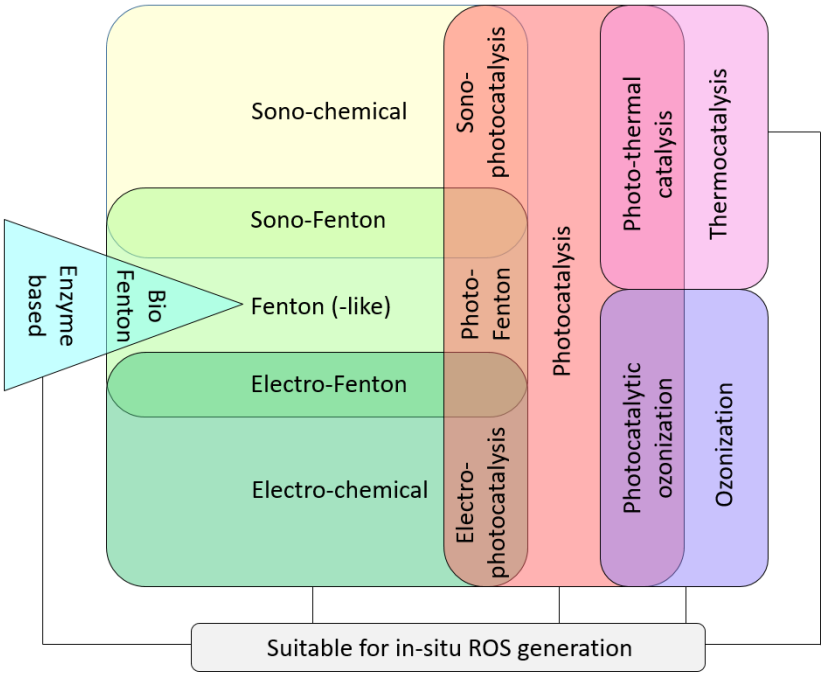

Figure 1. Scenario of AOPs exploiting hydrogen peroxide and derived ROS.

In Figure 1, the methods that are mainly recognized to be capable of inducing an in situ generation of ROS [17,25–27] have been underlined since the use of such methods can overcome the problems related to high costs and excessive consumption of hydrogen peroxide, as well as avoid the hazards associated with its transport, handling, and storage in significant quantities [25,27,28]. A further distinction can be made considering homogeneous and heterogeneous processes. In this latter category, solid catalytic materials are applied for the generation of active species in the aqueous medium through catalytic ozonation, photocatalytic and electrochemical systems, heterogeneous Fenton-like processes, etc. [29–31]. Heterogeneous catalyst-based methods are considered greener to permit both easier recycling of active materials and a decrease in costs and pollution [4]. For this reason, these will be more explore more in depth in this excursus.

From what has been seen so far, the two most common methods to produce hydrogen peroxide in heterogeneous systems are photocatalysis and electrocatalysis (Figure 2). In order to briefly introduce the basilar mechanism of a photocatalytic process (Figure 2A), it is possible to use the well-known semiconductor TiO_2 as an example. The mechanism of the UV/TiO_2 implies that when titania is irradiated with light energy equal to or higher than its band gap, an electron (e^-) can be excited from the valence band to the conduction band, leaving a hole (h^+) in the valence band. If charge separation is maintained, the paired e^--h^+ may migrate to the surface of the photocatalyst. In the aqueous phase, the photoinduced h^+ can oxidize surface hydroxyl groups or surface-bond water molecules to produce hydroxyl radicals and other ROS [32,33]. Regarding electrocatalysts, they have to initiate an Oxygen Reduction Reaction (ORR) to generate hydrogen peroxide via two e^- or four e^- processes (Figure 2B). Therefore, the involved materials have to possess suitable

electronic configuration and redox properties, conductivity, low overpotential, fast kinetics and good Faraday efficiency to allow for oxygen reduction [34–37].

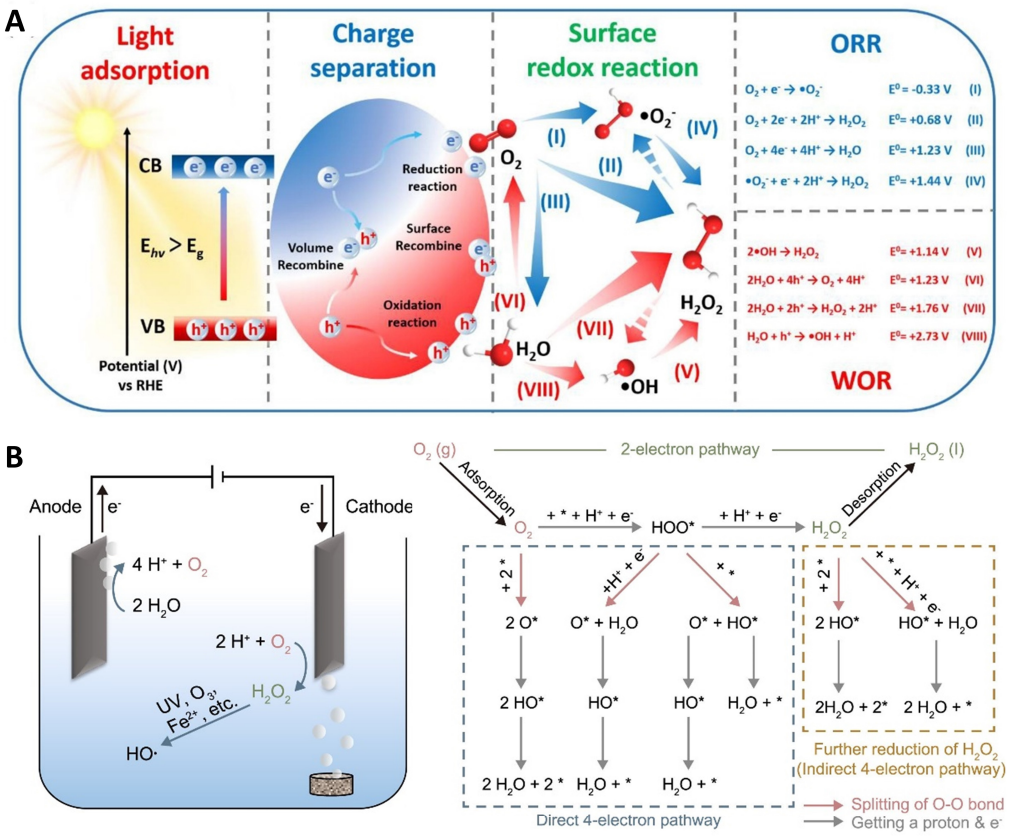

Figure 2. (**A**) Photocatalytic H_2O_2 production with a semiconducting-based process (ORR = Oxygen Reduction Reaction; WOR = Water Oxidation Reaction). (**B**) Electrochemical H_2O_2 generation and related two- and four-electron oxygen reduction reaction pathways. Images reproduced with permission of the authors of [38,39].

The methods based on the use/production of hydrogen peroxide and related ROS are mainly founded on the following reactions (1–19) [8,17,21,22,40]. Equation (1) is related to ozone-related systems, Equations (2)–(6) to the peroxone (O_3/H_2O_2) system, Equations (5)–(11) to photolysis and photocatalytic (hν)/thermocatalytic (ΔT) reactions in the presence of a heterogeneous catalyst ("Cat." refers to a generic semiconductor), and Equations (6) and (12)–(18) to Fenton and Fenton-like processes. Equation (18), in particular, is an example of radical recombination that can restore H_2O_2 [15]. Equation (19) is related to ultrasound (US)-assisted reactions, in which sound waves can lead to cavitation phenomena, involving vapor- and gas-filled microbubbles, and to the generation of high temperature and high pressure. Finally, the formation of organic radicals ($R^\bullet$) during these processes introduces new variables into this chain of reactions [41].

$$3O_3 + H_2O \rightarrow 2\,^\bullet OH + 4O_2 \quad (1)$$

$$H_2O_2 \rightarrow HO_2^- + H^+ \quad (2)$$

$$HO_2^- + O_3 \rightarrow {}^\bullet OH + O_2^- + O_2 \quad (3)$$

$$O_3 + H_2O + h\nu \rightarrow H_2O_2 + O_2 \quad (4)$$

$$H_2O_2 + h\nu \rightarrow 2\,^\bullet OH \quad (5)$$

$$H_2O_2 + {}^\bullet OH \rightarrow H_2O + HOO^\bullet \quad (6)$$

$$\text{Cat.} + h\nu/\Delta T \rightarrow e^{-}{}_{\text{(conduction band)}} + \text{hole}^{+}{}_{\text{(valence band)}} \quad (7)$$

$$\text{hole}^{+}{}_{\text{(valence band)}} + OH^{-}{}_{\text{(surface)}} \rightarrow {}^{\bullet}OH \quad (8)$$

$$\text{hole}^{+}{}_{\text{(valence band)}} + H_2O_{\text{(adsorbed)}} \rightarrow {}^{\bullet}OH + H^{+} \quad (9)$$

$$e^{-}{}_{\text{(conduction band)}} + O_{2\,\text{(adsorbed)}} \rightarrow O_2{}^{\bullet-} \quad (10)$$

$$H^{+} + O_2{}^{\bullet-} \rightarrow HOO^{\bullet} \quad (11)$$

$$H_2O + h\nu \rightarrow {}^{\bullet}OH + H^{\bullet} \text{ when } \lambda(h\nu) < 242 \text{ nm} \quad (12)$$

$$Fe^{2+} + H_2O_2 \rightarrow Fe^{3+} + {}^{\bullet}OH + OH^{-} \quad (13)$$

$$Fe^{3+} + H_2O_2 \rightarrow Fe^{2+} + HOO^{\bullet} + H^{+} \quad (14)$$

$${}^{\bullet}OH + Fe^{2+} \rightarrow Fe^{3+} + OH^{-} \quad (15)$$

$$Fe^{3+} + HOO^{\bullet} \rightarrow Fe^{2+} + O_2H^{+} \quad (16)$$

$$Fe^{2+} + HOO^{\bullet} + H^{+} \rightarrow Fe^{3+} + H_2O_2 \quad (17)$$

$$2HOO^{\bullet} \rightarrow H_2O_2 + O_2 \quad (18)$$

$$H_2O + US \rightarrow {}^{\bullet}OH + H^{\bullet} \quad (19)$$

It is worth briefly discussing the Fenton processes and the distinction between Fenton and Fenton-like ones. In the classical homogeneous Fenton process, low pH values (around 3.0) are necessary to avoid the precipitation of iron oxyhydroxides from Fe(II), resulting in higher costs [42–44]. Furthermore, when complex real matrices have to be depolluted, there is the risk of precipitation of the iron catalyst, leading to the formation of sludge and undesired by-products [7]. To overcome these limitations, Fenton-like processes are designed to use oxidants other than hydrogen peroxide and/or transition metals other than Fe^{2+} (e.g., Fe^{3+}, Cu^{2+}/Cu^{+}, iron-based minerals, nano zero-valent iron, etc.), and/or employ heterogeneous catalysts and/or external energy sources to create similar reactions [29,44–47]. All the aspects concerning the chemical development of AOP methods involving H_2O_2 will be addressed in Section 2.1.

As anticipated, another important point that must be considered concerns the production of H_2O_2 to be used in these reactions. In recent years, biological systems for the in situ generation of H_2O_2 have been carefully taken into account since they allow for the production of hydrogen peroxide under mild conditions, avoiding the use of critical solvents and reducing or avoiding the formation of toxic by-products.

One of the most exploited enzymes for this purpose is Glucose Oxidase (GOx), which catalyzes the oxidation of β-*d*-glucose to *d*-glucono-δ-lactone (further hydrolyzed into gluconic acid) and hydrogen peroxide in the presence of molecular dioxygen, as summarized in Equation (20).

$$\beta\text{-}d\text{-glucose} + O_2 + H_2O \rightarrow \text{gluconic acid} + H_2O_2 \quad (20)$$

This catalytic mechanism is also widely exploited in Bio-Fenton processes that actually use H_2O_2 enzymatically produced as a reagent for the Fenton reaction [48]. Unlike the classic Fenton reaction, the Bio-Fenton process also occurs at pH values near neutrality owing to the synergy with all the GOx reaction products [49]. A wide discussion about the environmental application of the Bio-Fenton technique will be made in Section 2.2 of this review, together with a description of innovative bi-enzymatic systems coupling GOx and other enzymes.

Finally, a section about H_2O_2 detection techniques and another on the critical assessment of the whole H_2O_2-mediated systems will be presented to enrich the overview of the practical implications of these depuration treatments. The global structure of this review will cover the topics indicated in Figure 3.

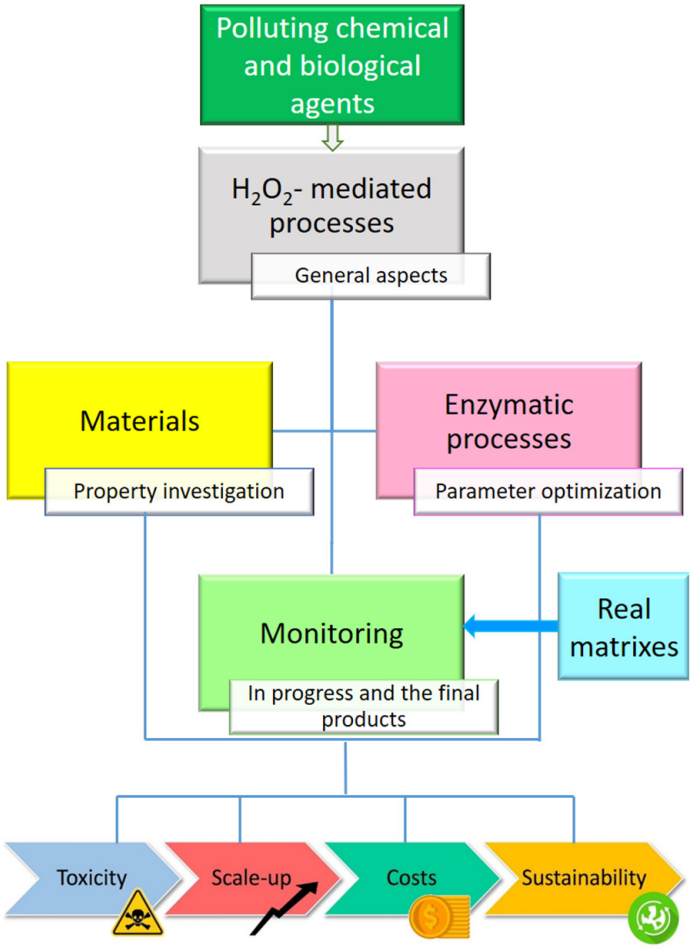

Figure 3. Workflow at the basis of this review, indicating the core topics.

2. Recent Developments in AOP Systems Involving H_2O_2

This section will examine different material- and enzyme-based systems involving hydrogen peroxide and its derived ROS for decontaminating wastewater from several types of contaminating agents, ranging from synthetic dyes (often found downstream textile industries) to pharmaceuticals and other harmful chemicals derived from different production activities to biological pathogens.

2.1. Advanced Materials

By searching on the Scopus database for studies with the query "H_2O_2 AND generation AND wastewater" and further limiting the search to the keywords "Hydrogen peroxide", 407 documents were found. Of these research studies, 96 possess "Iron", 77 "Iron compounds", 32 "Ferric Ion", 17 "Ferric compounds", 38 "Ferrous Ion", 109 "Fenton", 23 "Photo-Fenton", and 42 "Electro-Fenton" as further keywords. This circumstance makes clear the strong contribution of iron-based chemistry and Fenton-type reactions when environmental decontamination mediated by hydrogen peroxide is attempted. Table 1 shows a selection of recent works reporting iron as the main component or coadjuvant in remediation routes. Indeed, the opportunities of obtaining Fe-containing materials from natural sources (entries 10, 23 and 24 in Table 1) or preparing different kinds of iron-based compounds are uncountable [41,47,50–53]. Moreover, even in Fenton and photo-Fenton processes defined as "heterogeneous", iron can be added as a homogeneous reactant (entries 13, 15 and 21 in Table 1).

Table 1. Iron-based systems for pollutant removal mediated by H_2O_2 (except for two cases, all the works reported were published within the last 5 years) *.

System	Pollutants	Conditions	Performance	Mechanism and Notes	Ref.
1. Fe(III)-functionalized polyacrylonitrile/polypropylene fiber mesh	Bisphenol A (BPA)	Best setup: 75 ppm of BPA, 300 ppm of H_2O_2, pH = 3, 60 °C.	100% BPA abatement in <30 min; effects of temperature and pH. Fast degradation in Rotating Catalytic Reactor.	Fenton process; reusable catalyst but poisoning by the intermediates.	[54]
2. Zn-Carbon Nanotubes (CNTs) in the presence of Fe^{2+}	4-chlorophenol (4-CP)	Conc. 4-CP = 50 mg L^{-1}; Conc. Fe^{2+} 20 mg L^{-1}, pH = 2.0. O_2 was fed in the reaction mixture (400 mL min^{-1}).	Abatement of 4-CP and TOC: 98.8% and 87.4%, respectively (20 min). When 4-CP was spiked in real wastewater, the abatements of 4-CP and TOC were 47.0% and 45.6%. Effects of pH, Zn-CNTs dosage and Fe^{2+} amount.	Fenton: in situ generation of a high concentration of H_2O_2, rapid regeneration of Fe^{2+} from the reduction of Fe^{3+} by Zn and high adsorption ability of Zn-CNT towards pollutants.	[55]
3. Graphitic-C_3N_4 QDs with FeOOH	Tetracycline (TC), p-nitrophenol (PNP), 2,4-dinitrophenol (2,4-DNP)	500 W Xe lamp with a 420 nm cut-off; addition of H_2O_2; optimal pH = 7.	Abatement: TC ca. 90% (2 min), PNP 90% (10 min), 2,4-DNP ca. 90% (5 min). Dependence on catalyst/pollutant ratio, pH, conc. H_2O_2.	Photo-Fenton: main action of $^{\bullet}OH$ with the aid of $O_2^{\bullet-}$ and h^+; photogenerated e^- in CB favored Fe^{3+}/Fe^{2+} cycling.	[56]
4. Ultrathin porous Graphitic-C_3N_4 nanosheets with amorphous FeOOH QDs	Oxytetracycline (OTC)	300 W Xe lamp with a 420 nm cut-off; pH = 7.	Highest efficiency for 20%FeOOH-composite degrading 86.23% of OTC (120 min) and TOC removal of 48.6%.	Photo-Fenton; Graphitic-C_3N_4 in situ produced H_2O_2, improving transport of photogenerated e^--h^+ pairs; FeOOH generated $^{\bullet}OH$.	[57]
5. α-Fe_2O_3/Graphitic-C_3N_4	Rhodamine B (RhB), tetracycline hydrochloride (TC-H)	Simulated solar light with 300 W Xe lamp; neutral pH.	Degradation of RhB 96% (90 min) and TC-H 95% (150 min).	Photo-Fenton: effective separation and transfer of photogenerated charge carriers; H_2O_2 photoproduction on g-C_3N_4; $^{\bullet}OH$ generation from H_2O_2 decomposition on α-Fe_2O_3; $O_2^{\bullet-}$ and h+ played supporting role.	[58]
6. Magnetite/maghemite NPs coated with waste-sourced bio-based substances (BBS)	Phenol (PH)	For Fenton: addition of H_2O_2 5×10^{-4} M; photoactivation by a lamp with max emission at 365 nm; pH = 3.5.	100% PH degradation (5 min). Reusability allowed by the constant Fe release from NPs.	Fenton and photo-Fenton processes, but higher efficiency in Fenton mode. In photo-Fenton $^{\bullet}OH$ are generated. BBS acted preventing catalyst oxidation and Fe precipitation.	[59]

Table 1. *Cont.*

System	Pollutants	Conditions	Performance	Mechanism and Notes	Ref.
7. Glucose-mediated Fe_3O_4 magnetic NPs	Methylene blue (MB), Cr(VI)	For Fenton and photo-Fenton: addition of H_2O_2; photocatalytic reduction of Cr(VI); photoactivation with vis. light (250 W).	MB degradation at pH 9: 93% in 75 min by photo-Fenton and 92% in 120 min by Fenton process. 100% photoreduction of Cr(VI) in 25 min. Influence of H_2O_2 concentration, pH, catalyst/pollutant dosage.	Higher efficiency of both Fenton and photo-Fenton ascribed to the novel synthesis method. $^{\bullet}OH$ was detected as primary ROS. The catalyst was stable and reusable.	[60]
8. CuO-Fe_2O_3 heterojunction	Quinoline Yellow (QY)	Best setup: H_2O_2 and QY concentrations 27.6 mM and 100 mg L^{-1}, respectively; pH = 3, 40 °C.	100% QY removal in ca. 60 min. Dependence on pH, conc. H_2O_2 and dye, catalyst dose, temperature.	Photo-Fenton and Fenton (no strong effect of irradiation); recyclability.	[61]
9. Fe_3O_4/Cu magnetic NPs prepared using *Rosmarinus officinalis* leaves aqueous extract	Methyl Orange (MO), imipenem (IMI), imatinib mesylate (IMA)	300 W Xe lamp with a 420 nm cut-off.	MO, IMI, IMA degradation of 96.6%, 81.8% and 84%, respectively, after 5400 s; TOC decrement.	Photocatalytic process with production of H_2O_2 and $O_2^{\bullet-}$ as main ROS; reusability of the catalyst; beneficial effect of *R. officinalis* leaves extract.	[62]
10. Mexican Natural Zeolite-based Membrane	Reactive Black 5 (RB5)	Best setup: pH= 3, conc. H_2O_2 = 3 g L^{-1}, conc. RB5 = 100 mg L^{-1}, added $FeCl_3$ = 0.013 g L^{-1}, LED lamp emission at 405 nm (2.2 W), permeation flux ≅ 467 cm^3 m^{-2} h^{-1}.	92.3% discoloration in 30 min; progressive TOC decrement.	Photo-Fenton; reusable membranes, but possible Fe leaching.	[63]
11. Triphase MIL-101(Fe)/Graphitic-C_3N_4/hydrophobic carbon cloth	Methyl Orange (MO), methylene blue (MB), rhodamine B (RhB), rhodamine 6G (Rh6G)	300 W Xe lamp; dye solution = 10 ppm, pH = 3. Catalyst (size: 2.5 cm^2) hydrophilic surface immersed in solution, while the hydrophobic part was exposed to air for O_2 supply.	Abatement: MO 99%, MB 99%, RhB 98%, Rh6G 97% (130 min); high reaction rate constant.	Photo-Fenton with photoactivated in situ production of H_2O_2, promoted by triphase design of the Z-scheme heterojunction with a favored pathway for O_2 transfer. Photoinduced e^- and h^+ separation efficiency; $^{\bullet}OH$ and $O_2^{\bullet-}$ were the main ROS.	[64]

Table 1. *Cont.*

System	Pollutants	Conditions	Performance	Mechanism and Notes	Ref.
12. MoS_2-Fe_x composite	Sulfadiazine (SD)	Best catalyst: MoS_2-Fe_{75}; Optimal conditions: H_2O_2 addition, SD = 10 mg L^{-1}, pH = 6.5.	SD degradation 91.1% (90 min); effect of catalyst dosage, pH, H_2O_2 feeding way.	Fenton: MoS_2-Fe_x selectivity for $^1O_2$. "Small amount for multiple times" feeding way of H_2O_2 increased MoS_2-Fe_x stability and SD degradation rate, reducing H_2O_2 decomposition. Formation of Fe sludge was much reduced than nano-iron powder. Long-term effectiveness of the MoS_2-Fe_x/H_2O_2 system.	[65]
13. MoS_2 in the presence of Fe^{3+}	Bisphenol A (BPA), benzoic acid (BA), sulfadiazine (SDZ), rhodamine B (RhB), carbamazepine (CBZ), 4-acetamidophenol (APAP), ciprofloxacin (CIP), tetracycline hydrochloride (TC-H)	Optimal system: 1.0 mM H_2O_2, 0.3 g L^{-1} MoS_2 and 0.15 mM Fe^{3+}, pH = 3.0.	Abatement (60 min): CBZ 65.9%, APAP 79.1%, SDZ 84.1%, BA 86.0%, RhB 90.8%, CIP 92.5%, BPA 93.0%, TC 100%. Effects of pH and concentrations of pollutant, H_2O_2, Fe^{3+}, MoS_2.	Fenton: strong oxidative intermediate Mo^{6+} peroxo-complexes besides $^{\bullet}OH$ radicals. Stable and reusable catalyst.	[66]
14. TiO_2-supported Fe (FeTi-ox)	Acetaminophen (AAP), benzoic acid (BA), carbamazepine (CBZ), phenol (PH)	Conc. H_2O_2 = 10 mM and conc. pollutant = 5−10 μM, pH = 7.	Degradations (2 h): AAP 100%, PH 55%, while BA and CBZ were not removed. Pollutants selectively reacted with $^{\bullet}OH$ (BA and CBZ) or with both $^{\bullet}OH$ and Fe(IV) (AAP and PH).	Fenton: relevant interaction H_2O_2-TiO_2 forms a peroxo−titania complex Fe(III)-Ti-OOH, which reacted further with H_2O to give surface oxidant Fe[IV]-O^{2+} even in the presence of Cl^-, HCO_3^- ions and organic matter. Reusability of FeTi-ox.	[67]
15. P25 (TiO_2) in the presence of US and Fe^{2+}/Fe^{3+}	Bisphenol A (BPA), sulfadiazine (SDZ)	US at 400 kHz alone or in the presence of P25 under vis. light (LED lamp emitting at 400–630 nm).	With US and Fe^{2+}: >90% degradation of BPA and >80% for SDZ in 30 min. In the presence of Fe^{2+}/Fe^{3+}, US, P25 and vis. light, 100% SDZ abatement in 60 min.	Homogeneous sono-Fenton: in situ generation of H_2O_2 and $^{\bullet}OH$. Sono-photo-Fenton: P25 promoted Fe^{2+}/Fe^{3+} cycling by the photoproduced e^-. P25 favored reaction at circumneutral pH and pollutant mineralization.	[68]

Table 1. *Cont.*

System	Pollutants	Conditions	Performance	Mechanism and Notes	Ref.
16. Iron-cobalt oxide nanosheets (CoFe-ONSs)	Tetracycline (TC)	Conc. TC 50 mg L^{-1}, conc. H_2O_2 20mM, neutral pH.	TC removal 83.5% (50 min). Effects of catalyst dosage, conc. H_2O_2, pH, temperature, conc. TC, anions and water sources.	Fenton: $^{\bullet}OH$ were the main ROS. Redox cycles of FeII/FeIII and CoII/CoIII enhanced $^{\bullet}OH$ generation. Negligible Fe ions leaching from catalyst (reusability).	[69]
17. Magnetic $ZnO@Fe_3O_4$ composite	p-nitrophenol (p-NP)	Conc. p-NP 35 mg L^{-1}, pH = 3 (optimal); 100 W incandescent lamp (400–1700 nm).	100% p-NP removal in 60 min. Effect of temperature.	Photo-Fenton: self-generation of H_2O_2, with primary role of $^{\bullet}OH$; catalyst reusability.	[70]
18. $ZnFe_2O_4/BiVO_4$ heterojunction	Methylene blue (MB).	Best composition: $0.15ZnFe_2O_4/BiVO_4$.MB conc. 40 mg L^{-1}, eventual addition of H_2O_2; photoactivation with 300 W Xe lamp.	MB degradation with photocatalytic method (2 h): 83.7%; with Photo-Fenton (1 h): 98.8%.	Photocatalysis: h^+ had a main role in degrading MB; photo-Fenton: activation of H_2O_2 ($^{\bullet}OH$ production) by photogenerated e^-; photogenerated carriers separation efficiency.	[71]
19. $LaFeO_3$ prepared from citric acid and $LaFeO_3$ synthesized from waste-sourced bio-based substances	4-methylphenol (4-MP) and crystal violet (CV)	Conc. pollutant 10 mg L^{-1}; pH = 8–10; 1500 W Xe lamp with a 340 nm cut-off.	$LaFeO_3$ prepared from waste-sourced bio-based substances removed 100% CV and ca. 40% 4-MP. The citric acid-derived $LaFeO_3$ photodegraded 90% of 4-MP and 30% of CV.	Photocatalysis: different $LaFeO_3$ efficiencies were ascribed to different ζ-potentials. A homogeneous photo-Fenton process can occur when $LaFeO_3$ synthesized from waste-derived substances releases Fe and carboxylate ions.	[72, 73]
20. Cerium, Cobalt, Copper-doped Strontium Ferrate (SCFCC)	*Escherichia Coli*	Best material with 20% Cu doping. Bacteria conc. 1.0–3.0 $\times 10^5$ CFU/mL. SCFCC/inoculum ratio = 1 g/50 mL. Tests in the dark, and after thermo- or UV-activation (max 70 °C heating and UV-A 300 W lamp, respectively).	Max. bacterial removal 55% in the dark, 98% after UV, 40% after thermal activation.	Photo/Thermo-catalysis: formation of H_2O_2 and $^{\bullet}OH$. Activity was also influenced by SCFCC metal ions' redox couples and oxygen vacancies.	[74]

Table 1. *Cont.*

System	Pollutants	Conditions	Performance	Mechanism and Notes	Ref.
21. Peanut shell-derived biochar (PBC) in the presence of Fe^{2+}	Bisphenol A (BPA), dimethyl phthalate (DMP), sulfamethoxazole (SMX)	Degradation tests conducted in a three-electrode cell aerated with O_2 (0.4 L min^{-1}); voltage applied 0.5–1.1 V; pH = 3.0, conc. Fe^{2+} 0.2 mM and conc. pollutants 20 mg L^{-1}.	Removal efficiencies of 98–100% within 15 min; mineralization efficiencies of 83–100%.	Electro-Fenton: PBC hierarchical porous structure and defects caused a high surface area, electrical and ionic conductivity. The presence of OOH/C–O–C and N on the surface ensured a high two-electron ORR selectivity for H_2O_2 production, accelerated Fe^{2+} regeneration, also enabling $^{\bullet}OH$ accumulation.	[75]
22. Ferromagnetic activated carbon from rubber seed hull	Bezaktiv Brilliant Blue (BBB)	Best setup: pH = 3, conc. H_2O_2= 17 mol L^{-1}, conc. BBB = 100 mg L^{-1}.	BBB removal > 75% in all conditions (4 h). Effects of pH, conc. H_2O_2 and pollutant, catalyst dosage.	Fenton; reusable catalyst.	[76]
23. Natural pyrite (FeS_2)	Carbamazepine (CBZ)	Addition of tartaric acid (TA), citric acid (CA), ascorbic acid (AA); simulated sunlight (300 W Xe lamp).	No CBZ degradation with pyrite; CBZ abatement: 70%, 60%, 53% in pyrite/TA, pyrite/CA, pyrite/AA systems, respectively under irradiation (30 min). Effect of catalyst dosage, pH, conc. CBZ.	Photo-Fenton; in situ generated H_2O_2 without extra pH adjustment; organic acids can form complex with Fe in pyrite, promoting Fe(II) dissolution. Upon irradiation, pyrite is excited to generate photo-e^-, able to reduce oxygen to produce H_2O_2 and $^{\bullet}OH$.	[77]
24. Goethite (α-FeOOH)	Bisphenol A (BPA)	H_2O_2 addition (1.0 mM), conc. BPA 0.1 mM; reaction allowed under acidic, neutral and weakly alkaline conditions.	BPA degradation 75.9% after 240 min; pH dependency.	Fenton; $^{\bullet}OH$ production. Good structural stability of catalyst; higher efficiency with H_2O_2 in comparison to persulfate oxidation system due to the limited radical scavenging.	[78]

Table 1. *Cont.*

System	Pollutants	Conditions	Performance	Mechanism and Notes	Ref.
25. Heterogeneous Nanoscale Zero Valent Ion (n-ZVI)	Glyphosate (GLY)	Eventual addition of H_2O_2. Optimal pH 3–4.	Up to 87% of GLY removal (30 min) in Fenton mode. Effects of pH, conc. H_2O_2, n-ZVI dosage. Efficiency also in tap water (100% degradation in 40 min), despite potentially interfering ions.	Adsorption and Fenton (after H_2O_2 addition).	[79]

* Legend: QDs = Quantum Dots; CB = conduction band; e^- = electrons; h^+ = holes; λ cut-off < 420 nm indicates visible light; TOC = Total Organic Carbon; NPs = nanoparticles; ORR = Oxygen Reduction Reaction. For the sake of clarity, when mechanisms are indicated as "Fenton" for brevity, they have to be considered Fenton-like processes.

In the next subsections, the discussion, starting from the data of Table 1, will bring up several subjects, citing material types from 0D to 3D, from inorganic catalysts to organic substances, and from mono-element to binary and mixed systems, referring to the possibility of tuning the compositions with dopants or with the formation of composites/hybrids. The surface physical properties (area, porosity, surface charge), the chemical defects, such as oxygen vacancies, and a hint regarding the role of synthesis have also been taken into account. In Figure 4, the main points of this study are depicted.

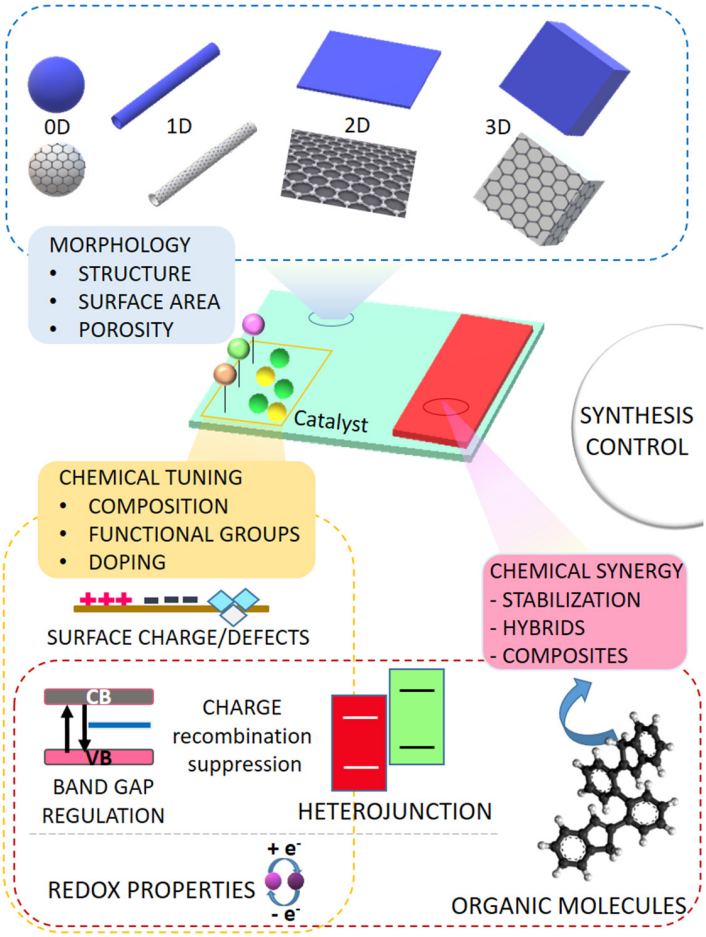

Figure 4. Focus on inorganic catalytic material properties that can be subjected to fine-tuning devoted to enhancing pollutant degradation efficiencies.

2.1.1. Considerations on Structures and Morphologies

In heterogeneous systems, the role of materials is determined not only by their chemical activity in a strict sense, but also by other physical–chemical characteristics, such as the materials' structures and morphologies. As the catalyst surface in the H_2O_2-mediated processes is involved in the adsorption and dissociation of oxygen/water molecules and oxygenated intermediates, a favorable surface charge, and the increase in the specific surface area and, thus, the number of active sites has been pursued as strategies to accelerate the reactions [80,81]. In this regard, Farhadian et al. [82] highlighted the importance of the support within composites/functionalized materials in a review focused on mesoporous silica with high surface area and high pore volume, capable of loading and dispersing catalytically active iron species for heterogeneous Fenton oxidation reactions. Indeed, the large cavities of the silica support can facilitate the mass transfer processes, and the high surface area of these materials increases the number of active sites, allowing for a more intimate contact with contaminants. Strategies for enhancing the catalytic performance of iron/silica composites were indicate, such as the simultaneous loading of different metals and the design of multimodal pore supports, surface functionalization to favor the distribution of active sites, and the use of radiation, ultrasound, and electrolysis.

In the same direction, entries 1–5 and 11 in Table 1 report the presence of 0D (quantum dots), 1D (carbon nanotubes) and 2D materials (polyacrylonitrile fiber mesh, graphitic carbon nitride, carbon cloth), also in combination. Salunkhe et al. [83] dedicated a review to 0D–2D synergistic nanocomposites for photocatalytic applications: the size-dependent bandgap tunability and effective charge carrier production of quantum dots can be exploited together with graphitic-C_3N_4 features, such as low toxicity, chemical and thermal stability, visible light absorption, n-type semiconducting property, and a configurable bandgap. Graphitic-C_3N_4 has been widely used for the photocatalytic degradation of pollutants alone or in co-presence with other compounds, such as MgO, Bi_2O_3, MoO_3/Ag, Au/Ni_2P, etc. [84–91]. Among the attempts to exploit graphitic-C_3N_4, Torres-Pinto et al. prepared these materials as metal-free photocatalysts able to generate hydrogen peroxide and, in turn, $^{\bullet}OH$ in the presence of dissolved oxygen when irradiated by visible light [92]. Adding low dosages of dissolved iron promoted a Fenton process and the C_3N_4 photocatalytic system improved the mineralization of resorcinol, phenol, gallic acid, and benzoic acid at a natural pH by approximately 1.2 times.

Graphene and reduced graphene oxide (rGO), 2D versatile carbon materials, have demonstrated excellent mechanical properties, high charge-carrier mobility, high specific surface area, a large number of functional groups and good electrocatalytic activity, attracting increasing attention for environmental applications as adsorbents, photocatalysts and electrocatalysts [93]. Many composites have been designed, as well, with doping elements, nano zero-valent iron, oxides, mixed oxides, and sulfides in binary and ternary systems [94–100]. An interesting application of these materials is also the possibility of transforming them from 2D to 3D systems, such as aerogels, sponges and foams, which possess enhanced porosity and lightness as inner characteristics [101,102]. For instance, a novel cathode of macroporous graphene aerogel (GA) with a high specific surface area was proposed for the electro-Fenton reaction, efficiently and continuously producing in situ H_2O_2 to degrade antibiotic ciprofloxacin [97]. The good mineralization efficiency was attributed to the relevant number of macropores of GA that acted as reaction traps to accelerate the electro-generation of H_2O_2, subsequently decomposed by Fe^{2+} to form $^{\bullet}OH$. Simultaneously, the strong charge transfer ability of GA was beneficial to the conversion of Fe^{3+}/Fe^{2+}, making this material a promising candidate material for electro-Fenton cathode due to its low cost, high efficiency and corrosion resistance.

For similar reasons connected to morphology, biochars and active carbons have been widely employed in H_2O_2-mediated processes (entries 21 and 22 in Table 1). Indeed, active carbons are produced from carbon-based compounds—often non-renewable (i.e., coal, petroleum residues, peat, lignite and polymers)—by the combination of a pyrolytic process and chemical or physical treatments through activators such as chemicals (acids, alkalis,

salts) or gases (i.e., steam, CO_2, N_2) [103,104]. Biochars, instead, were initially defined as carbonized biomass (formed under a low O_2 environment from agricultural residue, animal waste, or refuse of woody plants) and they can also be subjected to further physical–chemical transformations to improve surface features [103,104]. For both active carbons and biochars, the raw material, together with the production technique and operating temperature, have an important influence on product yield and composition [101]. In their review, for instance, Ribeiro et al. [105] discussed the various activities of carbon materials as catalysts on their own and hybrid magnetic carbon nanocomposites in catalytic wet peroxide oxidation reactions for the degradation of organic pollutants. Apart from purely iron-based compounds that are currently being developed [106,107], several other doping/functionalizing moieties have been used on biochar and active carbons, such as Ag_3PO_4 [108], MnO_2, nitrogen [109], boron [110], B/N/graphene [111], N/S/Fe [112], FeAl-layered double hydroxide [113], copper oxides [114–116], CuNi [117], and Sr/Ce [118].

Other efforts to improve the morphological and textural features have been made by acting directly on inorganic active phases, as in the examples of entries 10 and 11 in Table 1, where crystalline porous solids [119] (zeolites and a metal–organic framework, MOF) have been used, taking advantage of to their large surface area, tunable porosity and chemistry [120–122]. In particular, in entry 11, MIL (Materials of Institute Lavoisier) indicates one of the most popular MOFs and MIL-101 (Fe) is the one assembled by 1,4-benzene dicarboxylate ligand and iron(III) cation [123].

2.1.2. Considerations on Chemical Compositions and Stability

Among the inorganic species used as active phases in hydrogen-peroxide-mediated processes, the simplest compositions are zero-valent metal nanoparticles (e.g., Fe^0, Al^0, Zn^0, Cu^0) [124–130], which bear strong chemical reducibility, high efficiency, and large specific surface although the main drawbacks are the tendency towards agglomeration and oxidization [131]. Nanoscale zero-valent iron (n-ZVI) is certainly the most utilized in environmental applications, see entry 25 in Table 1. The typical reaction initiating the whole process is the slow-releasing source of dissolved Fe^{2+} in acidic solutions, starting a Fenton-like pathway [41,79,127]. Al^0 was reported to be able to produce hydrogen peroxide in situ in water at neutral conditions and further decompose H_2O_2 into $^{\bullet}OH$ in an acidic solution [125]. Other reaction types that zero-valent metal nanoparticles can support are, for example, simple photocatalysis or ozone-based processes [124,128].

Other important categories of materials exploited in H_2O_2-mediated processes are metal sulfides, metal oxides and mixed oxides. Metal sulfides have been presented in Table 1 (entries 12 and 13) in combination with iron since they can accelerate the Fe^{3+}/Fe^{2+} cycle through the exposed reducing metal active sites or directly participate as a co-catalyst in the reaction, activating the oxidant to generate active radicals [41]. However, these compounds can be employed as principal active phases. According to the previous findings, there are two general mechanisms commonly proposed for metal sulfide-based AOPs. One is the improvement of the electron transfer efficiency resulting from the reductive S^{2-} on the catalyst surface; the other one is the protons' capture by unsaturated S atoms on the surface of the metal sulfide, resulting in the formation of H_2S and exposition of metal active sites with reducing properties [132]. In general, the behavior of these compounds can be designed by choosing the most adequate metal (Fe, W, Co, Zn, Mo, Pb, Cr, Cu) in the sulfide since this factor has been reported to influence the performances [41,132]. An example of a further fine-tuning effort was conducted by Bai et al. [133], who synthesized MoS_2 photocatalysts with sulfur vacancies that in situ produced H_2O_2 and hydroxyl radicals. The reaction was favored by the transformation of variable metal molybdenum atom, Mo(IV)/Mo(VI), that effectively enhanced the degradation efficiency towards tetracycline and diclofenac.

Among binary oxides, one of the first and most studied is TiO_2, which is very well known as a semiconductor photocatalyst, as explained in the Introduction. The limitations of this system are mainly attributable to the high band gap of TiO_2, which requires UV light

to trigger the titania activity, and the rapid recombination of e^--h^+ pairs, with consequent photocatalytic efficiency reduction and radiation energy loss [134]. For this reason, many efforts have been made to overcome these issues through metal and non-metal doping, surface modification, and fabrication of composites with other materials. Iron and/or H_2O_2 assistance is a popular strategy in the literature [135–137]; here, two significant examples of the combination of titania with iron, H_2O_2 and ultrasound to start different Fenton-like processes are reported in Table 1, entries 14 and 15. More detailed information on the modulation titania band gap, surface reactivity, charge transfer, and stability, among other properties, has been extensively reported in ad hoc reviews [138–142].

To break free from titanium oxide in photocatalysis and iron oxides in Fenton-like systems (entries 5–9, 16 and 17 in Table 1), a plethora of other binary oxides and their various combinations have been developed, such as cobalt, copper, zinc, cerium, tin, and tungsten oxides [143–152]. Different but interesting studies also concern metal peroxides able to release H_2O_2, as recently reported for MgO_2 in dye degradation and bacterial decontamination [153], and for CaO_2 in trichloroethylene abatement [154].

Mixed oxides in different crystalline structures, such as perovskite (ABO_3), scheelite (ABO_4) and spinel types (AB_2O_4) [155–157], have been widely employed in environmental depollution (entries 18–20 in Table 1). They are exploited for their ability to degrade pollutants both in the presence and in the absence of hydrogen peroxide through their inherent semiconducting and redox properties, or by forming heterojunction structures. Often, they are employed as photocatalysts and electrocatalysts [158–165]. These materials with at least two metal elements in the basic structure have the advantage of being regulable in many characteristics, starting from the composition, which can bear multiple doping elements, creating several combinations. Moreover, in many studies, the possibility of inducing non-stoichiometry and charge compensation mechanisms is considered another important tool to create defects such as oxygen vacancies inducing high oxygen mobility, unusual element valence states, such as Fe(IV), and active redox couples [18]. For perovskite-type oxides, for instance, activity descriptors based on the occupancy by electrons in the orbitals of the active metal were proposed to explain material catalytic properties [166].

In general, when oxide materials are involved, catalytic activities have also been related to the degree and symmetry of the crystalline structure [80,167].

Regarding the use of magnetic iron-based oxides, they have been presented as a convenient tool not only to perform heterogeneous Fenton-like reactions, but also to allow for a better and easier separation from the water medium [50]. Many works have described these systems; for instance, in Table 1, they are exemplified in entries 6, 7, 9, and 17. Actually, the possibility of recovery, regeneration and reuse of the active phase in decontamination procedures is a fundamental parameter to define their sustainability. This aspect has been stressed in many studies and is highlighted in Table 1 (entries 1, 6–10, 13, 14, 16, 17, 22).

As partially anticipated in Section 2.1.1 discussing 2D carbon materials, such as graphitic carbon nitride, a novel frontier of H_2O_2 generation through photocatalysis is the replacement of traditional inorganic photocatalysts with organic ones, addressing remarkable advantages, such as narrow bandgap, adjustable band edge potentials, ability to control surface configurations, and tunability of structural units to promote efficient charge separation and transfer [168]. Various strategies to improve the activity and stability of organic photocatalysts have been explored, such as the construction of donor–acceptor structures, the design of conjugated structures, the incorporation of heteroatoms, the enhancement of the internal electric field, and the substitution of functional groups. Some examples of these compounds considered by Zhang et al. [168] are resorcinol-formaldehyde resins, poly(3-(4-ethylnylphenyl)ethynyl)pyridine, and Covalent Heptazine Frameworks, among others. Hydrogen peroxide generation was reported to occur by the anthraquinone-mediated oxygen reduction reaction (ORR), the radical-related ORR, the water oxidation reaction (WOR), and the dual ORR and WOR pathways.

Moreover, the role of natural-inspired organic substances as coadjutants in catalytic and Fenton-like reactions for water depollution has been explored both in homogeneous

and heterogeneous systems. In particular, humic-like substances (HLSs), given the intrinsic influence of humic acids in natural ecosystems, have been investigated [4]. In a recent review, García-Ballesteros et al. [169] pointed out that HLSs, which can even be isolated from different wastes, are photosensitive and are able to generate ROS such as hydroxyl radicals and singlet oxygen or triplet excited states upon irradiation (Equations (21)–(24)) [4,170]. This circumstance is particularly convenient when HLSs are complexed with iron to promote homogeneous (photo)-Fenton-like processes at mild pH, preventing Fe deactivation [171].

$$\mathrm{HLS} + h\nu \rightarrow {}^{3}\mathrm{HLS}^{*} \quad (21)$$

$$\mathrm{HLS} + h\nu \rightarrow \mathrm{HLS}^{+\bullet} + e^{-}_{aq} \quad (22)$$

$${}^{3}\mathrm{HLS}^{*} + \text{H-Substrate} \rightarrow \mathrm{HLS}^{\bullet} + \text{Substrate}^{\bullet} \quad (23)$$

$$\mathrm{HLSH}^{\bullet} + O_2 \rightarrow \mathrm{HLS} + \mathrm{HOO}^{\bullet} \quad (24)$$

Novel hybrid materials for heterogeneous catalysis have also been synthesized using HLSs to induce photocatalytic properties [172,173]. In some cases, these materials were produced by combining HLSs with iron-based oxides to drive heterogeneous (photo)-Fenton (or mixed heterogeneous/homogeneous) processes (as in entries 6 and 19 in Table 1) [170].

The effects of ligands in heterogeneous Fenton-like systems have also been explored with different chemical substances, like organic acids (entry 23 in Table 1). For instance, EDTA (ethylenediaminetetraacetic acid) was found to be able to enhance the activation rate of H_2O_2 via the decrease in the redox potential of the Fe(III)/Fe(II) pair. Additionally, it improved the utilization efficiency of hydrogen peroxide by preserving the electron-rich Fe(II) under the attack of $O_2^{\bullet-}$ and $HOO^{\bullet}$ [174]. Also, in the case of semiconductor oxides, the influence of ligands and complexes has been studied to enhance the photocatalytic performances [175–177], and this further underlines the importance of even more careful engineering of materials to make decontamination processes more efficient.

Lastly, the modulation of the physical–chemical properties of catalysts has also been carried out by fine-regulating, during the synthesis, both the operating parameters and the precursors' types, which act to stabilize the final materials as well as impart specific properties, for instance, specific surface charge and exposed functional groups [178–180] (see entries 7, 9 and 19 in Table 1). A simplified roadmap for the development of functional materials for H_2O_2-mediated processes is summarized in Figure 5.

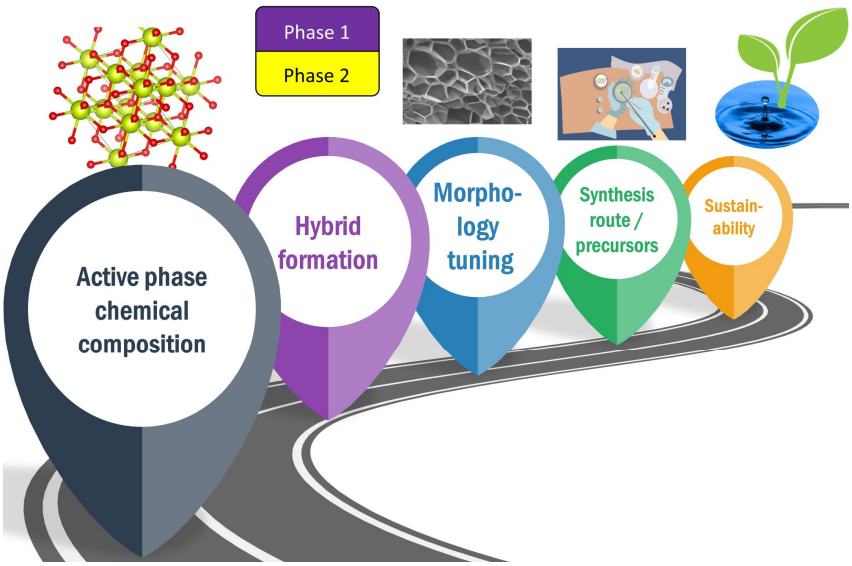

Figure 5. Strategies to obtain environmentally active materials in H_2O_2-based reactions.

2.2. Enzyme-Driven Processes

2.2.1. Glucose-Oxidase-Based Bio-Fenton

The applications of the Bio-Fenton approach in water remediation are increasing since the range of treatable pollutants is quite broad. In Bio-Fenton remediation processes, the hydrogen peroxide necessary to activate the Fenton reaction is mainly provided by an enzymatic reaction catalyzed by Glucose Oxidase (GOx) that occurs in mild pH conditions. GOx is a stable oxidoreductase able that use oxygen as an electron acceptor to catalyze β-*d*-glucose to *d*-glucono-δ-lactone by using the coenzyme FAD (Flavin Adenine Dinucleotide) as an electron carrier [181]. The oxidation of β-*d*-glucose leads to the reduction of one FAD molecule to the hydrogenated form $FADH_2$; successively, *d*-glucono-δ-lactone is non-enzymatically hydrolyzed to gluconic acid and the reduced coenzyme is re-oxidized to FAD by a molecule of dioxygen, producing a molecule of H_2O_2 for each reaction cycle, as in Figure 6.

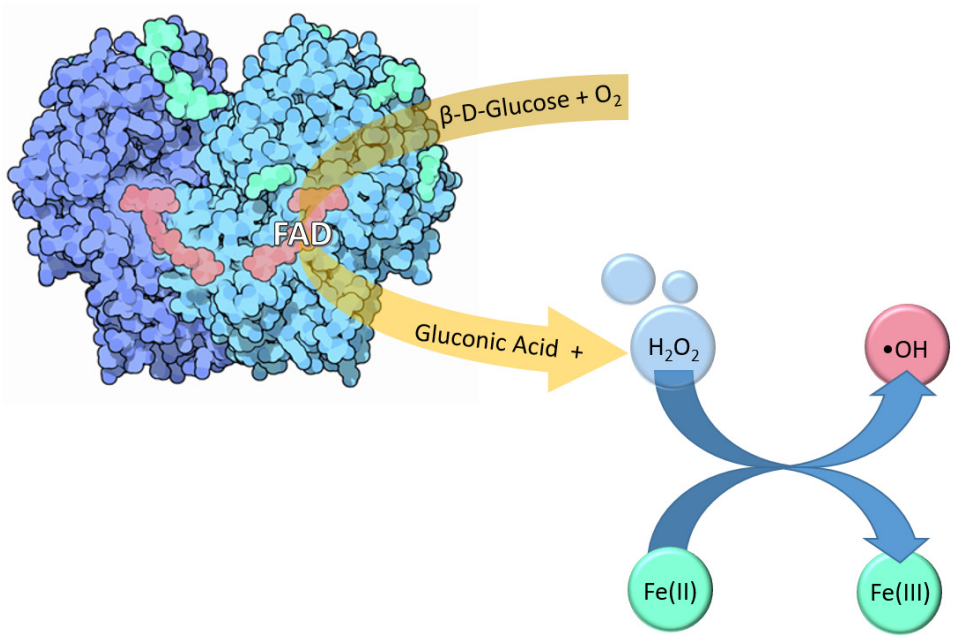

Figure 6. Schematic representation of Bio-Fenton reaction mediated by GO_x (3D structure of GOX by Protein Data Bank, entry: 1GPE) [182].

GOx in vivo is usually coupled with Catalase, which rapidly causes the dismutation of H_2O_2; on the contrary, in environmental applications, GOx is mainly exploited when coupled to a system able to activate Fenton or Fenton-like reactions. Table 2 provides a summary of recent studies concerning several classes of environmental contaminants removed by the Bio-Fenton reaction. To optimize the hydrogen peroxide production, different aspects have to be taken into consideration. The amount of H_2O_2 produced depends on both the concentration of the biocatalyst and glucose. Indeed, according to the Michaelis–Menten model, at low concentrations of glucose, the rate of H_2O_2 production is linearly proportional to its initial amount, but the reaction rate decreases when the glucose concentration increases until reaching a maximum value, which, in turn, depends on the concentration of GOx [48,183].

Huang and co-workers [184] highlighted the complex role of glucose in the Bio-Fenton reaction, reporting that, at a too-high concentration, it could also act as a hydroxyl radical scavenger, inhibiting the oxidation reaction. The optimization of hydrogen peroxide generation could be obtained, therefore, by using specific techniques, which allow for the evaluation of the influence of different variables on the reaction outcomes [185].

Gluconic acid formed from the oxidation of glucose makes the process a chelate-Bio-Fenton, since it is a well-known chelating agent for ferrous and ferrate ions and is also

used in non-enzymatic AOP processes to avoid precipitation of iron hydroxides at neutral pH [186]. Ahuja et al. [49] observed a 100% Fe(III) chelation with a ligand–ion ratio of 1:1 at pH 4 and an increasing concentration of chelate complexes with pH, demonstrating the advantage of using Bio-Fenton at circumneutral pH. The same authors [49] also demonstrated that the gluconate-complex could directly react with H_2O_2 or be the source of iron ions.

In order to ensure high efficiency in milder conditions, the Bio-Fenton reaction can be performed with iron citrate instead of iron sulfate [187–190]. However, in general, the introduction of iron as a homogeneous reactant can lead to the formation of iron-containing sludge [191,192]. Therefore, heterogeneous Fe sources such as iron oxides and oxyhydroxides, like Fe_3O_4 (magnetite), γ-Fe_2O_3 (maghemite), α-Fe_2O_3 (hematite), α-FeOOH (goethite) [193], or green rust [194] have also been employed. These solids prevent sludge formation, improve Fenton efficiency in a wider range of pH, and allow for their reuse.

A change in concentration and availability of iron ions with pH is a fundamental factor that influences the efficiency of the Fenton reaction [195]; furthermore, it is well known that pH affects the enzymatic activity. Wang et al. [196] found that the removal of trichloroethene by a Bio-Fenton reaction carried out with GOx immobilized on magnetic particles at the equilibrium state did not depend on the pH, but this parameter affected the reaction rate that decreased by approximately 60% when the pH increased from 3.6 to 9. Liu and co-workers [197] demonstrated that strongly acidic and alkaline environments significantly inhibited the 4-chlorophenol degradation, decreasing from 87.6% at pH 7 to only 55.2% at pH 3 and 35.8% at pH 11. This degradation trend follows the hydrogen peroxide production, which is minimal at pH 3 and 11, while it has a maximum at pH 7. The authors underlined that during the Bio-Fenton reaction, whatever the initial pH value, there was an increase in the acidity of the solution due to the production of gluconic acid. Therefore, the efficiency of the reaction was only maintained if the variation in pH was limited within the activity range (4.5–7).

Another crucial factor is the temperature. An optimal range between 25 and 60 °C for GOx catalytic capability was reported. As for the pH, the temperature mainly influences the kinetics of the reaction more than its final outcome. Huang et al. [184] found a 2.8-fold increase in k_{obs} for trichloroethene degradation when the temperature increased from 15 to 40 °C. A similar trend was also reported by Karimi et al. [198] for the decolorization of malachite green; in this case, a slight reduction in the decolorization kinetic was already observed at 35 °C, probably due to a partial denaturation of the enzyme. On the contrary, Wang et al. [196] showed that enzyme immobilization could improve enzyme thermal stability, reporting for GOx immobilized on magnetic particles an enhancement in activity with increasing the temperature from 15 to 40 °C, with consequent reduction in the time needed to reach the equilibrium from 96 h to 24 h.

The coupled effect of thermal stability and improvement in the enzymatic activity was also reported by Zhao et al., who found that 3,4-dimethylaniline was removed with a higher rate by GOx immobilized on Kaoline (Kaoline@GOx) than a free GOx system [183]. The authors suggested that this effect was due to an enhancement in GOx spatial conformation when the enzyme was fixed on the support.

Recently, some studies have reported an improvement in Bio-Fenton efficiency when appropriate UV-light irradiation was applied. Liu and co-workers [197] observed the evolution of hydrogen peroxide produced by GOx immobilized on Kaoline in the presence of organic green rust as a source of iron. Changing the UV-light intensity, the equilibrium concentration of H_2O_2 first increased with the irradiation (from 0 to 150 μW cm^{-2}) and then decreased with further raising the irradiance up to 400 μW cm^{-2}. Consequently, the degradation percentage of 4-chlorophenol followed the same trend. The authors proposed that the mechanism at the basis of the variation in the enzymatic activity could be related to the photo-excitation of the cofactor FAD into FAD*, which induced a glucose oxidase stronger reactivity. Indeed, the FAD cofactor shows high absorption capacity at 250–300 nm

and strong UV light tolerance [199]. Obviously, excessive light intensity causes enzyme inhibition and denaturation.

Very few works investigate the Bio-photo-Fenton strategy for environmental remediation. Ghatge and co-workers [200] studied the degradation of sulfonated polyethylene employing glucose oxidase immobilized on TiO_2. They demonstrate the synergy between Bio-Fenton and light irradiation in the production of reactive species following the concentration of the degradation products. Indeed, compared to the Bio-Fenton degradation using free GOx, 21-fold and 17-fold higher amounts of acetic acid and butanoic acid were, respectively, released by the Bio-photo-Fenton reaction after incubation for 6 h.

Table 2. GOx Bio-Fenton systems for pollutant removal mediated by H_2O_2 (acronym not explicated elsewhere: COD = Chemical Oxygen Demand, U = unit).

Pollutant	Performances	Conditions	Notes	Ref
1.Trichloroethene (TCE)	Removal after 192 h - TCE 5 mg L^{-1}: 76.2% - TCE 50 mg L^{-1}: 94.1%.	200 mg magnetic nanoparticles (MIG); 2.5 mM Glucose.	- Gox immobilized on MIG - Recycled for 4 cycles - Effectiveness in the ranges of T 15–45 °C and of pH 3.6–9.0 - Influence of inorganic ions: Ca^{2+} >Mg^{2+} >Cu^{2+} and $H_2PO_4^-$> Cl^-> SO_4^{2-}.	[196]
2. 4-chlorophenol (4-CP)	Removal after 250 min - GOx@Kaolin/OGR: 77.5% - GOx@Kaolin/OGR/UV: 96.1%.	4-CP: 5 mg L^{-1} UV: 150 µW cm^{-2} T: 25 ± 1 °C OGR: 250 mg L^{-1} GOx@Kaolin: 2.5 U mL^{-1} Glucose: 5 mmol L^{-1}.	- GOx immobilized on Kaolin (GOx@Kaolin) coupled with organic green rust (OGR, source of iron) and enhanced by UV light - Reusability 6 cycles.	[197]
3.Trichloroethylene (TCE)	- After 24 h at pH 7 Ground water: 30% or 48% if doped with additional H_2O_2 (after 3 h).	TCE: 60 mg L^{-1} Glucose: 60 mM GOx: 1 mg mL^{-1} Fe: 25 mg L^{-1}.	- GOx in solution - Organic matter of ground water acts as a radical scavenger.	[201]
4. Polycyclic aromatic hydrocarbons (PAHs): Naphthalene (NAP), Anthracene (ANT), Pyrene (PYR)	- After 48 h, neutral pH, removal%: 95.1%, 75.4%, and 85.2% for NAP, ANT, and PYR - COD reduction%: 28.6%, 13.8%, and 30.8% for NAP, ANT, and PYR.	PAH: 50 mg L^{-1} each GOx: 10 U Fe(III)citrate: 0.1 mM Glucose: 2 mM.	- GOx in solution - Evaluation of PAHs concentration and COD to evaluate the mineralization - Bio-Fenton as pre-treatment to enhance PAHs removal by activated sludge: COD removal from 33% to 72%.	[189]
5. Bisphenol A (BPA)	After 10 days of incubation Removal of 80%.	BPA: 0.1 mM GOx: 10 U Glucose: 32 mM Fe(III)citrate: 0.5 mM pH 5.3.	- GOx in solution.	[188]
6. Chloro-acetanilide herbicides: acetochlor, alachlor, metolachlor, propachlor, butachlor	After 5 days, degradation %: acetochlor: 72.8% alachlor: 73.4% metolachlor: 74.0% propachlor: 47.4% butachlor: 43.8%.	GOx: 10 U pH 5.5 Fe(III)citrate: 0.5 mM Glucose: 32 mM Each herbicide 0.1 mM.	- GOx in solution - Influence of chemical structure of herbicides and particularly of R-O-R' groups.	[187]

Table 2. *Cont.*

Pollutant	Performances	Conditions	Notes	Ref
7. Trace organic contaminant (TrOCs) (mefenamic acid, ketoprofen, caffeine, carbamazepine, trimethoprim, fenofibrate, diuron, carbendazim, thiabendazole)	After 360 min pH 7 mefenamic acid: 68.54% ketoprofene: 44.7% caffeine: 36.1% carbamazepine: 44.1% trimethoprim: 46.4% fenofibrate: 20.3% diuron: 89.4% carbendazim: 73.1% thiabendazole: 88.9%.	Glucose: 1 M GOx: 100 U mL^{-1} pH 7 50 µg L^{-1} mix of TrOCs T: 30 °C H_2O_2:$FeSO_4$ = 50:1.	- GOx produced from *Aspergillus niger* using *Casuarina equisetifolia* biomass in a pilot-scale - Municipal wastewater as a matrix - Influence of the rate H_2O_2: $FeSO_4$.	[185]
8. Trichloroethylene (TCE)	After 8 h Removal of 78%.	Glucose: 2.5 mM Fe(II): 0.5 mM GOx: 10 U mL^{-1}.	- GOx in solution - Efficiency maintained in the pH range 3–6 and in a T range 15–30 °C.	[184]
9. Sulfonated polyethylene (SPE)	After 6 h with free GOx, concentration degradation products: Acetic acid: 0.22 mM Butanoic acid: 0.01 mM; After 6 h with TiO_2-GOx: degradation product conc.: Acetic acid 4.78 mM Butanoic acid 0.17 mM.	GOx free: Glucose: 32 mM GOx: 1 U mL^{-1} pH 5.5, T: 30 °C SPE: 1 mg mL^{-1}; TiO_2-GOx: As above, except for 10 U of TiO_2-GOx Xe lamp 150 W, 400 nm cut off.	- GOx both free and immobilized on TiO_2 particles - Degradation follows studying the product formation (acetic acid, butanoic acid, isovaleric acid, 1,2-ethanediol monoacetate).	[200]
10. Atrazine (ATZ)	After 360 min 72.8% removal.	Phosphate buffer: 5 mM GOx: 10 µmol min^{-1} Glucose: 3 mM Ferric citrate: 0.5 mM ATZ: 0.1 mM pH 5.8.	- GOx in solution - Toxicological assay and by-products study.	[190]
11. 3, 4-Dimethylaniline (3, 4 DMA)	After 180 min, removal of 86.55%.	3, 4-DMA: 30 mg L^{-1} Green Rush: 1 mM in Fe(II) and 1 mM in Fe(III) Glucose: 5 mM pH 7 Kaolin@GOx: 2.5 U mL^{-1}.	- GOx immobilized on Kaolin (Kaolin@GOx) - Organic green rust as a source of iron.	[183]

2.2.2. Bi-Enzymatic Processes for Water Treatment

Enzymatic Cycles Activated by H_2O_2

Many enzymes require H_2O_2 to carry out their catalytic activity. Among them, peroxidases are the most studied for environmental applications.

Peroxidases are able to bind H_2O_2 to their Fe-heme prosthetic group. In the resting state, the Fe(III) is coordinated by four nitrogen atoms belonging to heme pyrrolic groups and one N atom of the side chain of an amino acid. As shown in Figure 7, the fifth ligand can be the nitrogen of the distal histidine or the sulfur of a cysteine residue. The sixth coordination position is usually free or occupied by a water molecule [202], which is easily substituted by an H_2O_2 molecule. In a typical peroxidase active site, the distal side of the heme is characterized by the presence of one histidine and one arginine residues, which stabilize the coordination with the H_2O_2 molecule and favor the subsequent steps of the catalytic cycle [203,204].

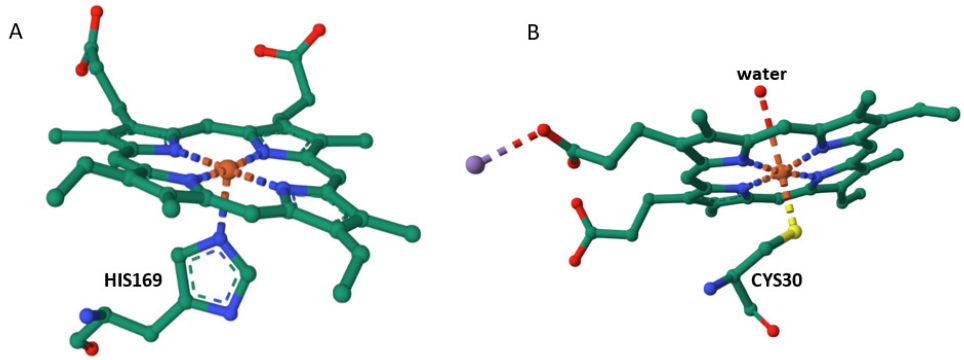

Figure 7. 3D structure of Fe-heme site in (**A**) soybean peroxidase; (**B**) chloroperoxidase. Images built by data from Protein Data Bank. Color legend: orange = iron; blue = nitrogen; red = oxygen; green = carbon, yellow = sulfur; violet = manganese.

In the presence of organic or inorganic substrates, H_2O_2 oxidizes the Fe(III) to a ferryl (Fe(IV)=O) radical, which can be reduced by inducing two steps of one-electron oxidation of a wide variety of compounds with the production of two molecules of organic or inorganic radicals and water (Figure 8A) [205].

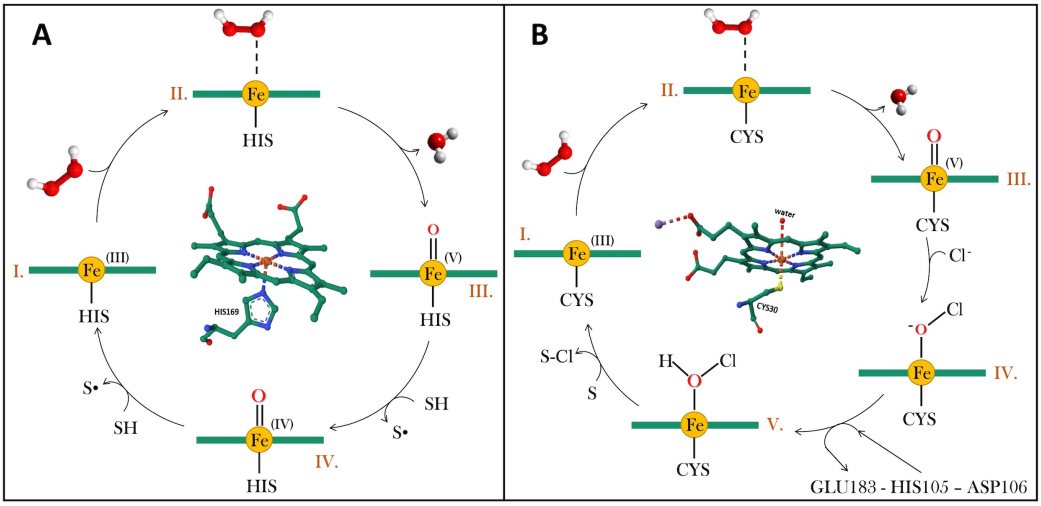

Figure 8. Summary of catalytic cycles. (**A**) Horseradish peroxidase (HIS = histidine, SH = substrate; S• = radical product); (**B**) Chloroperoxidase (CYS = cysteine, GLU = glutamic acid, HIS = histidine, ASP = aspartic acid, S = substrate, S-Cl = chlorinated product).

A quite different mechanism was reported for the heme-thiolate peroxidases, such as chloroperoxidase (CPOs) and aromatic-peroxygenase (APOs).

CPO from *Caldariomyces fumago* fungi was the first discovered halogenating enzyme [206,207]. In addition to substrate halogenation, it also exhibits peroxidase, catalase, and cytochrome P450-like activities [208]. The catalytic cycle leads to halide (chloride, bromide, and iodide, but not fluoride) oxidation, but this is not fully understood.

Wagenknecht and Woggon [209] proposed the mechanism reported in Figure 8B, in which the ferryl cation radical reacts with halides, reducing to Fe(III) and forming a complex capable of catalyzing the chlorination of the substrate. The Fe(V)=O reduction is favored by the three amino acid residues (GLU183, HIS105 and ASP106) that directly take part in its protonation. In the absence of halides, this enzyme could act as a normal peroxidase and follow the scheme in Figure 8A.

APOs are peroxygenases, enzymes able to transfer oxygen from peroxides to organic substrates (aliphatic, aromatic and heterocyclic) [210]. For these reasons, they are very useful for organic functionalization and synthesis reactions.

Dye-decolorizing peroxidases (DyPs) are probably the most recent heme-containing enzyme family discovered. Indeed, they were isolated in 1999 from the basidiomycetous fungus *Bjerkandera adusta* Dec 1 strain [211]. DyPs are so called due to their capability to oxidize synthetic high-redox potential anthraquinone-type dyes [212], but they can also react with other substrates like β-carotene and aromatic sulfides [213]. This different catalytic activity is probably related to some differences in the active site, which contains an aspartate residue in place of the histidine on the distal side [213], and a different arrangement of the secondary structure with the presence of β-sheets. Recent studies on the catalytic cycle suggest an electron transfer from the active site to the enzyme's surface occurs, allowing for the oxidation of large molecules that cannot physically enter the active site and favoring the relatively low specificity of these enzymes. This long electron transfer pathway seems to involve tryptophan and tyrosine residues that can form stable radicals and directly participate in the transfer [214].

Glucose Oxidase Coupling with Peroxidases

There is extensive research about the employment of free enzymes, such as peroxidases, for environmental applications [215], but in the last few decades, articles relating to immobilized enzymes have become increasingly widespread. As reported by Rigoletto et al. [216], different inorganic supports have been developed not only to improve enzymes' stability but also to produce in situ H_2O_2 to initiate the catalytic cycle [217–219].

It is well known that peroxidases could be inactivated by high concentrations of hydrogen peroxide [220–222]; therefore, a controlled in situ H_2O_2 production could be useful to avoid these drawbacks and maintain a stable enzymatic activity.

The possibility of exploiting the enzymatic generation of hydrogen peroxide coupling a peroxidase with GOx in a self-sustaining bi-enzymatic system has become widely studied, mainly for bio-sensing [223,224], but also more recently for environmental application. Although, in some studies, GOx is added to the solution as a homogeneous reagent together with glucose [225], the most widespread trend is to immobilize GOx on a solid support or to co-immobilize it with peroxidase in order to guarantee its reuse.

Co-immobilization of enzymes could enhance the system performances due to a reduction in mass transfer between peroxidase and H_2O_2. Furthermore, the formation of gluconic acid induced by GOx in the peroxidase microenvironment helps to reach a favorable pH value for peroxidase, thereby accelerating the reaction and enhancing the catalytic cycle. The resulting consumption of H_2O_2 prevents its accumulation on GOx, avoiding its inactivation [226,227]. This synergy ensures improved system performances, as reported by Gao and co-workers, who observed a higher Orange G decolorization with GOx and CPO co-immobilized on magnetic graphene oxide (MGO) with respect to those obtained employing GOx and CPO immobilized individually [228]. The co-immobilization on magnetic material also permitted an easy recovery of the support and the reusability of the system. Indeed, the authors reported that GOx-CPO-MGO could be employed for six cycles of water treatment with more than 38% residual activity retained after the last cycle.

Enhanced performances of co-immobilized enzymes have also been reported by Gu and co-workers [229]. The authors employed dopamine and modified cellulose–chitosan composite beads for a covalent loading of Horseradish peroxidase (HRP) and GOx and tested them to degrade acridine in wastewater, obtaining an almost complete removal. However, the removal efficiency was reduced from 99.0% to 61.2% after six reaction cycles; the decrease was tentatively ascribed to the mediator attack on the amino acid groups on the surface of the bi-enzyme system or to the loss of enzymes during application and washing.

Studies on reusability and stability for long storage periods are fundamental to estimating the real applicability of the bi-enzymatic systems in industrial applications. Actually, the literature confirms the possibility of adopting this strategy for the treatment of a large number of contaminants, from dyes [230,231] to other organic contaminants such as ferulic and caffeic acids [232], Bisphenol A [226], and endocrine disruptors [233].

3. Detection Methods for H_2O_2

In this work, different strategies for in situ hydrogen peroxide production have been identified. Important tools for the optimization of these reactions are represented by H_2O_2 detection and quantification methods.

According to most of the studies cited in this review, the commonest strategies employed in the environmental field are colorimetric assays. They are widely used because of their simple setup and easy spectrophotometric detection. They are usually based on chemical reactions involving hydrogen peroxide as a reagent with the formation of colored products. A summary of the literature concerning these methods is shown in Table 3.

Some colorimetric assays date back to the 1980s, but they are still employed, such as the I^{3-} assay, in which the H_2O_2 concentration is determined following the changes in absorption at 352 nm wavelength [57,133,184,234,235], or the reaction between 4-aminoantipyrine and phenol in the presence of peroxidase where the maximum absorption at 505 nm of the red product is monitored [234,236,237]. Another method is the vanadate one, based on the measure of 450 nm [238–240]. Moreover, some colorimetric assays are commercialized as a kit, like the Amplex^{TM} red hydrogen peroxide/peroxidase assay kit [241] (Thermofisher, Waltham, MA, USA) and the PAKTEST [242] (Kiouritsu Chemical Check Lab., Yokohama, Japan). However, not all colorimetric methods are exploitable for monitoring hydrogen peroxide production during AOP treatments. For example, permanganate titration cannot be used since Fe^{2+} ions react with permanganate, affecting H_2O_2 detection [240].

Recently, enzyme-mimetic materials have been developed for luminescent sensing of H_2O_2 in bioassays. They show a very low limit of detection (LOD) and are based on fluorescence [243,244].

Another important class of hydrogen peroxide detection methods is represented by electrochemical sensors in which H_2O_2 can be oxidized or reduced on the electrodes' surface. They show higher sensitivity and selectivity, cost-effectiveness, relatively shorter response time, and miniaturization capabilities. The research in this field is focused on overcoming drawbacks such as overpotentials and low kinetics by modifying the electrode surfaces with different materials, including dyes, redox proteins, metal oxides, and redox polymers, among others [245]. Recently, the interest in nanomaterials has grown and there is no shortage of combinations with the materials listed above that can improve H_2O_2 electrocatalytic sensing.

As seen in the previous paragraphs, a wide range of heme-containing proteins exists in nature that can use H_2O_2 in their catalytic cycles (peroxidases, cytochrome-c, hemoglobin, myoglobin, hemin, etc.), and, for this reason, they are also exploitable in H_2O_2 detection. Different studies suggest that HRP-based electrodes show good affinity with H_2O_2 and noticeable performances [246,247]. In order to ensure an optimized electron transfer, these proteins are often immobilized on highly conductive materials, both organic and inorganic, with a large surface area [248]. Interesting examples of these materials that also find application in the bio-medical sector are gold nanoparticles [249–251], nanometric metal oxides [252,253], metal nanoparticle–MOF [254–257], carbon nanotube–MOF [258] and metal nanoparticle–polymers [259,260].

Despite their efficiency, redox proteins could degrade over time and in harsh environmental conditions. To overcome these drawbacks, the development of inorganic materials with enzyme-mimetic activity is becoming more and more attractive. Most of these inorganic materials are mono- and bi-metals nanoparticles (AuNPs, Ag-NPs, Pt-NPs, Ag-AuNPs, Ni-CoNPs, etc.) or transition metals oxides and, often, to avoid aggregation on the electrode surface, they have been dispersed in polymeric matrices or introduced in MOFs. A broad description of these electrodes can be found in the comprehensive review carried out by Duanghathaipornsuk and co-workers [248].

Among electrochemical sensors with peroxidase-like activity, those based on Prussian Blue (PB) and its Analogues (PBAs) are largely used. They are metals hexacyanoferrate and can catalyze the reduction of H_2O_2 at low potentials. There is a wide variety of PBAs containing one or two transition metals that occupy the outer coordination sphere and that

define the selectivity for the detection of different analytes, both organic and inorganic [261]. PBAs employed for H_2O_2 detection usually contain iron coupled with another transition metal like Ni [262,263], Co [264,265] or Mn [264,266].

With the enhancement of nanotechnologies, researchers developed PB nanoparticles [267] to improve pH stability and sensitivity. Zang and co-workers studied the influence of nanoparticle size on electrocatalytic performance, finding that the sensitivity drops exponentially with increasing particle dimensions [268]. These nanozyme-based electrodes could also be affected by PB degradation during the electrochemical H_2O_2 reduction due to the solubilization of ferric hexacyanoferrate induced by the formation of reactive species [269]. Since this could limit the real use of the sensor, stabilization strategies, such as nanoparticles' coverage or dispersion in different polymers, have been designed. For example, Unzuncar et al. [270] developed a two-layer interface based on carboxymethyl cellulose and poly(3,4-ethylene dioxythiophene) with high stability and sensing behavior, not affected by interfering molecules present in tap water. More detailed syntheses of PB and PBA for electrochemical sensing can be found in some recent reviews [261,271].

Finally, many other enzyme-free electrochemical-based sensors for H_2O_2 are based on a wide range of materials, i.e., metal–organic frameworks [272], carbon nanocomposites [273], graphene oxide [274], and MXenes [275].

It must also be mentioned that some methods employing liquid-chromatographic analysis for the detection and quantification of hydrogen peroxide concentration in solution were developed. Some of them are based on the deprotonation of H_2O_2 to HO_2^-, which occurs when the pH of the eluent is higher than the acid-dissociation coefficient of H_2O_2 (pKa = 11.6). The revelation via a UV-detector can be carried out after separation in an ionic chromatography column with a LOD of 0.027 mg L^{-1} [276]. Other studies proposed the use of acidified potassium iodide solution as a mobile phase and the replacement of the reverse phase column with a series of capillary columns. Tantawi et al. [277] found a LOD of 8.29×10^{-4} mM employing this detection strategy. The authors reported that the method also shows high robustness by maintaining a high regression coefficient and excellent sensitivity in real matrices.

Since H_2O_2-mediated processes lead to the formation of ROS, their quantification is also extremely important for monitoring the depuration stages. Although it is not within the scope of this review, we can cite Electron Paramagnetic Resonance (EPR) and scavenging techniques as the main strategies for ROS identification. Specific papers have been devoted to summarizing the state-of-the-art on these topics [278,279].

Table 3. Spectrophotometric methods for H_2O_2 detection and quantification (acronyms not explicated elsewhere: NADPH = reduced Nicotinamide Adenine Dinucleotide Phosphate; TMB = 3,3′,5,5′-tetramethylbenzidine; ABTS = 2,2′-Azino-bis(3-ethylbenzothiazoline-6-sulfonic acid).

System	Wavelength	Conditions	Ref
1. Phenolphthalein method	552 nm	- 0.24 mL of phenolphthalein stock solution: 0.02 g mL^{-1} Phenolphthalein solution containing 10 g of NaOH, 5 g of zinc - $CuSO_4$ solution: 0.48 mL, 0.01 M - 100 mL of water.	[234]
2. Iodide method	352 nm	- 2 mL of solution A (66 g L^{-1} KI; 0.2 g L^{-1} of $(NH_4)_6Mo_7O_{24}$; 2 g L^{-1} of NaOH) - 2 mL of solution B (20 g L^{-1} of potassium hydrogen phthalate) - 6 mL of Peroxide samples.	[57,133,234,235]

Table 3. *Cont.*

System	Wavelength	Conditions	Ref
3. Oxidation of NADPH	340 nm	- Phosphate buffer: 0.04 M, pH 7.75 - EDTA: 4×10^{-4} M - Sodium azide: 4.2×10^{-3} M - Glutathione peroxidase: 8×10^{-8} M - Reduced glutathione: 3×10^{-3} M - NADPH: 5.6×10^{-5} M - Glutathione reductase: 1 U -Peroxide sample.	[234]
4. DMAB/MBTH/HRP	590 nm	- 3-(dimethylamino)benzoic acid (DMAB): 5×10^{-4} M - 3-methyl-2-benzothiazolinonehydrazone (MBTH): 2×10^{-5} M - Acetate buffer: 0.1 M, pH 5.5 -HRP.	[280]
5. 4-aminoantypirine/phenol/HRP	505 nm	- 4 mL of 4-aminoantipyrine/phenol reagent (2.34 g L^{-1} of phenol, 1g L^{-1} of 4-aminoantipyrine, 0.001 M phosphate buffer pH 6.9, 2.5 µM HRP) - 6 mL of peroxide sample.	[234,236,237]
6. Nanoparticles decorated $Ce_2(WO_4)_3$ nanosheets (CWNSs)	652 nm	- TMB: 100 µL 8 mM - CWNSs: 70 µL, 1000 µg mL^{-1} - Phosphate buffer: 400 µL, 50 mM pH 4 - MilliQ water: 330 µL - H_2O_2: 100 µL - LOD: 0.15 µM.	[281]
7. Ammonium metavanadate	450 nm	- Metavanadate 6.2 mM - Sulfuric acid 0.058 M - LOD: 143 µM.	[238–240]
8. Fe_3O_4 magnetic nanoparticles (MNPs) with peroxidase mimetics	545 nm	- ABTS: 24 µL, 60 mM - Fe_3O_4 MNPs: 10 µL, 3.74 mg mL^{-1} - Acetate buffer: pH 4185 µL - H_2O_2: 24 µL - Incubation 45 °C for 10 min and then diluted with 900 µL of water (after MNPs removal) and analyzed.	[282]
9. Peroxidase-mimicking metal−organic framework containing catalytic Cu^{2+} and luminescent Tb^{3+}: PA-Tb-Cu MOF (PA = m-phthalic acid)	545 nm Fluorescence (310 nm exciting wavelength)	- Acetate buffer: 960 µL, 10 mM, pH 5.05 - 20 µL of PA-Tb-Cu - MOF suspension: 11.73 mg mL^{-1} - Ascorbic acid: 10 µL, 200 mM - H_2O_2 sample + water up to a final volume of 1 mL - Measure after 20 min incubation - LOD: 0.2 µM.	[244]
10. CeO_2 nanoparticles doped with Eu^{3+}	590 nm Fluorescence (330 nm exciting wavelength)	- Samples prepared in potassium phosphate buffer (KPi) or Phosphate Buffered Saline (PBS) or 10% Farmigene Stain Buffer (FBS) - 125 g L^{-1} of nanoparticles - Measure after 30 min of incubation - LOD: 150 nM.	[243]

Table 3. *Cont.*

System	Wavelength	Conditions	Ref
11. Cobalt/bicarbonate system	260 nm	- Sodium oxalate: 25 µL,16.34 mM - Cobalt chloride: 25 µL, 67.8 mM - 2 mL of sample Finally, the reaction volume is made up to 2.5 mL with 270 µL of saturated sodium bicarbonate solution.	[185,201,283,284]
12. Titanium oxalate	385 nm	- 10 mL of peroxide sample - 1 mL of 1 M sulfuric acid - 1 mL of 50 g L^{-1} potassium titanium oxalate solution - 13 mL of water - Measure after 5 min of incubation - LOD: 29 µM.	[77,125,285]
13. *N*,*N*-diethyl-p-phenylenediamine (DPD)	551 nm	- DPD reagent (27 mL water, 3 mL phosphate buffer, 6 µL methanol, 50 µL of 10 g L^{-1} of DPD solution prepared in sulfuric acid 0.5 M, 50 µL HRP 1g L^{-1}) - LOD: 0.77 µM.	[64,285,286]
14. p-hydroxyphenyl acetic acid (POHPAA)	406–410 nm Fluorescence (315 nm exciting wavelength)	- POHPAA reagent (POHPAA 270 mg L^{-1}, HRP 30 mg L^{-1}, NaOH 1 M, potassium hydrogen phthalate 8.2 g L^{-1} pH 5.8) - LOD: 0.16 µM.	[285,287,288]

4. Criticalities and Perspectives

The processes based on H_2O_2 reactivity for environmental remediation have been investigated in depth in terms of general lab-scale degrading performances, as revealed from the significant number of research documents reported in this review. However, for applicability in real-scale conditions, other aspects have to be taken into account, whose schematic representation is depicted in Figure 9.

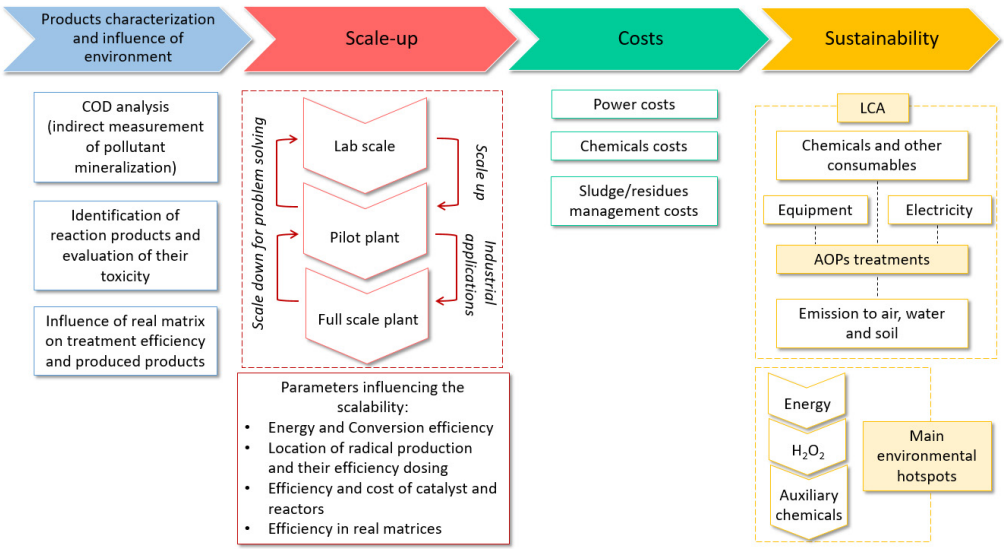

Figure 9. Aspects to be deepened in H_2O_2-mediated processes for real applications.

4.1. Product Characterization, Toxicity and Influence of Environmental Factors

The first point concerns the properties' study of the products formed during the depuration procedure and their impact on the environment. The optimum should be to

reach the complete mineralization of the pollutants into water and carbon dioxide, but this is not straightforward, not only because the degradation efficiency can be lower than 100%, but also because some treatments, such as those based on enzymes, occur through radical reactions, which do not lead to the mineralization of the contaminants.

Therefore, toxic intermediates and by-products can be produced [289,290]. In this sense, Hofman-Caris et al. [291] found that UV/hydrogen peroxide processes in drinking water treatment may generate mutagenic by-products in particular conditions, mainly influenced by parameters such as nitrate concentration (that can be subjected to photolysis), the presence of natural organic matter, the UV spectrum of the lamps, and the UV dose applied. The role of UV light has also been described in [292]. The comparison among the toxicity levels of H_2O_2/UV, photo-Fenton and heterogeneous photocatalysis (TiO_2/H_2O_2/UV) processes for the treatment of strongly polluted colored wastewater was analyzed as well [293,294]. The use of the system with titania resulted in the most effective method to remove toxins, organic material, and color.

It is, therefore, necessary not only to identify the formed by-products [187,188], but also to evaluate the toxicity of the resulting solution [190] and estimate COD values as an indirect measurement of pollutant mineralization [189,295]. In this regard, Liu et al. compared the COD values after the classic Fenton treatment and Bio-Fenton pre-treatment, followed by active sludge treatment of real wastewater spiked with chlorophenol [197]. The authors found that the resulting COD after the combined treatment was two times lower than that obtained with classic Fenton only, suggesting that the combination of different approaches improves the biodegradability of the selected contaminant.

Regarding biological contaminants, urban wastewater treatment plants are among the main hotspots of antibiotic resistance spread into the environment. It was found that UV/H_2O_2 processes may not be effective in minimizing the antibiotic resistance spread potential into the environment since the death of bacterial cells, which results in DNA release into treated water, may pose a risk for antibiotic resistance transfer to other bacteria present in the receiving water body [296].

Moreover, the control of the hydrogen peroxide quantity used as the oxidant is important since it was found that toxicity increases by increasing H_2O_2 addition, causing not only its undesirable excess in the effluent, but, in the absence of effective separation from the heterogeneous active phase, also catalyst poisoning [38,293].

In general, applying remediation strategies to real conditions means considering the influence of all the environmental factors that are intrinsic to the complexity of real systems, such as the co-presence of ions and organic matter in water matrices that can compete with the target chemical pollutants [201,297,298].

Indeed, wastewater or natural water contains inorganic ions (Ca^{2+}, Mg^{2+}, Cl^-, $H_2PO_4^-$, etc.) and dissolved organic matter that can influence the efficiency of the treatments. For instance, the reduction of trichloroethene removal by Bio-Fenton treatment in the presence of Cu^{2+} was demonstrated [196], as well as the inhibition of the GOx activity due to the reaction with H_2O_2, which resulted in a reduced production of hydroxyl radical [299]. A similar effect was also observed for Mg^{2+}, which is known to hinder the Fenton reaction [300]. Anions, such as $H_2PO_4^-$, Cl^- and SO_4^{2-}, can form complexes with iron ions, reducing their availability for the Fenton reaction [196]. Dissolved organic matter (DOM) in natural water, similarly, can act as a radical scavenger, limiting the number of reactive species available for substrate oxidation and leading to a decrement in pollutant degradation [301]. This kind of competition was also observed by Ravi et al., who reported a reduction in trichloroethylene degradation by the Bio-Fenton reaction carried out with free GOx in groundwater [201].

Also, in the case of pathogen contamination, this control is fundamental. Malvestiti et al. [302] verified the efficiency of O_3, O_3/H_2O_2 and UV/H_2O_2 treatments to disinfect municipal effluents and the influence of carbonate, nitrate and industrial contaminants. The results showed that all AOP treatments were affected by the presence of nitrate and, particularly, carbonate. These ions

reduced the inactivation of total coliforms and *Escherichia coli*. Ozone disinfection was the most affected method by scavenging compounds.

Additionally, the selectivity of the decontamination process towards specific pollutants is, in general, another rising theme in environmental research to ensure a higher low-cost/effectiveness ratio and lower secondary pollution [303].

4.2. Processes' Scalability, Cost Analysis and Environmental Impact

Real applications presuppose the scalability of the processes moving from laboratory scale to pilot plants and full-scale plants. At the basis of the scalability process, there are several critical points that have to be considered, such as oxidant conversion efficiency, location of radical production and delivery (i.e., in situ generation or need for a transport step) [304], and the study of kinetic parameters and degradation pathways [305]. All of these have to be initially optimized through the development of proper catalysts with high stability and activity; for instance, in the case of electrodes, they have to be characterized by high activity and corrosion resistance, long working life span and limited synthesis costs [305].

At the same time, the geometry and configuration of the reactors (e.g., batch mode vs. continuous-flow systems), integration with different depuration systems (like biological treatments), and operational costs have to be considered [304,306–308].

Obviously, each strategy shows intrinsic strengths and critical aspects that can limit its development on a large scale. For instance, the high operational costs of lamps, together with the difficult design of photoreactors and lower performances at neutral pH, are challenges for photo-Fenton full-scale applications [45], whereas the difficulty in distributing the formation of cavities in the reactor could be the limiting factor of sono-Fenton scale-up [309]. More complete considerations on AOP scalability have been discussed in [289,304], which also reported lists of pilot plants and full-scale plants of these wastewater remediation approaches.

It is clear that the overall evaluation of the feasibility of depuration procedures must involve the techno-economic aspects together with the environmental impact [101,310].

One widespread factor in evaluating the AOP processes is the consideration of the demand for energy. An example of compared systems was reported by Maniakova et al. [298]; the authors claimed that a solar-driven process catalyzed by N-doped TiO_2 was not yet competitive with the system of Fe^{2+}/H_2O_2/ethylenediamine-*N*,*N*′-disuccinic acid (EDDS, chelating agent) under sunlight in the removal of CECs from secondary treated urban wastewater because higher irradiation times were necessary, which would result in a larger surface area for solar reactors.

From an economic point of view, the criterion of Electric Energy per Order (EEO), which takes into account the electric power, the removal efficiency and the flow rate [311], could be used to compare the cost of different AOP strategies [311,312], but it does not consider other operating costs.

To have a more comprehensive overview of total process expense, several authors proposed to evaluate the sum of the single source of cost: (i) power, (ii) chemicals, and (iii) sludge/waste management (including transportation and disposal) [313,314].

A new criterion to compare AOPs has been proposed, namely the Accumulated Oxygen-equivalent Chemical-oxidation Dose (AOCD), which comprises the accumulation of the oxidant dose normalized to the treatment time. AOCD also takes into account other important parameters such as current density, irradiance, wavelength, active surface area and lamp, distance of the lamp, faradaic and quantum yields, number of electrons exchanged, residence time, etc., depending on the AOP technique considered. The development of tools for AOP comparison is fundamental to help legislators determine and choose the best available techniques for water reuse as defined by the Industrial Emissions European Union Directive 2010/75/EU [315].

Regarding the evaluation of the processes' environmental impacts, the life cycle assessment (LCA) methodology is a valuable and widespread support tool [316]. What

emerges from most of the LCA outputs is that the main environmental hotspots of AOP strategies are, in order of relevance, the energy supply, the H_2O_2 employment, and, finally, the auxiliary chemicals.

Since energy is recognized as the main impacting factor, an appropriate choice of energy source is fundamental. For instance, García-Montaño et al. [317] compared different photo-Fenton strategies and noticed that the use of solar irradiation decreased the environmental impacts between 8.3 and 57.3%. Similar results have been reported by Ttofa et al. [318], who found that using solar energy to also power auxiliary equipment, such as pumps, lessened the calculated environmental impacts by up to 83%.

It can, therefore, be stated that investment in renewable energy could be effective in decreasing the environmental repercussions of AOPs.

In studies that report a lower energy imprint, the contribution of chemicals to the environmental impact grows, with a particular influence brought about by the use of hydrogen peroxide and auxiliary chemicals (i.e., NaOH necessary to reach a proper water pH after the treatment), or because of the substances released during the process [316].

From the materials' and chemicals' point of view, Costamagna et al. [319] investigated the photo-Fenton processes through LCA methodology. The photo-Fenton reaction carried out at circumneutral conditions, using the already mentioned soluble bio-organic substances (BBS) as auxiliary agents, was compared with the traditional photo-Fenton run at pH 2.8. The evaluation was carried out both at the laboratory level and at the pilot plant scale. Working in mild conditions reduced the environmental burden associated with the use of chemicals, but the decrement in effectiveness significantly increased the overall impact of the system.

In the case of heterogeneous catalysis, the focus is primarily on the sustainability of the materials, from their synthesis, possibly using greener strategies, to performances and recyclability [101,320,321]. Some studies highlight that the choice of heterogeneous Fenton can significantly reduce the environmental impact of the water treatments owing to the reuse of the catalyst. On the other hand, a higher amount of H_2O_2 seems to be required to degrade the same amount of pollutant, making the research of the least impactful compromise necessary [322].

4.3. Final Considerations

As emerges from the discussion of the recent literature, the panorama of AOP techniques is very diversified and effective for the remediation of different contaminated aqueous matrices. An example of the evolution of depuration systems over time is represented by Fenton-like processes, which can overcome the main issues of classical Fenton reactions, such as the addition of hydrogen peroxide, careful pH regulation in a narrow acid pH range and formation of sludge, although other drawbacks are still required to be solved. The regulation of the amount and type of energy involved, the low on-site production efficiency of hydrogen peroxide, the design of reactors (not only in terms of operation modes, but also chemical stability) and operational costs have to be optimized [16,27,45,323–326]. Issues related to the best compromise among efficiency, energy and chemical demand, operating and monitoring aspects together with the economic convenience must similarly be adjusted in processes based on photo-, electro-catalysis, etc.

It is, therefore, difficult to establish an absolute ranking of all the different techniques since there are a multitude of facets that should be taken into consideration. However, it is possible to summarize the main aspects emerging from the comparative reading of the literature as follows:

- The use of AOPs in mild pH conditions can reduce additional process costs related to the salinity increase, as it is induced in classic Fenton treatment by acidification and further neutralization [315];
- In situ hydrogen peroxide production avoids high costs and hazards associated with its transport, handling, and storage;

- Homogeneous processes such as ozonization have been investigated and already applied in the full-scale treatment of urban wastewater effluents [327];
- Heterogeneous catalysis shows several advantages with respect to homogeneous processes, such as the recyclability of the catalyst, which can contribute both to cost reduction and limitation of the environmental impact. However, this strategy does not seem completely ready for full-scale application due to catalyst preparation costs, effectiveness, stability, and reactor configurations [328];
- The main hotspot of the environmental impact is energy and, consequently, an appropriate choice of energy source can significantly reduce the total impact of the process; thus, investment in renewable energies should be preferred;
- Since wastewaters are characterized by a complex composition, their contamination cannot be solved by employing a single remediation technique. Effective hybrid systems combining AOP techniques and/or biological treatments are reported in the literature [315];
- AOP strategies have been reported among the best available technologies in a recent review about wastewater reuse in European countries [315];
- Limited scale-up and techno-economic analysis are available for Bio-Fenton treatments. Enzyme cost and stability could represent critical points for its real applications; however, some studies suggest that GOx production could be cost-effective and scalable [185]. Moreover, as widely described above, the immobilization of glucose oxidase improves its stability towards oxidation and deactivation due to environmental factors and ensures its reusability, making Bio-Fenton suitable for actual wastewater treatment;
- Although, to the best of the authors' knowledge, there are no reported pilot or full-scale plants that integrate Bio-Fenton in wastewater treatments, its effectiveness as a pretreatment to be coupled with conventional active sludge was highlighted by Wang et al. [189].

Author Contributions: Conceptualization, M.R., E.L. and M.L.T.; writing—original draft preparation, M.R. and M.L.T.; writing—review and editing, M.R., E.L. and M.L.T. All authors have read and agreed to the published version of the manuscript.

Funding: This research received no external funding.

Data Availability Statement: No new data were created or analyzed in this study. Data sharing is not applicable to this article.

Acknowledgments: This work was supported by Project CH4.0 under the MUR program "Dipartimenti di Eccellenza 2023–2027" (CUP: D13C22003520001).

Conflicts of Interest: The authors declare no conflicts of interest.

References

1. Hossain, M.F. Water. In *Sustainable Design and Build*; Butterworth-Heinemann: Oxford, UK, 2019; pp. 301–418. ISBN 9780128167229.
2. Velasco-Muñoz, J.; Aznar-Sánchez, J.; Belmonte-Ureña, L.; Román-Sánchez, I. Sustainable Water Use in Agriculture: A Review of Worldwide Research. *Sustainability* **2018**, *10*, 1084. [CrossRef]
3. Kokkinos, P.; Venieri, D.; Mantzavinos, D. Advanced Oxidation Processes for Water and Wastewater Viral Disinfection. A Systematic Review. *Food Environ. Virol.* **2021**, *13*, 283–302. [CrossRef]
4. Testa, M.L.; Tummino, M.L. Lignocellulose Biomass as a Multifunctional Tool for Sustainable Catalysis and Chemicals: An Overview. *Catalysts* **2021**, *11*, 125. [CrossRef]
5. Abou-Shady, A.; Siddique, M.S.; Yu, W. A Critical Review of Recent Progress in Global Water Reuse during 2019–2021 and Perspectives to Overcome Future Water Crisis. *Environments* **2023**, *10*, 159. [CrossRef]
6. Roy, A.; Sharma, A.; Yadav, S.; Jule, L.T.; Krishnaraj, R. Nanomaterials for Remediation of Environmental Pollutants. *Bioinorg. Chem. Appl.* **2021**, *2021*, 1764647. [CrossRef]
7. Lama, G.; Meijide, J.; Sanromán, A.; Pazos, M. Heterogeneous Advanced Oxidation Processes: Current Approaches for Wastewater Treatment. *Catalysts* **2022**, *12*, 344. [CrossRef]
8. Deng, Y.; Zhao, R. Advanced Oxidation Processes (AOPs) in Wastewater Treatment. *Curr. Pollut. Rep.* **2015**, *1*, 167–176. [CrossRef]

9. Arifin, M.N.; Jusoh, R.; Abdullah, H.; Ainirazali, N.; Setiabudi, H.D. Recent Advances in Advanced Oxidation Processes (AOPs) for the Treatment of Nitro- and Alkyl-Phenolic Compounds. *Environ. Res.* **2023**, *229*, 115936. [CrossRef]
10. Kumari, P.; Kumar, A. ADVANCED OXIDATION PROCESS: A Remediation Technique for Organic and Non-Biodegradable Pollutant. *Results Surf. Interfaces* **2023**, *11*, 100122. [CrossRef]
11. Garcia-Costa, A.L.; Casas, J.A. Intensification Strategies for Thermal H_2O_2-Based Advanced Oxidation Processes: Current Trends and Future Perspectives. *Chem. Eng. J. Adv.* **2022**, *9*, 100228. [CrossRef]
12. Wang, Y.; Lin, Y.; He, S.; Wu, S.; Yang, C. Singlet Oxygen: Properties, Generation, Detection, and Environmental Applications. *J. Hazard. Mater.* **2024**, *461*, 132538. [CrossRef] [PubMed]
13. Ikhlaq, A.; Brown, D.R.; Kasprzyk-Hordern, B. Mechanisms of Catalytic Ozonation: An Investigation into Superoxide Ion Radical and Hydrogen Peroxide Formation during Catalytic Ozonation on Alumina and Zeolites in Water. *Appl. Catal. B Environ.* **2013**, *129*, 437–449. [CrossRef]
14. Li, W.; Zhang, M.; Wang, H.; Lian, J.; Qiang, Z. Removal of Recalcitrant Organics in Reverse Osmosis Concentrate from Coal Chemical Industry by UV/H_2O_2 and UV/PDS: Efficiency and Kinetic Modeling. *Chemosphere* **2022**, *287*, 131999. [CrossRef] [PubMed]
15. Pandis, P.K.; Kalogirou, C.; Kanellou, E.; Vaitsis, C.; Savvidou, M.G.; Sourkouni, G.; Zorpas, A.A.; Argirusis, C. Key Points of Advanced Oxidation Processes (AOPs) for Wastewater, Organic Pollutants and Pharmaceutical Waste Treatment: A Mini Review. *ChemEngineering* **2022**, *6*, 8. [CrossRef]
16. An, J.; Li, N.; Wu, Y.; Wang, S.; Liao, C.; Zhao, Q.; Zhou, L.; Li, T.; Wang, X.; Feng, Y. Revealing Decay Mechanisms of H_2O_2-Based Electrochemical Advanced Oxidation Processes after Long-Term Operation for Phenol Degradation. *Environ. Sci. Technol.* **2020**, *54*, 10916–10925. [CrossRef] [PubMed]
17. Wang, X.; Jing, J.; Zhou, M.; Dewil, R. Recent Advances in H_2O_2-Based Advanced Oxidation Processes for Removal of Antibiotics from Wastewater. *Chin. Chem. Lett.* **2023**, *34*, 107621. [CrossRef]
18. Tummino, M.L. $SrFeO_3$ Peculiarities and Exploitation in Decontamination Processes and Environmentally-Friendly Energy Applications. *Curr. Res. Green Sustain. Chem.* **2022**, *5*, 100339. [CrossRef]
19. Qu, C.; Liang, D.W. Novel Electrochemical Advanced Oxidation Processes with H_2O_2 Generation Cathode for Water Treatment: A Review. *J. Environ. Chem. Eng.* **2022**, *10*, 107896. [CrossRef]
20. Pi, L.; Cai, J.; Xiong, L.; Cui, J.; Hua, H.; Tang, D.; Mao, X. Generation of H2O2 by On-Site Activation of Molecular Dioxygen for Environmental Remediation Applications: A Review. *Chem. Eng. J.* **2020**, *389*, 123420. [CrossRef]
21. Wang, L.; Zhang, J.; Zhang, Y.; Yu, H.; Qu, Y.; Yu, J. Inorganic Metal-Oxide Photocatalyst for H_2O_2 Production. *Small* **2022**, *18*, 2104561. [CrossRef]
22. Mansour, M.S.; Farid, Y.; Nosier, S.A.; Adli, O.; Abdel-Aziz, M.H. Removal of Eosin Yellow Dye from Industrial Wastewater Using UV/H2O2 and Photoelectro-Fenton Techniques. *J. Photochem. Photobiol. A Chem.* **2023**, *436*, 114411. [CrossRef]
23. Wang, J.; Li, C.; Rauf, M.; Luo, H.; Sun, X.; Jiang, Y. Gas Diffusion Electrodes for H2O2 Production and Their Applications for Electrochemical Degradation of Organic Pollutants in Water: A Review. *Sci. Total Environ.* **2021**, *759*, 143459. [CrossRef]
24. Muruganandham, M.; Suri, R.P.S.; Jafari, S.; Sillanpää, M.; Lee, G.J.; Wu, J.J.; Swaminathan, M. Recent Developments in Homogeneous Advanced Oxidation Processes for Water and Wastewater Treatment. *Int. J. Photoenergy* **2014**, *2014*, 821674. [CrossRef]
25. Asghar, A.; Raman, A.A.A.; Daud, W.M.A.W. Advanced Oxidation Processes for In-Situ Production of Hydrogen Peroxide/Hydroxyl Radical for Textile Wastewater Treatment: A Review. *J. Clean. Prod.* **2015**, *87*, 826–838. [CrossRef]
26. Ji, J.; Wang, Z.; Xu, Q.; Zhu, Q.; Xing, M. In Situ H_2O_2 Generation and Corresponding Pollutant Removal Applications: A Review. *Chem.—A Eur. J.* **2023**, *29*, e202203921. [CrossRef]
27. Liu, Y.; Zhao, Y.; Wang, J. Fenton/Fenton-like Processes with in-Situ Production of Hydrogen Peroxide/Hydroxyl Radical for Degradation of Emerging Contaminants: Advances and Prospects. *J. Hazard. Mater.* **2021**, *404*, 124191. [CrossRef]
28. Popat, A.; Nidheesh, P.V.; Anantha Singh, T.S.; Suresh Kumar, M. Mixed Industrial Wastewater Treatment by Combined Electrochemical Advanced Oxidation and Biological Processes. *Chemosphere* **2019**, *237*, 124419. [CrossRef]
29. Rezaei, F.; Vione, D. Effect of PH on Zero Valent Iron Performance in Heterogeneous Fenton and Fenton-like Processes: A Review. *Molecules* **2018**, *23*, 3127. [CrossRef]
30. Kamali, M.; Aminabhavi, T.M.; Costa, M.E.V.; Ul Islam, S.; Appels, L.; Dewil, R. Heterogeneous Advanced Oxidation Processes (HE-AOPs) for the Removal of Pharmaceutically Active Compounds—Pros and Cons. In *Advanced Wastewater Treatment Technologies for the Removal of Pharmaceutically Active Compounds. Green Energy and Technology*; Springer: Cham, Switzerland, 2023; pp. 211–239.
31. Rodríguez-Chueca, J.; Carbajo, J.; García-Muñoz, P. Intensification of Photo-Assisted Advanced Oxidation Processes for Water Treatment: A Critical Review. *Catalysts* **2023**, *13*, 401. [CrossRef]
32. Mazumder, A.; Bhattacharya, S.; Bhattacharjee, C. Role of Nano-Photocatalysis in Heavy Metal Detoxification. In *Nanophotocatalysis and Environmental Applications*; Springer Nature Switzerland: Cham, Switzerland, 2020; pp. 1–33.
33. Tseng, D.H.; Juang, L.C.; Huang, H.H. Effect of Oxygen and Hydrogen Peroxide on the Photocatalytic Degradation of Monochlorobenzene in TiO2 Aqueous Suspension. *Int. J. Photoenergy* **2012**, *2012*, 328526. [CrossRef]
34. Huang, X.; Song, M.; Zhang, J.; Shen, T.; Luo, G.; Wang, D. Recent Advances of Electrocatalyst and Cell Design for Hydrogen Peroxide Production. *Nano-Micro Lett.* **2023**, *15*, 86. [CrossRef]

35. Kim, D.J.; Zhu, Q.; Rigby, K.; Wu, X.; Kim, J.H.; Kim, J.-H. A Protocol for Electrocatalyst Stability Evaluation: H_2O_2 Electrosynthesis for Industrial Wastewater Treatment. *Environ. Sci. Technol.* **2022**, *56*, 1365–1375. [CrossRef]
36. Zhou, W.; Meng, X.; Gao, J.; Alshawabkeh, A.N. Hydrogen Peroxide Generation from O2 Electroreduction for Environmental Remediation: A State-of-the-Art Review. *Chemosphere* **2019**, *225*, 588–607. [CrossRef]
37. Knowles, R.R. Reaching Your Full (Over)Potential: A Novel Approach to Electrocatalytic Oxygen Reduction. *ACS Cent. Sci.* **2015**, *1*, 224–225. [CrossRef]
38. Chen, Z.; Yao, D.; Chu, C.; Mao, S. Photocatalytic H2O2 Production Systems: Design Strategies and Environmental Applications. *Chem. Eng. J.* **2023**, *451*, 138489. [CrossRef]
39. An, J.; Feng, Y.; Zhao, Q.; Wang, X.; Liu, J.; Li, N. Electrosynthesis of H2O2 through a Two-Electron Oxygen Reduction Reaction by Carbon Based Catalysts: From Mechanism, Catalyst Design to Electrode Fabrication. *Environ. Sci. Ecotechnol.* **2022**, *11*, 100170. [CrossRef]
40. Qian, W.; Wu, Z.; Jia, Y.; Hong, Y.; Xu, X.; You, H.; Zheng, Y.; Xia, Y. Thermo-Electrochemical Coupling for Room Temperature Thermocatalysis in Pyroelectric ZnO Nanorods. *Electrochem. Commun.* **2017**, *81*, 124–127. [CrossRef]
41. Luo, H.; Zeng, Y.; He, D.; Pan, X. Application of Iron-Based Materials in Heterogeneous Advanced Oxidation Processes for Wastewater Treatment: A Review. *Chem. Eng. J.* **2021**, *407*, 127191. [CrossRef]
42. Litter, M.I.; Slodowicz, M. An Overview on Heterogeneous Fenton and PhotoFenton Reactions Using Zerovalent Iron Materials. *J. Adv. Oxid. Technol.* **2017**, *20*, 20160164. [CrossRef]
43. Clarizia, L.; Russo, D.; Di Somma, I.; Marotta, R.; Andreozzi, R. Homogeneous Photo-Fenton Processes at near Neutral PH: A Review. *Appl. Catal. B Environ.* **2017**, *209*, 358–371. [CrossRef]
44. Rodríguez-Narváez, O.M.; Pérez, L.S.; Yee, N.G.; Peralta-Hernández, J.M.; Bandala, E.R. Comparison between Fenton and Fenton-like Reactions for l-Proline Degradation. *Int. J. Environ. Sci. Technol.* **2019**, *16*, 1515–1526. [CrossRef]
45. Wang, N.; Zheng, T.; Zhang, G.; Wang, P. A Review on Fenton-like Processes for Organic Wastewater Treatment. *J. Environ. Chem. Eng.* **2016**, *4*, 762–787. [CrossRef]
46. Jiang, C.; Gao, Z.; Qu, H.; Li, J.; Wang, X.; Li, P.; Liu, H. A New Insight into Fenton and Fenton-like Processes for Water Treatment: Part II. Influence of Organic Compounds on Fe(III)/Fe(II) Interconversion and the Course of Reactions. *J. Hazard. Mater.* **2013**, *250–251*, 76–81. [CrossRef]
47. Lai, L.; He, Y.; Zhou, H.; Huang, B.; Yao, G.; Lai, B. Critical Review of Natural Iron-Based Minerals Used as Heterogeneous Catalysts in Peroxide Activation Processes: Characteristics, Applications and Mechanisms. *J. Hazard. Mater.* **2021**, *416*, 125809. [CrossRef]
48. Kahoush, M.; Behary, N.; Cayla, A.; Nierstrasz, V. Bio-Fenton and Bio-Electro-Fenton as Sustainable Methods for Degrading Organic Pollutants in Wastewater. *Process Biochem.* **2018**, *64*, 237–247. [CrossRef]
49. Ahuja, D.K.; Bachas, L.G.; Bhattacharyya, D. Modified Fenton Reaction for Trichlorophenol Dechlorination by Enzymatically Generated H_2O_2 and Gluconic Acid Chelate. *Chemosphere* **2007**, *66*, 2193–2200. [CrossRef]
50. Tummino, M.L.; Nisticò, R.; Franzoso, F.; Bianco Prevot, A.; Calza, P.; Laurenti, E.; Paganini, M.C.; Scalarone, D.; Magnacca, G. The "Lab4treat" Outreach Experience: Preparation of Sustainable Magnetic Nanomaterials for Remediation of Model Wastewater. *Molecules* **2021**, *26*, 3361. [CrossRef]
51. Zhang, W.; Jiang, X.; Ralston, J.; Cao, J.; Jin, X.; Sun, W.; Gao, Z. Efficient Heterogeneous Photodegradation of Eosin Y by Oxidized Pyrite Using the Photo-Fenton Process. *Miner. Eng.* **2023**, *191*, 107972. [CrossRef]
52. Guo, S.; Huang, R.; Yuan, J.; Chen, R.; Chen, F. Efficient Removal of Aromatic Pollutants via Catalytic Wet Peroxide Oxidation over Synthetic Anisotropic Ilmenite/Carbon Nanocomposites. *npj Clean Water* **2023**, *6*, 74. [CrossRef]
53. Thomas, N.; Dionysiou, D.D.; Pillai, S.C. Heterogeneous Fenton Catalysts: A Review of Recent Advances. *J. Hazard. Mater.* **2021**, *404*, 124082. [CrossRef]
54. Wang, J.; Farias, J.; Tiwary, A.; Tangyie, G.C.; Huddersman, K. Advance Oxidation Process (AOP) of Bisphenol A Using a Novel Surface-Functionalised Polyacrylonitrile (PAN) Fibre Catalyst. *Water* **2022**, *14*, 640. [CrossRef]
55. Liu, Y.; Liu, Y.; Yang, Z.; Wang, J. Fenton Degradation of 4-Chlorophenol Using H2O2: In Situ Generated by Zn-CNTs/O2 System. *RSC Adv.* **2017**, *7*, 49985–49994. [CrossRef]
56. Zhao, P.; Jin, B.; Zhang, Q.; Peng, R. Graphitic-C3N4 Quantum Dots Modified FeOOH for Photo-Fenton Degradation of Organic Pollutants. *Appl. Surf. Sci.* **2022**, *586*, 152792. [CrossRef]
57. Shi, W.; Sun, W.; Liu, Y.; Zhang, K.; Sun, H.; Lin, X.; Hong, Y.; Guo, F. A Self-Sufficient Photo-Fenton System with Coupling in-Situ Production H2O2 of Ultrathin Porous g-C3N4 Nanosheets and Amorphous FeOOH Quantum Dots. *J. Hazard. Mater.* **2022**, *436*, 129141. [CrossRef]
58. Wang, Y.; Song, H.; Chen, J.; Chai, S.; Shi, L.; Chen, C.; Wang, Y.; He, C. A Novel Solar Photo-Fenton System with Self-Synthesizing H2O2: Enhanced Photo-Induced Catalytic Performances and Mechanism Insights. *Appl. Surf. Sci.* **2020**, *512*, 145650. [CrossRef]
59. Calza, P.; Di Sarro, J.; Magnacca, G.; Bianco Prevot, A.; Laurenti, E. Use of Low-Cost Magnetic Materials Containing Waste Derivatives for the (Photo)-Fenton Removal of Organic Pollutants. *Materials* **2019**, *12*, 3942. [CrossRef]
60. Chavan, R.; Bhat, N.; Parit, S.; Narasimharao, K.; Devan, R.S.; Patil, R.B.; Karade, V.C.; Pawar, N.V.; Kim, J.H.; Jadhav, J.P.; et al. Development of Magnetically Recyclable Nanocatalyst for Enhanced Fenton and Photo-Fenton Degradation of MB and Cr(VI) Photo-Reduction. *Mater. Chem. Phys.* **2023**, *293*, 126964. [CrossRef]

61. Bousalah, D.; Zazoua, H.; Boudjemaa, A.; Benmounah, A.; Messaoud-Boureghda, M.Z.; Bachari, K. Enhanced Reactivity of the CuO-Fe_2O_3 Intimate Heterojunction for the Oxidation of Quinoline Yellow Dye (E104). *Environ. Sci. Pollut. Res.* **2022**, *29*, 69988–69999. [CrossRef]
62. Mirsadeghi, S.; Zandavar, H.; Rajabi, H.R.; Sajadiasl, F.; Ganjali, M.R.; Pourmortazavi, S.M. Superior Degradation of Organic Pollutants and H_2O_2 Generation Ability on Environmentally-Sound Constructed Fe_3O_4-Cu Nanocomposite. *J. Mater. Res. Technol.* **2021**, *14*, 808–821. [CrossRef]
63. Domenzain-Gonzalez, J.; Castro-Arellano, J.J.; Galicia-Luna, L.A.; Rodriguez-Cruz, M.; Hernandez-Lopez, R.T.; Lartundo-Rojas, L. Photocatalytic Membrane Reactor Based on Mexican Natural Zeolite: RB5 Dye Removal by Photo-Fenton Process. *J. Environ. Chem. Eng.* **2021**, *9*, 105281. [CrossRef]
64. Ju, Y.; Li, H.; Wang, Z.; Liu, H.; Huo, S.; Jiang, S.; Duan, S.; Yao, Y.; Lu, X.; Chen, F. Solar-Driven on-Site H_2O_2 Generation and Tandem Photo-Fenton Reaction on a Triphase Interface for Rapid Organic Pollutant Degradation. *Chem. Eng. J.* **2022**, *430*, 133168. [CrossRef]
65. Chen, Z.; Lian, C.; Huang, K.; Ji, J.; Yan, Q.; Zhang, J.; Xing, M. "Small Amount for Multiple Times" of H_2O_2 Feeding Way in MoS2-Fex Heterogeneous Fenton for Enhancing Sulfadiazine Degradation. *Chin. Chem. Lett.* **2022**, *33*, 1365–1372. [CrossRef]
66. Luo, H.; Cheng, Y.; Zeng, Y.; Luo, K.; Pan, X. Enhanced Decomposition of H2O2 by Molybdenum Disulfide in a Fenton-like Process for Abatement of Organic Micropollutants. *Sci. Total Environ.* **2020**, *732*, 139335. [CrossRef] [PubMed]
67. Kim, H.H.; Lee, H.; Lee, D.; Ko, Y.J.; Woo, H.; Lee, J.; Lee, C.; Pham, A.L.T. Activation of Hydrogen Peroxide by a Titanium Oxide-Supported Iron Catalyst: Evidence for Surface Fe(IV) and Its Selectivity. *Environ. Sci. Technol.* **2020**, *54*, 15424–15432. [CrossRef] [PubMed]
68. Xu, L.; Zhang, X.; Han, J.; Gong, H.; Meng, L.; Mei, X.; Sun, Y.; Qi, L.; Gan, L. Degradation of Emerging Contaminants by Sono-Fenton Process with in Situ Generated H_2O_2 and the Improvement by P25-Mediated Visible Light Irradiation. *J. Hazard. Mater.* **2020**, *391*, 122229. [CrossRef] [PubMed]
69. Nie, M.; Li, Y.; Li, L.; He, J.; Hong, P.; Zhang, K.; Cai, X.; Kong, L.; Liu, J. Ultrathin Iron-Cobalt Oxide Nanosheets with Enhanced H_2O_2 Activation Performance for Efficient Degradation of Tetracycline. *Appl. Surf. Sci.* **2021**, *535*, 147655. [CrossRef]
70. Liu, Q.; Zhou, L.; Liu, L.; Li, J.; Wang, S.; Znad, H.; Liu, S. Magnetic ZnO@Fe_3O_4 Composite for Self-Generated H2O2 toward Photo-Fenton-like Oxidation of Nitrophenol. *Compos. Part B Eng.* **2020**, *200*, 108345. [CrossRef]
71. Cao, Y.; Ren, Y.; Zhang, J.; Xie, T.; Lin, Y. Activation of H_2O_2 by Photo-Generated Electrons for Enhanced Visible Light Driven Methylene Blue Degradation with $ZnFe_2O_4/BiVO_4$ Heterojunction. *Opt. Mater.* **2021**, *121*, 111637. [CrossRef]
72. Deganello, F.; Tummino, M.L.; Calabrese, C.; Testa, M.L.; Avetta, P.; Fabbri, D.; Prevot, A.B.; Montoneri, E.; Magnacca, G. A New, Sustainable $LaFeO_3$ Material Prepared from Biowaste-Sourced Soluble Substances. *New J. Chem.* **2015**, *39*, 877–885. [CrossRef]
73. Bianco Prevot, A.; Fabbri, D.; Bernardini, E.; Deganello, F.; Tummino, M.L.; Magnacca, G. Insights on the Photocatalytic Performances of LaFeO3 Synthesized by Solution Combustion Synthesis. In *Materials Science in Photocatalysis*; Elsevier: Amsterdam, The Netherlands, 2021; pp. 357–370. ISBN 9780128218594.
74. Tummino, M.L.; Vineis, C.; Varesano, A.; Liotta, L.F.; Rigoletto, M.; Laurenti, E.; Deganello, F. $Sr_{0.85}Ce_{0.15}Fe_{0.67}Co_{0.33}$-$XCu_xO_3$ Perovskite Oxides: Effect of B-Site Copper Codoping on the Physicochemical, Catalytic and Antibacterial Properties upon UV or Thermal Activation. *Front. Environ. Eng.* **2023**, *2*, 1249931. [CrossRef]
75. Luo, Z.; Liu, M.; Tang, D.; Xu, Y.; Ran, H.; He, J.; Chen, K.; Sun, J. High H_2O_2 Selectivity and Enhanced Fe^{2+} Regeneration toward an Effective Electro-Fenton Process Based on a Self-Doped Porous Biochar Cathode. *Appl. Catal. B Environ.* **2022**, *315*, 121523. [CrossRef]
76. Mafo, S.G.M.; Tchuifon, D.R.T.; Ngakou, C.S.; Fotsop, C.G.; Kouteu, P.A.N.; Doungmo, G.; Ndifor-Angwafor, G.N.; Anagho, S.G. Study of the Degradation of Bezaktiv Brilliant Blue by the Fenton Process Using a Prepared Ferromagnetic Activated Carbon from Rubber Seed Hull as Heterogeneous Catalyst. *Desalin. Water Treat.* **2023**, *287*, 200–213. [CrossRef]
77. Guo, Q.; Zhu, W.; Yang, D.; Wang, X.; Li, Y.; Gong, C.; Yan, J.; Zhai, J.; Gao, X.; Luo, Y. A Green Solar Photo-Fenton Process for the Degradation of Carbamazepine Using Natural Pyrite and Organic Acid with in-Situ Generated H_2O_2. *Sci. Total Environ.* **2021**, *784*, 147187. [CrossRef] [PubMed]
78. Ding, J.; Shen, L.; Yan, R.; Lu, S.; Zhang, Y.; Zhang, X.; Zhang, H. Heterogeneously Activation of H_2O_2 and Persulfate with Goethite for Bisphenol A Degradation: A Mechanistic Study. *Chemosphere* **2020**, *261*, 127715. [CrossRef] [PubMed]
79. Ahmed, N.; Vione, D.; Rivoira, L.; Castiglioni, M.; Beldean-Galea, M.S.; Bruzzoniti, M.C. Feasibility of a Heterogeneous Nanoscale Zero-Valent Iron Fenton-like Process for the Removal of Glyphosate from Water. *Molecules* **2023**, *28*, 2214. [CrossRef] [PubMed]
80. Deganello, F.; Oko, D.N.; Testa, M.L.; La Parola, V.; Tummino, M.L.; Soares, C.O.; Rivera, J.G.; Orozco, G.; Guay, D.; Tavares, A.C. Perovskite-Type Catalysts Prepared by Nanocasting: Effect of Metal Silicates on the Electrocatalytic Activity toward Oxygen Evolution and Reduction Reactions. *ACS Appl. Energy Mater.* **2018**, *1*, 2565–2575. [CrossRef]
81. Huang, J.; Climent, V.; Groß, A.; Feliu, J.M. Understanding Surface Charge Effects in Electrocatalysis. Part 2: Hydrogen Peroxide Reactions at Platinum. *Chin. J. Catal.* **2022**, *43*, 2837–2849. [CrossRef]
82. Farhadian, N.; Liu, S.; Asadi, A.; Shahlaei, M.; Moradi, S. Enhanced Heterogeneous Fenton Oxidation of Organic Pollutant via Fe-Containing Mesoporous Silica Composites: A Review. *J. Mol. Liq.* **2021**, *321*, 114896. [CrossRef]
83. Salunkhe, T.T.; Gurugubelli, T.R.; Babu, B.; Yoo, K. Recent Innovative Progress of Metal Oxide Quantum-Dot-Integrated g-C3N4 (0D-2D) Synergistic Nanocomposites for Photocatalytic Applications. *Catalysts* **2023**, *13*, 1414. [CrossRef]

84. Liu, W.; Li, Z.; Kang, Q.; Wen, L. Efficient Photocatalytic Degradation of Doxycycline by Coupling α-Bi_2O_3/g-C_3N_4 Composite and H_2O_2 under Visible Light. *Environ. Res.* **2021**, *197*, 110925. [CrossRef]
85. Adhikari, S.; Lee, H.H.; Kim, D.-H. Efficient Visible-Light Induced Electron-Transfer in z-Scheme MoO_3/Ag/C_3N_4 for Excellent Photocatalytic Removal of Antibiotics of Both Ofloxacin and Tetracycline. *Chem. Eng. J.* **2020**, *391*, 123504. [CrossRef]
86. He, Y.Q.; Zhang, F.; Ma, B.; Xu, N.; Binnah Junior, L.; Yao, B.; Yang, Q.; Liu, D.; Ma, Z. Remarkably Enhanced Visible-Light Photocatalytic Hydrogen Evolution and Antibiotic Degradation over g-C_3N_4 Nanosheets Decorated by Using Nickel Phosphide and Gold Nanoparticles as Cocatalysts. *Appl. Surf. Sci.* **2020**, *517*, 146187. [CrossRef]
87. Jourshabani, M.; Asrami, M.R.; Lee, B.-K. An Efficient and Unique Route for the Fabrication of Highly Condensed Oxygen-Doped Carbon Nitride for the Photodegradation of Synchronous Pollutants and H_2O_2 Production under Ambient Conditions. *Appl. Catal. B Environ.* **2022**, *302*, 120839. [CrossRef]
88. Cui, Y.; Ding, Z.; Liu, P.; Antonietti, M.; Fu, X.; Wang, X. Metal-Free Activation of H_2O_2 by g-C_3N_4 under Visible Light Irradiation for the Degradation of Organic Pollutants. *Phys. Chem. Chem. Phys.* **2012**, *14*, 1455–1462. [CrossRef] [PubMed]
89. Chen, Q.-L.; Liu, Y.-L.; Tong, L.-G. Enhanced Visible Light Photocatalytic Activity of G-C3N4 Assisted by Hydrogen Peroxide. *Mater. Res. Express* **2018**, *5*, 046203. [CrossRef]
90. Li, T.; Ge, L.; Peng, X.; Wang, W.; Zhang, W. Enhanced Degradation of Sulfamethoxazole by a Novel Fenton-like System with Significantly Reduced Consumption of H_2O_2 Activated by g-C_3N_4/MgO Composite. *Water Res.* **2021**, *190*, 116777. [CrossRef] [PubMed]
91. Zhou, L.; Lei, J.; Wang, F.; Wang, L.; Hoffmann, M.R.; Liu, Y.; In, S.-I.; Zhang, J. Carbon Nitride Nanotubes with in Situ Grafted Hydroxyl Groups for Highly Efficient Spontaneous H_2O_2 Production. *Appl. Catal. B Environ.* **2021**, *288*, 119993. [CrossRef]
92. Torres-Pinto, A.; Sampaio, M.J.; Teixo, J.; Silva, C.G.; Faria, J.L.; Silva, A.M.T. Photo-Fenton Degradation Assisted by in Situ Generation of Hydrogen Peroxide Using a Carbon Nitride Photocatalyst. *J. Water Process Eng.* **2020**, *37*, 101467. [CrossRef]
93. Yang, Z.; Zhou, S.; Feng, X.; Wang, N.; Ola, O.; Zhu, Y. Recent Progress in Multifunctional Graphene-Based Nanocomposites for Photocatalysis and Electrocatalysis Application. *Nanomaterials* **2023**, *13*, 2028. [CrossRef] [PubMed]
94. Frindy, S.; Sillanpää, M. Synthesis and Application of Novel α-Fe_2O_3/Graphene for Visible-Light Enhanced Photocatalytic Degradation of RhB. *Mater. Des.* **2020**, *188*, 108461. [CrossRef]
95. Shi, W.; Wang, L.; Wang, J.; Sun, H.; Shi, Y.; Guo, F.; Lu, C. Magnetically Retrievable CdS/Reduced Graphene Oxide/$ZnFe_2O_4$ Ternary Nanocomposite for Self-Generated H_2O_2 towards Photo-Fenton Removal of Tetracycline under Visible Light Irradiation. *Sep. Purif. Technol.* **2022**, *292*, 120987. [CrossRef]
96. Tantubay, K.; Das, P.; Baskey (Sen), M. Hydrogen Peroxide–Assisted Photocatalytic Dye Degradation over Reduced Graphene Oxide Integrated $ZnCr_2O_4$ Nanoparticles. *Environ. Sci. Pollut. Res.* **2022**, *29*, 17309–17318. [CrossRef] [PubMed]
97. Wang, Y.; Chen, J.; Gao, J.; Meng, H.; Chai, S.; Jian, Y.; Shi, L.; Wang, Y.; He, C. Selective Electrochemical H2O2 Generation on the Graphene Aerogel for Efficient Electro-Fenton Degradation of Ciprofloxacin. *Sep. Purif. Technol.* **2021**, *272*, 118884. [CrossRef]
98. Abdelfatah, A.M.; El-Maghrabi, N.; Mahmoud, A.E.D.; Fawzy, M. Synergetic Effect of Green Synthesized Reduced Graphene Oxide and Nano-Zero Valent Iron Composite for the Removal of Doxycycline Antibiotic from Water. *Sci. Rep.* **2022**, *12*, 19372. [CrossRef] [PubMed]
99. Su, P.; Zhou, M.; Song, G.; Du, X.; Lu, X. Efficient H_2O_2 Generation and Spontaneous •OH Conversion for In-Situ Phenol Degradation on Nitrogen-Doped Graphene: Pyrolysis Temperature Regulation and Catalyst Regeneration Mechanism. *J. Hazard. Mater.* **2020**, *397*, 122681. [CrossRef] [PubMed]
100. Su, P.; Zhou, M.; Lu, X.; Yang, W.; Ren, G.; Cai, J. Electrochemical Catalytic Mechanism of N-Doped Graphene for Enhanced H_2O_2 Yield and in-Situ Degradation of Organic Pollutant. *Appl. Catal. B Environ.* **2019**, *245*, 583–595. [CrossRef]
101. Tummino, M.L.; Varesano, A.; Copani, G.; Vineis, C. A Glance at Novel Materials, from the Textile World to Environmental Remediation. *J. Polym. Environ.* **2023**, *31*, 2826–2854. [CrossRef]
102. Umar, E.; Ikram, M.; Haider, J.; Nabgan, W.; Imran, M.; Nazir, G. 3D Graphene-Based Material: Overview, Perspective, Advancement, Energy Storage, Biomedical Engineering and Environmental Applications a Bibliometric Analysis. *J. Environ. Chem. Eng.* **2023**, *11*, 110339. [CrossRef]
103. Heidarinejad, Z.; Dehghani, M.H.; Heidari, M.; Javedan, G.; Ali, I.; Sillanpää, M. Methods for Preparation and Activation of Activated Carbon: A Review. *Environ. Chem. Lett.* **2020**, *18*, 393–415. [CrossRef]
104. Tan, X.F.; Liu, S.B.; Liu, Y.G.; Gu, Y.L.; Zeng, G.M.; Hu, X.J.; Wang, X.; Liu, S.H.; Jiang, L.H. Biochar as Potential Sustainable Precursors for Activated Carbon Production: Multiple Applications in Environmental Protection and Energy Storage. *Bioresour. Technol.* **2017**, *227*, 359–372. [CrossRef]
105. Ribeiro, R.S.; Silva, A.M.T.; Figueiredo, J.L.; Faria, J.L.; Gomes, H.T. Catalytic Wet Peroxide Oxidation: A Route towards the Application of Hybrid Magnetic Carbon Nanocomposites for the Degradation of Organic Pollutants. A Review. *Appl. Catal. B Environ.* **2016**, *187*, 428–460. [CrossRef]
106. Zhang, X.; Sun, P.; Wei, K.; Huang, X.; Zhang, X. Enhanced H_2O_2 Activation and Sulfamethoxazole Degradation by Fe-Impregnated Biochar. *Chem. Eng. J.* **2020**, *385*, 123921. [CrossRef]
107. Li, X.; Jia, Y.; Zhang, J.; Qin, Y.; Wu, Y.; Zhou, M.; Sun, J. Efficient Removal of Tetracycline by H_2O_2 Activated with Iron-Doped Biochar: Performance, Mechanism, and Degradation Pathways. *Chin. Chem. Lett.* **2022**, *33*, 2105–2110. [CrossRef]

108. Bankole, O.M.; Adanlawo, O.S.; Ojubola, K.I.; Adeyemi, F.O.; Achadu, O.J.; Ogunniyi, J.A.; Olaseni, S.E.; Ogunlaja, A.S. Facile Synthesis of Solar Active Charcoal Passivated Ag_3PO_4 and Their Two-Channel Mechanisms for H_2O_2 Formation in Aerated Water. *J. Mol. Struct.* **2024**, *1300*, 137264. [CrossRef]
109. Compton, P.; Dehkordi, N.R.; Larese Casanova, P.; Alshawabkeh, A.N. Activated Carbon Modifications for Heterogeneous Fenton-Like Catalysis. *J. Chem. Eng. Catal.* **2022**, *1*, 203. [PubMed]
110. Chen, X.; Wang, L.; Sun, W.; Yang, Z.; Jin, J.; Huang, Y.; Liu, G. Boron Bifunctional Catalysts for Rapid Degradation of Persistent Organic Pollutants in a Metal-Free Electro-Fenton Process: O_2 and H_2O_2 Activation Process. *Environ. Sci. Technol.* **2023**, *57*, 15693–15702. [CrossRef]
111. Wu, Y.; Gao, Z.; Feng, Y.; Cui, Q.; Du, C.; Yu, C.; Liang, L.; Zhao, W.; Feng, J.; Sun, J.; et al. Harnessing Selective and Durable Electrosynthesis of H_2O_2 over Dual-Defective Yolk-Shell Carbon Nanosphere toward on-Site Pollutant Degradation. *Appl. Catal. B Environ.* **2021**, *298*, 120572. [CrossRef]
112. Yang, G.; Mo, S.; Xing, B.; Dong, J.; Song, X.; Liu, X.; Yuan, J. Effective Degradation of Phenol via Catalytic Wet Peroxide Oxidation over N, S, and Fe-Tridoped Activated Carbon. *Environ. Pollut.* **2020**, *258*, 113687. [CrossRef]
113. Fan, X.; Cao, Q.; Meng, F.; Song, B.; Bai, Z.; Zhao, Y.; Chen, D.; Zhou, Y.; Song, M. A Fenton-like System of Biochar Loading Fe–Al Layered Double Hydroxides (FeAl-LDH@BC)/H_2O_2 for Phenol Removal. *Chemosphere* **2021**, *266*, 128992. [CrossRef]
114. Fu, D.; Kurniawan, T.A.; Gui, H.; Li, H.; Feng, S.; Li, Q.; Wang, Y. Role of Cu x O-Anchored Pyrolyzed Hydrochars on H_2O_2 -Activated Degradation of Tetracycline: Effects of Pyrolysis Temperature and PH. *Ind. Eng. Chem. Res.* **2022**, *61*, 8847–8857. [CrossRef]
115. Liu, Z.; Meng, H.; Li, C.; Zhang, H.; Cao, J.; Meng, G. Degradation of Biologically Treated Coking Wastewater over CuOx/PAC, CuOx/GAC, and CuOx/ACF Catalysts under Microwave Irradiation in the Presence of H_2O_2. *J. Environ. Eng.* **2020**, *146*. [CrossRef]
116. Dong, H.; Zou, Y.; Zhang, K.; Sun, Y.; Hui, B.; Yang, D.; Cai, L.; Li, J. Biomimetic Design of Wood Carbon-Based Heterogeneous Catalysts for Enhanced Organic Pollutants Degradation. *Chem. Eng. J.* **2023**, *451*, 138568. [CrossRef]
117. Li, Z.; Liu, F.; Ding, Y.; Wang, F.; You, H.; Jin, C. Preparation and Properties of Cu-Ni Bimetallic Oxide Catalyst Supported on Activated Carbon for Microwave Assisted Catalytic Wet Hydrogen Peroxide Oxidation for Biologically Pretreated Coal Chemical Industry Wastewater Treatment. *Chemosphere* **2019**, *214*, 17–24. [CrossRef] [PubMed]
118. Sharma, G.; Dionysiou, D.D.; Sharma, S.; Kumar, A.; Al-Muhtaseb, A.H.; Naushad, M.; Stadler, F.J. Highly Efficient Sr/Ce/Activated Carbon Bimetallic Nanocomposite for Photoinduced Degradation of Rhodamine B. *Catal. Today* **2019**, *335*, 437–451. [CrossRef]
119. Valtchev, V.; Mintova, S. Zeolites and MOFs? In *Zeolites and Metal-Organic Frameworks*; Amsterdam University Press: Amsterdam, The Netherlands, 2018; pp. 13–24.
120. Rashed, M.N.; Palanisamy, P.N. Introductory Chapter: Adsorption and Ion Exchange Properties of Zeolites for Treatment of Polluted Water. In *Zeolites and Their Applications*; InTechOpen: London, UK, 2018.
121. Zhang, W.; Taheri-Ledari, R.; Saeidirad, M.; Qazi, F.S.; Kashtiaray, A.; Ganjali, F.; Tian, Y.; Maleki, A. Regulation of Porosity in MOFs: A Review on Tunable Scaffolds and Related Effects and Advances in Different Applications. *J. Environ. Chem. Eng.* **2022**, *10*, 108836. [CrossRef]
122. Jalali, S.; Ardjmand, M.; Ramavandi, B.; Nosratinia, F. Elimination of Amoxicillin Using Zeolite Y-Sea Salt as a Good Catalyst for Activation of Hydrogen Peroxide: Investigating Degradation Pathway and the Effect of Wastewater Chemistry. *J. Environ. Manag.* **2022**, *302*, 114045. [CrossRef]
123. Edebali, S. Synthesis and Characterization of MIL-101 (Fe) as Efficient Catalyst for Tetracycline Degradation by Using NaBH4: Artificial Neural Network Modeling. *Appl. Surf. Sci. Adv.* **2023**, *18*, 100496. [CrossRef]
124. Liú, D.; Wang, G.; Liŭ, D.; Lin, J.; He, Y.; Li, X.; Li, Z. Photocatalysis Using Zero-Valent Nano-Copper for Degrading Methyl Orange under Visible Light Irradiation. *Opt. Mater.* **2016**, *53*, 155–159. [CrossRef]
125. Liu, Y.; Guo, J.; Chen, Y.; Tan, N.; Wang, J. High-Efficient Generation of H_2O_2 by Aluminum-Graphite Composite through Selective Oxygen Reduction for Degradation of Organic Contaminants. *Environ. Sci. Technol.* **2020**, *54*, 14085–14095. [CrossRef]
126. Tan, N.; Yang, Z.; Gong, X.B.; Wang, Z.R.; Fu, T.; Liu, Y. In Situ Generation of H_2O_2 Using MWCNT-Al/O_2 System and Possible Application for Glyphosate Degradation. *Sci. Total Environ.* **2019**, *650*, 2567–2576. [CrossRef]
127. Lin, C.-C.; Cheng, Y.-J. Effectiveness of Using Nanoscale Zero-Valent Iron and Hydrogen Peroxide in Degrading Sulfamethazine in Water. *J. Taiwan Inst. Chem. Eng.* **2021**, *118*, 179–186. [CrossRef]
128. Zhang, J.; Wu, Y.; Liu, L.; Lan, Y. Rapid Removal of P-Chloronitrobenzene from Aqueous Solution by a Combination of Ozone with Zero-Valent Zinc. *Sep. Purif. Technol.* **2015**, *151*, 318–323. [CrossRef]
129. Zhong, W.; Peng, Q.; Liu, K.; Tang, X.; Zhang, Y.; Xing, J. Building $Cu_0/CuFe_2O_4$ Framework to Efficiently Degrade Tetracycline and Improve Utilization of H_2O_2 in Fenton-like System. *Chem. Eng. J.* **2023**, *474*, 145522. [CrossRef]
130. Devi, L.G.; Srinivas, M.; ArunaKumari, M.L. Heterogeneous Advanced Photo- Fenton Process Using Peroxymonosulfate and Peroxydisulfate in Presence of Zero Valent Metallic Iron: A Comparative Study with Hydrogen Peroxide Photo-Fenton Process. *J. Water Process Eng.* **2016**, *13*, 117–126. [CrossRef]
131. Li, L.; Hu, J.; Shi, X.; Fan, M.; Luo, J.; Wei, X. Nanoscale Zero-Valent Metals: A Review of Synthesis, Characterization, and Applications to Environmental Remediation. *Environ. Sci. Pollut. Res.* **2016**, *23*, 17880–17900. [CrossRef]

132. Wu, Z.; Xiong, Z.; Lai, B. Metal Sulfide-Based Catalysts in Advanced Oxidation Processes for Water Decontamination. *Environ. Funct. Mater.* **2022**, *1*, 298–315. [CrossRef]
133. Bai, X.; Wang, X.; Jia, T.; Guo, L.; Hao, D.; Zhang, Z.; Wu, L.; Zhang, X.; Yang, H.; Gong, Y.; et al. Efficient Degradation of PPCPs by Mo1−xS2−y with S Vacancy at Phase-Junction: Promoted by Innergenerate-H_2O_2. *Appl. Catal. B Environ.* **2022**, *310*, 121302. [CrossRef]
134. Moma, J.; Baloyi, J. Modified Titanium Dioxide for Photocatalytic Applications. In *Photocatalysts—Applications and Attributes*; IntechOpen: London, UK, 2019.
135. Zulfiqar, M.; Sufian, S.; Rabat, N.E.; Mansor, N. Photocatalytic Degradation and Adsorption of Phenol by Solvent-Controlled TiO2 Nanosheets Assisted with H_2O_2 and $FeCl_3$: Kinetic, Isotherm and Thermodynamic Analysis. *J. Mol. Liq.* **2020**, *308*, 112941. [CrossRef]
136. Popescu, T.; Oktaviani Matei, C.; Culita, D.C.; Maraloiu, V.-A.; Rostas, A.M.; Diamandescu, L.; Iacob, N.; Savopol, T.; Ilas, M.C.; Feder, M.; et al. Facile Synthesis of Low Toxicity Iron Oxide/TiO_2 Nanocomposites with Hyperthermic and Photo-Oxidation Properties. *Sci. Rep.* **2022**, *12*, 6887. [CrossRef]
137. dela Rosa, F.M.; Popović, M.; Papac Zjačić, J.; Radić, G.; Kraljić Roković, M.; Kovačić, M.; Farré, M.J.; Genorio, B.; Lavrenčič Štangar, U.; Kušić, H.; et al. Visible-Light Activation of Persulfate or H_2O_2 by Fe_2O_3/TiO_2 Immobilized on Glass Support for Photocatalytic Removal of Amoxicillin: Mechanism, Transformation Products, and Toxicity Assessment. *Nanomaterials* **2022**, *12*, 4328. [CrossRef]
138. Farhana Jaafar, N.; Farhana Jaafar, N.; Khairuddean, M.; Nordin, N. A Review on Recent Progression of Modifications on Titania Morphology and Its Photocatalytic Performance. *Acta Chim. Slov.* **2020**, *67*, 361–374. [CrossRef]
139. Daghrir, R.; Drogui, P.; Robert, D. Modified TiO_2 for Environmental Photocatalytic Applications: A Review. *Ind. Eng. Chem. Res.* **2013**, *52*, 3581–3599. [CrossRef]
140. Parangi, T.; Mishra, M.K. Titania Nanoparticles as Modified Photocatalysts: A Review on Design and Development. *Comments Inorg. Chem.* **2019**, *39*, 90–126. [CrossRef]
141. Kumar, S.G.; Devi, L.G. Review on Modified TiO_2 Photocatalysis under UV/Visible Light: Selected Results and Related Mechanisms on Interfacial Charge Carrier Transfer Dynamics. *J. Phys. Chem. A* **2011**, *115*, 13211–13241. [CrossRef]
142. Noureen, L.; Wang, Q.; Humayun, M.; Shah, W.A.; Xu, Q.; Wang, X. Recent Advances in Structural Engineering of Photocatalysts for Environmental Remediation. *Environ. Res.* **2023**, *219*, 115084. [CrossRef]
143. Covinich, L.; Felissia, F.; Massa, P.; Fenoglio, R.; Area, M.C. Kinetic Modeling of a Heterogeneous Fenton-Type Oxidative Treatment of Complex Industrial Effluent. *Int. J. Ind. Chem.* **2018**, *9*, 215–229. [CrossRef]
144. Bokhari, T.H.; Ahmad, N.; Jilani, M.I.; Saeed, M.; Usman, M.; Haq, A.U.; Rehman, R.; Iqbal, M.; Nazir, A.; Javed, T. UV/H_2O_2, UV/H_2O_2/SnO_2 and Fe/H_2O_2 Based Advanced Oxidation Processes for the Degradation of Disperse Violet 63 in Aqueous Medium. *Mater. Res. Express* **2020**, *7*, 015531. [CrossRef]
145. Habib, I.Y.; Burhan, J.; Jaladi, F.; Lim, C.M.; Usman, A.; Kumara, N.T.R.N.; Tsang, S.C.E.; Mahadi, A.H. Effect of Cr Doping in CeO_2 Nanostructures on Photocatalysis and H_2O_2 Assisted Methylene Blue Dye Degradation. *Catal. Today* **2021**, *375*, 506–513. [CrossRef]
146. Valles-Pérez, B.Y.; Badillo-Ávila, M.A.; Torres-Delgado, G.; Castanedo-Pérez, R.; Zelaya-Ángel, O. Photocatalytic Activity of ZnO + CuO Thin Films Deposited by Dip Coating: Coupling Effect between Oxides. *J. Sol-Gel Sci. Technol.* **2020**, *93*, 517–526. [CrossRef]
147. Mohammadzadeh, A.; Khoshghadam-Pireyousefan, M.; Shokrianfard-Ravasjan, B.; Azadbeh, M.; Rashedi, H.; Dibazar, M.; Mostafaei, A. Synergetic Photocatalytic Effect of High Purity ZnO Pod Shaped Nanostructures with H_2O_2 on Methylene Blue Dye Degradation. *J. Alloys Compd.* **2020**, *845*, 156333. [CrossRef]
148. Ene, C.D.; Patrinoiu, G.; Munteanu, C.; Ene, R.; Chifiriuc, M.C.; Carp, O. Multifunctional ZnO Materials Prepared by a Versatile Green Carbohydrate-Assisted Combustion Method for Environmental Remediation Applications. *Ceram. Int.* **2019**, *45*, 2295–2302. [CrossRef]
149. Pourmortazavi, S.M.; Rahimi-Nasrabadi, M.; Ahmadi, F.; Ganjali, M.R. $CuCO_3$ and CuO Nanoparticles; Facile Preparation and Evaluation as Photocatalysts. *J. Mater. Sci. Mater. Electron.* **2018**, *29*, 9442–9451. [CrossRef]
150. Kumar, S.G.; Rao, K.S.R.K. Comparison of Modification Strategies towards Enhanced Charge Carrier Separation and Photocatalytic Degradation Activity of Metal Oxide Semiconductors (TiO_2, WO_3 and ZnO). *Appl. Surf. Sci.* **2017**, *391*, 124–148. [CrossRef]
151. Karthikeyan, C.; Arunachalam, P.; Ramachandran, K.; Al-Mayouf, A.M.; Karuppuchamy, S. Recent Advances in Semiconductor Metal Oxides with Enhanced Methods for Solar Photocatalytic Applications. *J. Alloys Compd.* **2020**, *828*, 154281. [CrossRef]
152. Danish, M.S.S.; Estrella, L.L.; Alemaida, I.M.A.; Lisin, A.; Moiseev, N.; Ahmadi, M.; Nazari, M.; Wali, M.; Zaheb, H.; Senjyu, T. Photocatalytic Applications of Metal Oxides for Sustainable Environmental Remediation. *Metals* **2021**, *11*, 80. [CrossRef]
153. El-Shamy, A.G. Synthesis of New Magnesium Peroxide (MgO_2) Nano-Rods for Pollutant Dye Removal and Antibacterial Applications. *Mater. Chem. Phys.* **2020**, *243*, 122640. [CrossRef]
154. Ali, M.; Farooq, U.; Lyu, S.; Sun, Y.; Li, M.; Ahmad, A.; Shan, A.; Abbas, Z. Synthesis of Controlled Release Calcium Peroxide Nanoparticles (CR-NCPs): Characterizations, H_2O_2 Liberate Performances and Pollutant Degradation Efficiency. *Sep. Purif. Technol.* **2020**, *241*, 116729. [CrossRef]
155. Kowalkińska, M.; Głuchowski, P.; Swebocki, T.; Ossowski, T.; Ostrowski, A.; Bednarski, W.; Karczewski, J.; Zielińska-Jurek, A. Scheelite-Type Wide-Bandgap ABO 4 Compounds (A = Ca, Sr, and Ba; B = Mo and W) as Potential Photocatalysts for Water Treatment. *J. Phys. Chem. C* **2021**, *125*, 25497–25513. [CrossRef]

156. Kong, J.; Yang, T.; Rui, Z.; Ji, H. Perovskite-Based Photocatalysts for Organic Contaminants Removal: Current Status and Future Perspectives. *Catal. Today* **2019**, *327*, 47–63. [CrossRef]
157. Chandrasekaran, S.; Bowen, C.; Zhang, P.; Li, Z.; Yuan, Q.; Ren, X.; Deng, L. Spinel Photocatalysts for Environmental Remediation, Hydrogen Generation, CO 2 Reduction and Photoelectrochemical Water Splitting. *J. Mater. Chem. A* **2018**, *6*, 11078–11104. [CrossRef]
158. Wang, J.; Yang, L.; Zhang, L. Constructed 3D Hierarchical Micro-Flowers $CoWO_4$@Bi_2WO_6 Z-Scheme Heterojunction Catalyzer: Two-Channel Photocatalytic H_2O_2 Production and Antibiotics Degradation. *Chem. Eng. J.* **2021**, *420*, 127639. [CrossRef]
159. Das, K.C.; Dhar, S.S. Rapid Catalytic Degradation of Malachite Green by $MgFe_2O_4$ Nanoparticles in Presence of H_2O_2. *J. Alloys Compd.* **2020**, *828*, 154462. [CrossRef]
160. Hong, P.; Li, Y.; He, J.; Saeed, A.; Zhang, K.; Wang, C.; Kong, L.; Liu, J. Rapid Degradation of Aqueous Doxycycline by Surface $CoFe_2O_4/H_2O_2$ System: Behaviors, Mechanisms, Pathways and DFT Calculation. *Appl. Surf. Sci.* **2020**, *526*, 146557. [CrossRef]
161. Wei, Y.; Zhang, Y.; Miao, J.; Geng, W.; Long, M. In-Situ Utilization of Piezo-Generated Hydrogen Peroxide for Efficient p-Chlorophenol Degradation by Fe Loading Bismuth Vanadate. *Appl. Surf. Sci.* **2021**, *543*, 148791. [CrossRef]
162. Demircivi, P.; Simsek, E.B. Visible-Light-Enhanced Photoactivity of Perovskite-Type W-Doped BaTiO3 Photocatalyst for Photodegradation of Tetracycline. *J. Alloys Compd.* **2019**, *774*, 795–802. [CrossRef]
163. Vieten, J.; Bulfin, B.; Roeb, M.; Sattler, C. Citric Acid Auto-Combustion Synthesis of Ti-Containing Perovskites via Aqueous Precursors. *Solid State Ion.* **2018**, *315*, 92–97. [CrossRef]
164. Li, L.; Hu, Z.; Yu, J.C. On-Demand Synthesis of H_2O_2 by Water Oxidation for Sustainable Resource Production and Organic Pollutant Degradation. *Angew. Chem.* **2020**, *132*, 20719–20725. [CrossRef]
165. Li, M.; Han, N.; Zhang, X.; Wang, S.; Jiang, M.; Bokhari, A.; Zhang, W.; Race, M.; Shen, Z.; Chen, R.; et al. Perovskite Oxide for Emerging Photo(Electro)Catalysis in Energy and Environment. *Environ. Res.* **2022**, *205*, 112544. [CrossRef] [PubMed]
166. Nzuzo, Y.; Oseghale, C.O.; Chike-Ekwughe, A.; Maumela, M.; Bingwa, N. Electronic Distribution and Dynamics as Catalytic Descriptors in Heterogeneous Catalysis: A Mini Review. *Catal. Commun.* **2024**, 106901. [CrossRef]
167. Di Paola, A.; Bellardita, M.; Palmisano, L.; Barbieriková, Z.; Brezová, V. Influence of Crystallinity and OH Surface Density on the Photocatalytic Activity of TiO_2 Powders. *J. Photochem. Photobiol. A Chem.* **2014**, *273*, 59–67. [CrossRef]
168. Zhang, Y.; Pan, C.; Li, J.; Zhu, Y. Recent Progress in Nonsacrificial H_2O_2 Generation Using Organic Photocatalysts and In Situ Applications for Environmental Remediation. *Acc. Mater. Res.* **2024**, *5*, 76–88. [CrossRef]
169. García-Ballesteros, S.; García-Negueroles, P.; Amat, A.M.; Arques, A. Humic-Like Substances as Auxiliaries to Enhance Advanced Oxidation Processes. *ACS Omega* **2022**, *7*, 3151–3157. [CrossRef] [PubMed]
170. Bianco Prevot, A.; Testa, M.L.; Laurenti, E.; Tummino, M.L.; Magnacca, G. Soluble Bioorganic Substances from Compost as Photosensitizers for a Sustainable Homogeneous and Heterogeneous Photocatalysis. In *Materials Science in Photocatalysis*; Elsevier: Amsterdam, The Netherlands, 2021; pp. 589–601. ISBN 9780128218594.
171. Vallés, I.; Santos Juanes, L.; Amat, A.M.; Palma, D.; Laurenti, E.; Bianco Prevot, A.; Arques, A. Humic Acids as Complexing Agents to Drive Photo-Fenton at Mild PH in Saline Matrices: Process Performance and Mechanistic Studies. *J. Environ. Chem. Eng.* **2023**, *11*, 111391. [CrossRef]
172. Tummino, M.L.; Testa, M.L.; Malandrino, M.; Gamberini, R.; Bianco Prevot, A.; Magnacca, G.; Laurenti, E. Green Waste-Derived Substances Immobilized on SBA-15 Silica: Surface Properties, Adsorbing and Photosensitizing Activities towards Organic and Inorganic Substrates. *Nanomaterials* **2019**, *9*, 162. [CrossRef] [PubMed]
173. Testa, M.L.; Tummino, M.L.; Agostini, S.; Avetta, P.; Deganello, F.; Montoneri, E.; Magnacca, G.; Prevot, A.B. Synthesis, Characterization and Environmental Application of Silica Grafted Photoactive Substances Isolated from Urban Biowaste. *RSC Adv.* **2015**, *5*, 47920–47927. [CrossRef]
174. Huang, Q.Q.; Liu, H.Z.; Huang, M.; Wang, J.; Yu, H.Q. Ligand-Assisted Heterogeneous Catalytic H_2O_2 Activation for Pollutant Degradation: The Trade-off between Coordination Site Passivation and Adjacent Site Activation. *Appl. Catal. B Environ.* **2023**, *330*, 122592. [CrossRef]
175. Baran, T.; Wojtyła, S.; Minguzzi, A.; Rondinini, S.; Vertova, A. Achieving Efficient H_2O_2 Production by a Visible-Light Absorbing, Highly Stable Photosensitized TiO_2. *Appl. Catal. B Environ.* **2019**, *244*, 303–312. [CrossRef]
176. Zhang, M.; Lin, X.; Yi, Z.; Xu, X.; Yang, J.; Zhu, M. Enhanced Reactive Oxidation Species Generation by Ligand-to-Metal-Charge Transfer between Oxygen Vacancy-Rich ZnO Mesocrystal with Ciprofloxacin Pollutants. *Appl. Catal. B Environ.* **2023**, *321*, 122033. [CrossRef]
177. Fei, B.; Yan, Q.; Wang, J.; Liu, Q.; Long, J.; Li, Y.; Shao, K.; Su, Z.; Sun, W. Green Oxidative Degradation of Methyl Orange with Copper(II) Schiff Base Complexes as Photo-Fenton-Like Catalysts. *Z. Anorg. Allg. Chem.* **2014**, *640*, 2035–2040. [CrossRef]
178. Zhao, J.; Liu, Y.; Fan, M.; Yuan, L.; Zou, X. From Solid-State Metal Alkoxides to Nanostructured Oxides: A Precursor-Directed Synthetic Route to Functional Inorganic Nanomaterials. *Inorg. Chem. Front.* **2015**, *2*, 198–212. [CrossRef]
179. Paris, C.B.; Howe, A.G.; Lewis, R.J.; Hewes, D.; Morgan, D.J.; He, Q.; Edwards, J.K. Impact of the Experimental Parameters on Catalytic Activity When Preparing Polymer Protected Bimetallic Nanoparticle Catalysts on Activated Carbon. *ACS Catal.* **2022**, *12*, 4440–4454. [CrossRef] [PubMed]
180. Köwitsch, I.; Mehring, M. Carbon Nitride Materials: Impact of Synthetic Method on Photocatalysis and Immobilization for Photocatalytic Pollutant Degradation. *J. Mater. Sci.* **2021**, *56*, 18608–18624. [CrossRef]

181. Wang, F.; Chen, X.; Wang, Y.; Li, X.; Wan, M.; Zhang, G.; Leng, F.; Zhang, H. Insights into the Structures, Inhibitors, and Improvement Strategies of Glucose Oxidase. *Int. J. Mol. Sci.* **2022**, *23*, 9841. [CrossRef] [PubMed]
182. Wohlfahrt, G.; Witt, S.; Hendle, J.; Schomburg, D.; Kalisz, H.M.; Hecht, H.-J. 1.8 and 1.9 Å Resolution Structures of the Penicillium Amagasakiense and Aspergillus Niger Glucose Oxidases as a Basis for Modelling Substrate Complexes. *Acta Crystallogr. Sect. D Biol. Crystallogr.* **1999**, *55*, 969–977. [CrossRef] [PubMed]
183. Zhao, Z.; Li, M.; Du, N.; Li, Z.; Zhang, Y.; Zhang, Q. Fenton-like Reaction of Glucose Oxidase-Glucose@Kaolin Coupled with Green Rust: A Framework Triggering FeIV=O in Refractory Pollutants Degradation. *Sep. Purif. Technol.* **2022**, *301*, 122061. [CrossRef]
184. Huang, Y.; Liu, H.; Liu, S.; Li, C.; Yuan, S. Glucose Oxidase Modified Fenton Reactions for In-Situ ROS Generation and Potential Application in Groundwater Remediation. *Chemosphere* **2020**, *253*, 126648. [CrossRef] [PubMed]
185. Vaidyanathan, V.K.; Alanazi, A.K.; Senthil Kumar, P.; Rajendran, D.S.; Chidambaram, A.; Venkataraman, S.; Kumar, V.V.; Rangasamy, G.; Cabana, H.; Abo-Dief, H.M. Cost-Effective, Scalable Production of Glucose Oxidase Using Casuarina Equisetifolia Biomass and Its Application in the Bio-Fenton Oxidation Process for the Removal of Trace Organic Contaminants from Wastewater. *Bioresour. Technol.* **2023**, *377*, 128958. [CrossRef] [PubMed]
186. Krishnan, S.; Martínez-Huitle, C.A.; Nidheesh, P.V. An Overview of Chelate Modified Electro-Fenton Processes. *J. Environ. Chem. Eng.* **2022**, *10*, 107183. [CrossRef]
187. Yang, Y.; Ghatge, S.; Ko, Y.; Yoon, Y.; Ahn, J.-H.; Kim, J.J.; Hur, H.-G. Non-Specific Degradation of Chloroacetanilide Herbicides by Glucose Oxidase Supported Bio-Fenton Reaction. *Chemosphere* **2022**, *292*, 133417. [CrossRef]
188. An, S.; Yoon, Y.; Ahn, J.-H.; Kim, D.; Weon, H.-Y.; Kim, Y.; Hur, H.-G.; Yang, Y. Oxidative Degradation of Bisphenol A by Bio-Fenton Reaction Equipped with Glucose Oxidase and Ferric Citrate: Degradation Kinetics and Pathway. *J. Environ. Chem. Eng.* **2023**, *11*, 109349. [CrossRef]
189. Wang, X.; Song, C.; Liu, X.; Zhang, J.; Zhang, Y.; Shi, X.; Kim, D. Bio-Fenton-Assisted Biological Process for Efficient Mineralization of Polycyclic Aromatic Hydrocarbons from the Environment. *Processes* **2022**, *10*, 1316. [CrossRef]
190. Yoon, Y.; Cho, M. Understanding Atrazine Elimination via Treatment of the Enzyme-Based Fenton Reaction: Kinetics, Mechanism, Reaction Pathway, and Metabolites Toxicity. *Chemosphere* **2024**, *349*, 140982. [CrossRef] [PubMed]
191. Ioffe, M.; Kundu, S.; Perez-Lapid, N.; Radian, A. Heterogeneous Fenton Catalyst Based on Clay Decorated with Nano-Sized Amorphous Iron Oxides Prevents Oxidant Scavenging through Surface Complexation. *Chem. Eng. J.* **2022**, *433*, 134609. [CrossRef]
192. Wang, J.; Tang, J. Fe-Based Fenton-like Catalysts for Water Treatment: Catalytic Mechanisms and Applications. *J. Mol. Liq.* **2021**, *332*, 115755. [CrossRef]
193. Wang, J.; Tang, J. Fe-Based Fenton-like Catalysts for Water Treatment: Preparation, Characterization and Modification. *Chemosphere* **2021**, *276*, 130177. [CrossRef] [PubMed]
194. Bhave, C.; Shejwalkar, S. A Review on the Synthesis and Applications of Green Rust for Environmental Pollutant Remediation. *Int. J. Environ. Sci. Technol.* **2018**, *15*, 1243–1248. [CrossRef]
195. Neyens, E.; Baeyens, J. A Review of Classic Fenton's Peroxidation as an Advanced Oxidation Technique. *J. Hazard. Mater.* **2003**, *98*, 33–50. [CrossRef] [PubMed]
196. Wang, M.; Huang, Y.; Liu, H. Removal of Trichloroethene by Glucose Oxidase Immobilized on Magnetite Nanoparticles. *RSC Adv.* **2023**, *13*, 11853–11864. [CrossRef] [PubMed]
197. Liu, X.; Zhang, L.; Zhang, Q.; Li, M.; Zhao, Z.; Lin, B.; Peng, J.; Shen, H.; He, Q. Fenton-like System of UV/Glucose-Oxidase@Kaolin Coupled with Organic Green Rust: UV-Enhanced Enzyme Activity and the Mechanism of UV Synergistic Degradation of Photosensitive Pollutants. *Environ. Res.* **2024**, *247*, 118257. [CrossRef]
198. Karimi, A.; Aghbolaghy, M.; Khataee, A.; Shoa Bargh, S. Use of Enzymatic Bio-Fenton as a New Approach in Decolorization of Malachite Green. *Sci. World J.* **2012**, *2012*, 691569. [CrossRef]
199. Hakala, M. Photoinhibition of Manganese Enzymes: Insights into the Mechanism of Photosystem II Photoinhibition. *J. Exp. Bot.* **2006**, *57*, 1809–1816. [CrossRef] [PubMed]
200. Ghatge, S.; Yang, Y.; Ko, Y.; Yoon, Y.; Ahn, J.-H.; Kim, J.J.; Hur, H.-G. Degradation of Sulfonated Polyethylene by a Bio-Photo-Fenton Approach Using Glucose Oxidase Immobilized on Titanium Dioxide. *J. Hazard. Mater.* **2022**, *423*, 127067. [CrossRef] [PubMed]
201. Ravi, S.; Lonappan, L.; Touahar, I.; Fonteneau, É.; Vaidyanathan, V.K.; Cabana, H. Evaluation of Bio-Fenton Oxidation Approach for the Remediation of Trichloroethylene from Aqueous Solutions. *J. Environ. Manag.* **2020**, *270*, 110899. [CrossRef] [PubMed]
202. Banci, L. Structural Properties of Peroxidases. *J. Biotechnol.* **1997**, *53*, 253–263. [CrossRef] [PubMed]
203. Sugano, Y.; Sasaki, K.; Shoda, M. CDNA Cloning and Genetic Analysis of a Novel Decolorizing Enzyme, Peroxidase Gene Dyp from Geotrichum Candidum Dec 1. *J. Biosci. Bioeng.* **1999**, *87*, 411–417. [CrossRef] [PubMed]
204. Faraco, V.; Piscitelli, A.; Sannia, G.; Giardina, P. Identification of a New Member of the Dye-Decolorizing Peroxidase Family from Pleurotus Ostreatus. *World J. Microbiol. Biotechnol.* **2007**, *23*, 889–893. [CrossRef]
205. Battistuzzi, G.; Bellei, M.; Bortolotti, C.A.; Sola, M. Redox Properties of Heme Peroxidases. *Arch. Biochem. Biophys.* **2010**, *500*, 21–36. [CrossRef] [PubMed]
206. Nuell, M.J.; Fang, G.H.; Axley, M.J.; Kenigsberg, P.; Hager, L.P. Isolation and Nucleotide Sequence of the Chloroperoxidase Gene from Caldariomyces Fumago. *J. Bacteriol.* **1988**, *170*, 1007–1011. [CrossRef]

207. Conesa, A.; Punt, P.J.; van den Hondel, C.A.M.J.J. Fungal Peroxidases: Molecular Aspects and Applications. *J. Biotechnol.* **2002**, *93*, 143–158. [CrossRef]
208. Al-Maqdi, K.A.; Hisaindee, S.M.; Rauf, M.A.; Ashraf, S.S. Comparative Degradation of a Thiazole Pollutant by an Advanced Oxidation Process and an Enzymatic Approach. *Biomolecules* **2017**, *7*, 64. [CrossRef]
209. Wagenknecht, H.-A.; Woggon, W.-D. Identification of Intermediates in the Catalytic Cycle of Chloroperoxidase. *Chem. Biol.* **1997**, *4*, 367–372. [CrossRef] [PubMed]
210. Piontek, K.; Strittmatter, E.; Ullrich, R.; Gröbe, G.; Pecyna, M.J.; Kluge, M.; Scheibner, K.; Hofrichter, M.; Plattner, D.A. Structural Basis of Substrate Conversion in a New Aromatic Peroxygenase. *J. Biol. Chem.* **2013**, *288*, 34767–34776. [CrossRef] [PubMed]
211. Yoshida, T.; Sugano, Y. Unexpected Diversity of Dye-Decolorizing Peroxidases. *Biochem. Biophys. Rep.* **2023**, *33*, 101401. [CrossRef] [PubMed]
212. Hofrichter, M.; Ullrich, R.; Pecyna, M.J.; Liers, C.; Lundell, T. New and Classic Families of Secreted Fungal Heme Peroxidases. *Appl. Microbiol. Biotechnol.* **2010**, *87*, 871–897. [CrossRef] [PubMed]
213. Catucci, G.; Valetti, F.; Sadeghi, S.J.; Gilardi, G. Biochemical Features of Dye-decolorizing Peroxidases: Current Impact on Lignin Degradation. *Biotechnol. Appl. Biochem.* **2020**, *67*, 751–759. [CrossRef] [PubMed]
214. Uchida, T.; Sasaki, M.; Tanaka, Y.; Ishimori, K. A Dye-Decolorizing Peroxidase from Vibrio Cholerae. *Biochemistry* **2015**, *54*, 6610–6621. [CrossRef] [PubMed]
215. Sellami, K.; Couvert, A.; Nasrallah, N.; Maachi, R.; Abouseoud, M.; Amrane, A. Peroxidase Enzymes as Green Catalysts for Bioremediation and Biotechnological Applications: A Review. *Sci. Total Environ.* **2022**, *806*, 150500. [CrossRef] [PubMed]
216. Rigoletto, M.; Calza, P.; Gaggero, E.; Laurenti, E. Hybrid Materials for the Removal of Emerging Pollutants in Water: Classification, Synthesis, and Properties. *Chem. Eng. J. Adv.* **2022**, *10*, 100252. [CrossRef]
217. Calza, P.; Zacchigna, D.; Laurenti, E. Degradation of Orange Dyes and Carbamazepine by Soybean Peroxidase Immobilized on Silica Monoliths and Titanium Dioxide. *Environ. Sci. Pollut. Res.* **2016**, *23*, 23742–23749. [CrossRef]
218. Iñarritu, I.; Torres, E.; Topete, A.; Campos-Terán, J. Immobilization Effects on the Photocatalytic Activity of CdS Quantum Dots-Horseradish Peroxidase Hybrid Nanomaterials. *J. Colloid Interface Sci.* **2017**, *506*, 36–45. [CrossRef]
219. Wu, J.; He, T.; Ma, X.; Li, C.; Han, J.; Wang, L.; Dong, H.; Zhang, R.; Wang, Y. A Novel Immobilized Horseradish Peroxidase Platform Driven by Visible Light for the Complete Mineralization of Sulfadiazine in Water. *Int. J. Biol. Macromol.* **2023**, *253*, 127239. [CrossRef] [PubMed]
220. Baynton, K.J.; Bewtra, J.K.; Biswas, N.; Taylor, K.E. Inactivation of Horseradish Peroxidase by Phenol and Hydrogen Peroxide: A Kinetic Investigation. *Biochim. Biophys. Acta—Protein Struct. Mol. Enzymol.* **1994**, *1206*, 272–278. [CrossRef] [PubMed]
221. Nicell, J.A.; Wright, H. A Model of Peroxidase Activity with Inhibition by Hydrogen Peroxide. *Enzym. Microb. Technol.* **1997**, *21*, 302–310. [CrossRef]
222. Hiner, A.N.P.; Hernández-Ruiz, J.; Rodríguez-López, J.N.; Arnao, M.B.; Varón, R.; García-Cánovas, F.; Acosta, M. The Inactivation of Horseradish Peroxidase Isoenzyme AZ by Hydrogen Peroxide: An Example of Partial Resistance Due to the Formation of a Stable Enzyme Intermediate. *JBIC J. Biol. Inorg. Chem.* **2001**, *6*, 504–516. [CrossRef] [PubMed]
223. Chansaenpak, K.; Kamkaew, A.; Lisnund, S.; Prachai, P.; Ratwirunkit, P.; Jingpho, T.; Blay, V.; Pinyou, P. Development of a Sensitive Self-Powered Glucose Biosensor Based on an Enzymatic Biofuel Cell. *Biosensors* **2021**, *11*, 16. [CrossRef] [PubMed]
224. Zhang, H.; Chen, Z.; Dai, J.; Zhang, W.; Jiang, Y.; Zhou, A. A Low-Cost Mobile Platform for Whole Blood Glucose Monitoring Using Colorimetric Method. *Microchem. J.* **2021**, *162*, 105814. [CrossRef]
225. Pantić, N.; Prodanović, R.; Đurđić, K.I.; Polović, N.; Spasojević, M.; Prodanović, O. Optimization of Phenol Removal with Horseradish Peroxidase Encapsulated within Tyramine-Alginate Micro-Beads. *Environ. Technol. Innov.* **2021**, *21*, 101211. [CrossRef]
226. Babaei, H.; Ghobadi Nejad, Z.; Yaghmaei, S.; Farhadi, F. Co-Immobilization of Multi-Enzyme Cascade System into the Metal–Organic Frameworks for the Removal of Bisphenol A. *Chem. Eng. J.* **2023**, *461*, 142050. [CrossRef]
227. Yan, Y.; Liu, X.; Jiang, X.; Zhang, W.; Wang, Y.; Wang, Y.; Zhang, Y.; Luo, H.; Yao, B.; Huang, H.; et al. Surface Charge Modifications Modulate Glucose Oxidase PH-Activity Profiles for Efficient Gluconic Acid Production. *J. Clean. Prod.* **2022**, *372*, 133817. [CrossRef]
228. Gao, F.; Guo, Y.; Fan, X.; Hu, M.; Li, S.; Zhai, Q.; Jiang, Y.; Wang, X. Enhancing the Catalytic Performance of Chloroperoxidase by Co-Immobilization with Glucose Oxidase on Magnetic Graphene Oxide. *Biochem. Eng. J.* **2019**, *143*, 101–109. [CrossRef]
229. Gu, Y.; Yuan, L.; Li, M.; Wang, X.; Rao, D.; Bai, X.; Shi, K.; Xu, H.; Hou, S.; Yao, H. Co-Immobilized Bienzyme of Horseradish Peroxidase and Glucose Oxidase on Dopamine-Modified Cellulose–Chitosan Composite Beads as a High-Efficiency Biocatalyst for Degradation of Acridine. *RSC Adv.* **2022**, *12*, 23006–23016. [CrossRef] [PubMed]
230. Liu, X.; Zhang, Q.; Li, M.; Qin, S.; Zhao, Z.; Lin, B.; Ding, Y.; Xiang, Y.; Li, C. Horseradish Peroxidase (HRP) and Glucose Oxidase (GOX) Based Dual-Enzyme System: Sustainable Release of H_2O_2 and Its Effect on the Desirable Ping Pong Bibi Degradation Mechanism. *Environ. Res.* **2023**, *229*, 115979. [CrossRef] [PubMed]
231. Razzaghi, M.; Karimi, A.; Aghdasinia, H.; Joghataei, M.-T. Oxidase-Peroxidase Sequential Polymerization for Removal of a Dye from Contaminated Water by Horseradish Peroxidase (HRP)/Glucose Oxidase (GOx)/Polyurethane Hybrid Catalyst. *Korean J. Chem. Eng.* **2017**, *34*, 2870–2878. [CrossRef]
232. Pitzalis, F.; Monduzzi, M.; Salis, A. A Bienzymatic Biocatalyst Constituted by Glucose Oxidase and Horseradish Peroxidase Immobilized on Ordered Mesoporous Silica. *Microporous Mesoporous Mater.* **2017**, *241*, 145–154. [CrossRef]

233. Taboada-Puig, R.; Junghanns, C.; Demarche, P.; Moreira, M.T.; Feijoo, G.; Lema, J.M.; Agathos, S.N. Combined Cross-Linked Enzyme Aggregates from Versatile Peroxidase and Glucose Oxidase: Production, Partial Characterization and Application for the Elimination of Endocrine Disruptors. *Bioresour. Technol.* **2011**, *102*, 6593–6599. [CrossRef] [PubMed]
234. Frew, J.E.; Jones, P.; Scholes, G. Spectrophotometric Determination of Hydrogen Peroxide and Organic Hydroperoxides at Low Concentrations in Aqueous Solution. *Anal. Chim. Acta* **1983**, *155*, 139–150. [CrossRef]
235. Sekar, R.; DiChristina, T.J. Microbially Driven Fenton Reaction for Degradation of the Widespread Environmental Contaminant 1,4-Dioxane. *Environ. Sci. Technol.* **2014**, *48*, 12858–12867. [CrossRef] [PubMed]
236. Zhou, B.; Wang, J.; Guo, Z.; Tan, H.; Zhu, X. A Simple Colorimetric Method for Determination of Hydrogen Peroxide in Plant Tissues. *Plant Growth Regul.* **2006**, *49*, 113–118. [CrossRef]
237. Fernando, C.D.; Soysa, P. Optimized Enzymatic Colorimetric Assay for Determination of Hydrogen Peroxide (H_2O_2) Scavenging Activity of Plant Extracts. *MethodsX* **2015**, *2*, 283–291. [CrossRef]
238. Schüttler, S.; Jolmes, L.; Jeß, E.; Tschulik, K.; Golda, J. Validation of in Situ Diagnostics for the Detection of OH and H_2O_2 in Liquids Treated by a Humid Atmospheric Pressure Plasma Jet. *Plasma Process. Polym.* **2024**, *21*, e2300079. [CrossRef]
239. Oliveira, M.C.; Nogueira, R.F.P.; Gomes Neto, J.A.; Jardim, W.F.; Rohwedder, J.J.R. Sistema de Injeção Em Fluxo Espectrofotométrico Para Monitorar Peróxido de Hidrogênio Em Processo de Fotodegradação Por Reação Foto-Fenton. *Quim. Nova* **2001**, *24*, 188–190. [CrossRef]
240. Nogueira, R.; Oliveira, M.; Paterlini, W. Simple and Fast Spectrophotometric Determination of H_2O_2 in Photo-Fenton Reactions Using Metavanadate. *Talanta* **2005**, *66*, 86–91. [CrossRef] [PubMed]
241. Thermofisher Scientific AmplexTM Red Hydrogen Peroxide/Peroxidase Assay Kit. Available online: https://www.thermofisher.com/order/catalog/product/A22188?gclid=EAIaIQobChMI1eDRvZrGhAMVx6doCR1c2QCCEAAYASAAEgLFlvD_BwE&ef_id=EAIaIQobChMI1eDRvZrGhAMVx6doCR1c2QCCEAAYASAAEgLFlvD_BwE:G:s&s_kwcid=AL!3652!3!447292198748!!!g!!!10506731179!109642167571&cid=bid (accessed on 13 March 2024).
242. Kyoritsu Chemical-Check Lab Packtest Hydrogen Peroxide. Available online: https://en.kyoritsu-lab.co.jp/products/wak_h2o2 (accessed on 13 March 2024).
243. Pratsinis, A.; Kelesidis, G.A.; Zuercher, S.; Krumeich, F.; Bolisetty, S.; Mezzenga, R.; Leroux, J.-C.; Sotiriou, G.A. Enzyme-Mimetic Antioxidant Luminescent Nanoparticles for Highly Sensitive Hydrogen Peroxide Biosensing. *ACS Nano* **2017**, *11*, 12210–12218. [CrossRef] [PubMed]
244. Qi, Z.; Wang, L.; You, Q.; Chen, Y. PA-Tb-Cu MOF as Luminescent Nanoenzyme for Catalytic Assay of Hydrogen Peroxide. *Biosens. Bioelectron.* **2017**, *96*, 227–232. [CrossRef] [PubMed]
245. Chen, W.; Cai, S.; Ren, Q.-Q.; Wen, W.; Zhao, Y.-D. Recent Advances in Electrochemical Sensing for Hydrogen Peroxide: A Review. *Analyst* **2012**, *137*, 49–58. [CrossRef] [PubMed]
246. Peng, H.-P.; Liang, R.-P.; Qiu, J.-D. Facile Synthesis of Fe_3O_4@Al_2O_3 Core–Shell Nanoparticles and Their Application to the Highly Specific Capture of Heme Proteins for Direct Electrochemistry. *Biosens. Bioelectron.* **2011**, *26*, 3005–3011. [CrossRef] [PubMed]
247. WANG, S.; XIE, F.; LIU, G. Direct Electrochemistry and Electrocatalysis of Heme Proteins on SWCNTs-CTAB Modified Electrodes. *Talanta* **2009**, *77*, 1343–1350. [CrossRef]
248. Duanghathaipornsuk, S.; Farrell, E.J.; Alba-Rubio, A.C.; Zelenay, P.; Kim, D.-S. Detection Technologies for Reactive Oxygen Species: Fluorescence and Electrochemical Methods and Their Applications. *Biosensors* **2021**, *11*, 30. [CrossRef] [PubMed]
249. Chávez, M.; Fernandez-Merino, Á.; del Caño, R.; Sánchez-Obrero, G.; Madueño, R.; Blázquez, M.; Pineda, T. Behind the Optimization of the Sensor Film: Bioconjugation of Triangular Gold Nanoparticles with Hemoproteins for Sensitivity Enhancement of Enzymatic Biosensors. *Biosensors* **2023**, *13*, 467. [CrossRef]
250. Kanwal, A.; Saif, B.; Muhammad, A.; Liu, W.; Liu, J.; Ren, H.; Yang, P.; Lei, Z. Hemoglobin-Promoted Growth of Polyhedral Gold Nanoparticles for the Detection of Glucose, H_2O_2, and Ascorbic Acid. *ACS Appl. Nano Mater.* **2023**, *6*, 4734–4746. [CrossRef]
251. Elewi, A.S.; Al-Shammaree, S.A.W.; AL Sammarraie, A.K.M.A. Hydrogen Peroxide Biosensor Based on Hemoglobin-Modified Gold Nanoparticles–Screen Printed Carbon Electrode. *Sens. Bio-Sens. Res.* **2020**, *28*, 100340. [CrossRef]
252. Salimi, A.; Sharifi, E.; Noorbakhsh, A.; Soltanian, S. Direct Electrochemistry and Electrocatalytic Activity of Catalase Immobilized onto Electrodeposited Nano-Scale Islands of Nickel Oxide. *Biophys. Chem.* **2007**, *125*, 540–548. [CrossRef] [PubMed]
253. Rui, Q.; Komori, K.; Tian, Y.; Liu, H.; Luo, Y.; Sakai, Y. Electrochemical Biosensor for the Detection of H2O2 from Living Cancer Cells Based on ZnO Nanosheets. *Anal. Chim. Acta* **2010**, *670*, 57–62. [CrossRef] [PubMed]
254. Soto, D.; Alzate, M.; Gallego, J.; Orozco, J. Hybrid Nanomaterial/Catalase-Modified Electrode for Hydrogen Peroxide Sensing. *J. Electroanal. Chem.* **2021**, *880*, 114826. [CrossRef]
255. Yagati, A.K.; Ngoc Le, H.T.; Cho, S. Bioelectrocatalysis of Hemoglobin on Electrodeposited Ag Nanoflowers toward H2O2 Detection. *Nanomaterials* **2020**, *10*, 1628. [CrossRef] [PubMed]
256. Wang, H.; Chen, W.; Chen, Q.; Liu, N.; Cheng, H.; Li, T. Metal-Organic Framework (MOF)-Au@Pt Nanoflowers Composite Material for Electrochemical Sensing of H_2O_2 in Living Cells. *J. Electroanal. Chem.* **2021**, *897*, 115603. [CrossRef]
257. Dang, W.; Sun, Y.; Jiao, H.; Xu, L.; Lin, M. AuNPs-NH_2/Cu-MOF Modified Glassy Carbon Electrode as Enzyme-Free Electrochemical Sensor Detecting H_2O_2. *J. Electroanal. Chem.* **2020**, *856*, 113592. [CrossRef]
258. Ji, J.; Ko, S.Y.; Choi, K.M.; Kwon, Y. Hydrogen Peroxide Sensor Using the Biomimetic Structure of Peroxidase Including a Metal Organic Framework. *Appl. Surf. Sci.* **2021**, *554*, 148786. [CrossRef]

259. Tong, P.; Asif, M.; Ajmal, M.; Aziz, A.; Sun, Y. A Multicomponent Polymer-Metal-Enzyme System as Electrochemical Biosensor for H_2O_2 Detection. *Front. Chem.* **2022**, *10*, 874965. [CrossRef]
260. Manickam, P.; Vashist, A.; Madhu, S.; Sadasivam, M.; Sakthivel, A.; Kaushik, A.; Nair, M. Gold Nanocubes Embedded Biocompatible Hybrid Hydrogels for Electrochemical Detection of H_2O_2. *Bioelectrochemistry* **2020**, *131*, 107373. [CrossRef]
261. Matos-Peralta, Y.; Antuch, M. Review—Prussian Blue and Its Analogs as Appealing Materials for Electrochemical Sensing and Biosensing. *J. Electrochem. Soc.* **2020**, *167*, 037510. [CrossRef]
262. Narendra Kumar, A.V.; Harish, S.; Joseph, J.; Phani, K.L. Nix–Fe(1−x)Fe(CN)6 Hybrid Thin Films Electrodeposited on Glassy Carbon: Effect of Tuning of Redox Potentials on the Electrocatalysis of Hydrogen Peroxide. *J. Electroanal. Chem.* **2011**, *659*, 128–133. [CrossRef]
263. Ishizaki, M.; Ohshida, E.; Tanno, H.; Kawamoto, T.; Tanaka, H.; Hara, K.; Kominami, H.; Kurihara, M. H_2O_2-Sensing Abilities of Mixed-Metal (Fe-Ni) Prussian Blue Analogs in a Wide PH Range. *Inorg. Chim. Acta* **2020**, *502*, 119314. [CrossRef]
264. Li, J.; He, L.; Jiang, J.; Xu, Z.; Liu, M.; Liu, X.; Tong, H.; Liu, Z.; Qian, D. Facile Syntheses of Bimetallic Prussian Blue Analogues (KxM[Fe(CN)6]·nH_2O, M=Ni, Co, and Mn) for Electrochemical Determination of Toxic 2-Nitrophenol. *Electrochim. Acta* **2020**, *353*, 136579. [CrossRef]
265. Zhao, H.-C.; Zhang, P.; Li, S.-H.; Luo, H.-X. Cobalt Hexacyanoferrate-Modified Graphene Platform Electrode and Its Electrochemical Sensing toward Hydrogen Peroxide. *Chin. J. Anal. Chem.* **2017**, *45*, 830–836. [CrossRef]
266. Pang, H.; Zhang, Y.; Cheng, T.; Lai, W.-Y.; Huang, W. Uniform Manganese Hexacyanoferrate Hydrate Nanocubes Featuring Superior Performance for Low-Cost Supercapacitors and Nonenzymatic Electrochemical Sensors. *Nanoscale* **2015**, *7*, 16012–16019. [CrossRef]
267. Pakrudheen, I.; Bathinapatla, A.; Murugan, E. Amphiphilic Dendrimer Loaded Prussian Blue Nanoparticle for the Detection of Hydrogen Peroxide. *Indian J. Chem. Technol.* **2022**, *29*, 668–677. [CrossRef]
268. Zhang, M.; Zhang, W.; Engelbrekt, C.; Hou, C.; Zhu, N.; Chi, Q. Size-Dependent and Self-Catalytic Gold@Prussian Blue Nanoparticles for the Electrochemical Detection of Hydrogen Peroxide. *ChemElectroChem* **2020**, *7*, 3818–3823. [CrossRef]
269. Noël, J.; Médard, J.; Combellas, C.; Kanoufi, F. Prussian Blue Degradation during Hydrogen Peroxide Reduction: A Scanning Electrochemical Microscopy Study on the Role of the Hydroxide Ion and Hydroxyl Radical. *ChemElectroChem* **2016**, *3*, 1178–1184. [CrossRef]
270. Uzuncar, S.; Ozdogan, N.; Ak, M. Enzyme-Free Detection of Hydrogen Peroxide with a Hybrid Transducing System Based on Sodium Carboxymethyl Cellulose, Poly(3,4-Ethylenedioxythiophene) and Prussian Blue Nanoparticles. *Anal. Chim. Acta* **2021**, *1172*, 338664. [CrossRef]
271. Ying, S.; Chen, C.; Wang, J.; Lu, C.; Liu, T.; Kong, Y.; Yi, F. Synthesis and Applications of Prussian Blue and Its Analogues as Electrochemical Sensors. *Chempluschem* **2021**, *86*, 1608–1622. [CrossRef] [PubMed]
272. Sohrabi, H.; Maleki, F.; Khaaki, P.; Kadhom, M.; Kudaibergenov, N.; Khataee, A. Electrochemical-Based Sensing Platforms for Detection of Glucose and H_2O_2 by Porous Metal–Organic Frameworks: A Review of Status and Prospects. *Biosensors* **2023**, *13*, 347. [CrossRef]
273. Hu, Y.; Hojamberdiev, M.; Geng, D. Recent Advances in Enzyme-Free Electrochemical Hydrogen Peroxide Sensors Based on Carbon Hybrid Nanocomposites. *J. Mater. Chem. C* **2021**, *9*, 6970–6990. [CrossRef]
274. Shamkhalichenar, H.; Choi, J.-W. Review—Non-Enzymatic Hydrogen Peroxide Electrochemical Sensors Based on Reduced Graphene Oxide. *J. Electrochem. Soc.* **2020**, *167*, 037531. [CrossRef]
275. Wu, X.; Ma, P.; Sun, Y.; Du, F.; Song, D.; Xu, G. Application of MXene in Electrochemical Sensors: A Review. *Electroanalysis* **2021**, *33*, 1827–1851. [CrossRef]
276. Song, M.; Wang, J.; Chen, B.; Wang, L. A Facile, Nonreactive Hydrogen Peroxide (H_2O_2) Detection Method Enabled by Ion Chromatography with UV Detector. *Anal. Chem.* **2017**, *89*, 11537–11544. [CrossRef] [PubMed]
277. Tantawi, O.; Baalbaki, A.; El Asmar, R.; Ghauch, A. A Rapid and Economical Method for the Quantification of Hydrogen Peroxide (H_2O_2) Using a Modified HPLC Apparatus. *Sci. Total Environ.* **2019**, *654*, 107–117. [CrossRef]
278. Chiesa, M.; Giamello, E.; Livraghi, S.; Paganini, M.C.; Polliotto, V.; Salvadori, E. Electron Magnetic Resonance in Heterogeneous Photocatalysis Research. *J. Phys. Condens. Matter* **2019**, *31*, 444001. [CrossRef]
279. Fernández-Castro, P.; Vallejo, M.; San Román, M.F.; Ortiz, I. Insight on the Fundamentals of Advanced Oxidation Processes. Role and Review of the Determination Methods of Reactive Oxygen Species. *J. Chem. Technol. Biotechnol.* **2015**, *90*, 796–820. [CrossRef]
280. Ngo, T.T.; Lenhoff, H.M. A Sensitive and Versatile Chromogenic Assay for Peroxidase and Peroxidase-Coupled Reactions. *Anal. Biochem.* **1980**, *105*, 389–397. [CrossRef]
281. Cao, W.; Ju, P.; Wang, Z.; Zhang, Y.; Zhai, X.; Jiang, F.; Sun, C. Colorimetric Detection of H_2O_2 Based on the Enhanced Peroxidase Mimetic Activity of Nanoparticles Decorated Ce2(WO4)3 Nanosheets. *Spectrochim. Acta—Part A Mol. Biomol. Spectrosc.* **2020**, *239*, 118499. [CrossRef] [PubMed]
282. Wei, H.; Wang, E. Fe_3O_4 Magnetic Nanoparticles as Peroxidase Mimetics and Their Applications in H_2O_2 and Glucose Detection. *Anal. Chem.* **2008**, *80*, 2250–2254. [CrossRef] [PubMed]
283. Masschelein, W.; Denis, M.; Ledent, R. Spectrophotometric determination of residual hydrogen peroxide. *Water Sew. Work.* **1977**, *124*, 69–72.

284. Vaithyanathan, V.K.; Ravi, S.; Leduc, R.; Vaidyanathan, V.K.; Cabana, H. Utilization of Biosolids for Glucose Oxidase Production: A Potential Bio-Fenton Reagent for Advanced Oxidation Process for Removal of Pharmaceutically Active Compounds. *J. Environ. Manag.* **2020**, *271*, 110995. [CrossRef]
285. Kosaka, K.; Yamada, H.; Matsui, S.; Echigo, S.; Shishida, K. Comparison among the Methods for Hydrogen Peroxide Measurements To Evaluate Advanced Oxidation Processes: Application of a Spectrophotometric Method Using Copper(II) Ion and 2,9-Dimethyl-1,10-Phenanthroline. *Environ. Sci. Technol.* **1998**, *32*, 3821–3824. [CrossRef]
286. Bader, H.; Sturzenegger, V.; Hoigné, J. Photometric Method for the Determination of Low Concentrations of Hydrogen Peroxide by the Peroxidase Catalyzed Oxidation of N,N-Diethyl-p-Phenylenediamine (DPD). *Water Res.* **1988**, *22*, 1109–1115. [CrossRef]
287. Shaked, Y.; Armoza-Zvuloni, R. Dynamics of Hydrogen Peroxide in a Coral Reef: Sources and Sinks. *J. Geophys. Res. Biogeosci.* **2013**, *118*, 1793–1801. [CrossRef]
288. Schick, R.; Strasser, I.; Stabel, H.-H. Fluorometric Determination of Low Concentrations of H_2O_2 in Water: Comparison with Two Other Methods and Application to Environmental Samples and Drinking-Water Treatment. *Water Res.* **1997**, *31*, 1371–1378. [CrossRef]
289. Priyadarshini, M.; Das, I.; Ghangrekar, M.M.; Blaney, L. Advanced Oxidation Processes: Performance, Advantages, and Scale-up of Emerging Technologies. *J. Environ. Manag.* **2022**, *316*, 115295. [CrossRef]
290. Carvalho Neves, L.; Beber de Souza, J.; de Souza Vidal, C.M.; Herbert, L.T.; de Souza, K.V.; Geronazzo Martins, K.; Young, B.J. Phytotoxicity Indexes and Removal of Color, COD, Phenols and ISA from Pulp and Paper Mill Wastewater Post-Treated by UV/H_2O_2 and Photo-Fenton. *Ecotoxicol. Environ. Saf.* **2020**, *202*, 110939. [CrossRef]
291. Hofman-Caris, R.C.H.M.; Harmsen, D.J.H.; Puijker, L.; Baken, K.A.; Wols, B.A.; Beerendonk, E.F.; Keltjens, L.L.M. Influence of Process Conditions and Water Quality on the Formation of Mutagenic Byproducts in UV/H_2O_2 Processes. *Water Res.* **2015**, *74*, 191–202. [CrossRef]
292. Rozas, O.; Vidal, C.; Baeza, C.; Jardim, W.F.; Rossner, A.; Mansilla, H.D. Organic Micropollutants (OMPs) in Natural Waters: Oxidation by UV/H_2O_2 Treatment and Toxicity Assessment. *Water Res.* **2016**, *98*, 109–118. [CrossRef]
293. Lopez-Lopez, C.; Purswani, J.; Martín-Pascual, J.; Martínez-Toledo, M.V.; Muñío, M.M.; Poyatos, J.M. Toxic Effect of H_2O_2 in H_2O_2/UV, Photo-Fenton and Heterogeneous Photocatalysis (TiO_2/H_2O_2/UV) Systems to Treat Textile Wastewater. *Desalin. Water Treat.* **2015**, *56*, 3044–3053. [CrossRef]
294. Arshad, R.; Bokhari, T.H.; Javed, T.; Bhatti, I.A.; Rasheed, S.; Iqbal, M.; Nazir, A.; Naz, S.; Khan, M.I.; Khosa, M.K.K.; et al. Degradation Product Distribution of Reactive Red-147 Dye Treated by UV/H_2O_2/TiO_2 Advanced Oxidation Process. *J. Mater. Res. Technol.* **2020**, *9*, 3168–3178. [CrossRef]
295. Tony, M.A.; Lin, L.-S. Iron Coated-Sand from Acid Mine Drainage Waste for Being a Catalytic Oxidant Towards Municipal Wastewater Remediation. *Int. J. Environ. Res.* **2021**, *15*, 191–201. [CrossRef]
296. Ferro, G.; Guarino, F.; Castiglione, S.; Rizzo, L. Antibiotic Resistance Spread Potential in Urban Wastewater Effluents Disinfected by UV/H_2O_2 Process. *Sci. Total Environ.* **2016**, *560–561*, 29–35. [CrossRef]
297. Rioja, N.; Zorita, S.; Peñas, F.J. Effect of Water Matrix on Photocatalytic Degradation and General Kinetic Modeling. *Appl. Catal. B Environ.* **2016**, *180*, 330–335. [CrossRef]
298. Maniakova, G.; Kowalska, K.; Murgolo, S.; Mascolo, G.; Libralato, G.; Lofrano, G.; Sacco, O.; Guida, M.; Rizzo, L. Comparison between Heterogeneous and Homogeneous Solar Driven Advanced Oxidation Processes for Urban Wastewater Treatment: Pharmaceuticals Removal and Toxicity. *Sep. Purif. Technol.* **2020**, *236*, 116249. [CrossRef]
299. Wu, Y.; Chu, L.; Liu, W.; Jiang, L.; Chen, X.; Wang, Y.; Zhao, Y. The Screening of Metal Ion Inhibitors for Glucose Oxidase Based on the Peroxidase-like Activity of Nano-Fe_3O_4. *RSC Adv.* **2017**, *7*, 47309–47315. [CrossRef]
300. Vitale, A.A.; Bernatene, E.A.; Pomilio, A.B. Inhibition of Fenton Reaction of Glucose by Alcohols and Tetrahydrofuran in Catalytic Concentrations: Calculation of the Stability Constants of ROH/Fe^{2+} Complexes. *Curr. Phys. Chem.* **2022**, *12*, 76–87. [CrossRef]
301. Lindsey, M. Inhibited Hydroxyl Radical Degradation of Aromatic Hydrocarbons in the Presence of Dissolved Fulvic Acid. *Water Res.* **2000**, *34*, 2385–2389. [CrossRef]
302. Malvestiti, J.A.; Dantas, R.F. Disinfection of Secondary Effluents by O_3, O_3/H_2O_2 and UV/H_2O_2: Influence of Carbonate, Nitrate, Industrial Contaminants and Regrowth. *J. Environ. Chem. Eng.* **2018**, *6*, 560–567. [CrossRef]
303. Yang, Z.; Qian, J.; Shan, C.; Li, H.; Yin, Y.; Pan, B. Toward Selective Oxidation of Contaminants in Aqueous Systems. *Environ. Sci. Technol.* **2021**, *55*, 14494–14514. [CrossRef]
304. Mahbub, P.; Duke, M. Scalability of Advanced Oxidation Processes (AOPs) in Industrial Applications: A Review. *J. Environ. Manag.* **2023**, *345*, 118861. [CrossRef] [PubMed]
305. Zhang, M.; Dong, H.; Zhao, L.; Wang, D.; Meng, D. A Review on Fenton Process for Organic Wastewater Treatment Based on Optimization Perspective. *Sci. Total Environ.* **2019**, *670*, 110–121. [CrossRef] [PubMed]
306. Ghafoori, S.; Mehrvar, M.; Chan, P.K. Photoreactor Scale-up for Degradation of Aqueous Poly(Vinyl Alcohol) Using UV/H_2O_2 Process. *Chem. Eng. J.* **2014**, *245*, 133–142. [CrossRef]
307. Bar-Niv, N.; Azaizeh, H.; Kuc, M.E.; Azerrad, S.; Haj-Zaroubi, M.; Menashe, O.; Kurzbaum, E. Advanced Oxidation Process UV-H_2O_2 Combined with Biological Treatment for the Removal and Detoxification of Phenol. *J. Water Process Eng.* **2022**, *48*, 102923. [CrossRef]
308. Otálvaro-Marín, H.L.; González-Caicedo, F.; Arce-Sarria, A.; Mueses, M.A.; Crittenden, J.C.; Machuca-Martinez, F. Scaling-up a Heterogeneous H_2O_2/TiO_2/Solar-Radiation System Using the DamkÖhler Number. *Chem. Eng. J.* **2019**, *364*, 244–256. [CrossRef]

309. Pliego, G.; Zazo, J.A.; Garcia-Muñoz, P.; Munoz, M.; Casas, J.A.; Rodriguez, J.J. Trends in the Intensification of the Fenton Process for Wastewater Treatment: An Overview. *Crit. Rev. Environ. Sci. Technol.* **2015**, *45*, 2611–2692. [CrossRef]
310. Bashir, Y.; Raj, R.; Ghangrekar, M.M.; Nema, A.K.; Das, S. Critical Assessment of Advanced Oxidation Processes and Bio-Electrochemical Integrated Systems for Removing Emerging Contaminants from Wastewater. *RSC Sustain.* **2023**, *1*, 1912–1931. [CrossRef]
311. Sgroi, M.; Snyder, S.A.; Roccaro, P. Comparison of AOPs at Pilot Scale: Energy Costs for Micro-Pollutants Oxidation, Disinfection by-Products Formation and Pathogens Inactivation. *Chemosphere* **2021**, *273*, 128527. [CrossRef]
312. Yao, W.; Ur Rehman, S.W.; Wang, H.; Yang, H.; Yu, G.; Wang, Y. Pilot-Scale Evaluation of Micropollutant Abatements by Conventional Ozonation, UV/O3, and an Electro-Peroxone Process. *Water Res.* **2018**, *138*, 106–117. [CrossRef]
313. Mousset, E.; Loh, W.H.; Lim, W.S.; Jarry, L.; Wang, Z.; Lefebvre, O. Cost Comparison of Advanced Oxidation Processes for Wastewater Treatment Using Accumulated Oxygen-Equivalent Criteria. *Water Res.* **2021**, *200*, 117234. [CrossRef]
314. Cañizares, P.; Paz, R.; Sáez, C.; Rodrigo, M.A. Costs of the Electrochemical Oxidation of Wastewaters: A Comparison with Ozonation and Fenton Oxidation Processes. *J. Environ. Manag.* **2009**, *90*, 410–420. [CrossRef] [PubMed]
315. Rizzo, L.; Gernjak, W.; Krzeminski, P.; Malato, S.; McArdell, C.S.; Perez, J.A.S.; Schaar, H.; Fatta-Kassinos, D. Best Available Technologies and Treatment Trains to Address Current Challenges in Urban Wastewater Reuse for Irrigation of Crops in EU Countries. *Sci. Total Environ.* **2020**, *710*, 136312. [CrossRef] [PubMed]
316. Ribeiro, J.P.; Sarinho, L.; Nunes, M.I. Application of Life Cycle Assessment to Fenton Processes in Wastewater Treatment—A Review. *J. Water Process Eng.* **2024**, *57*, 104692. [CrossRef]
317. Garcia Montano, J.; Ruiz, N.; Munoz, I.; Domenech, X.; Garciahortal, J.; Torrades, F.; Peral, J. Environmental Assessment of Different Photo-Fenton Approaches for Commercial Reactive Dye Removal. *J. Hazard. Mater.* **2006**, *138*, 218–225. [CrossRef]
318. Ioannou-Ttofa, L.; Foteinis, S.; Chatzisymeon, E.; Michael-Kordatou, I.; Fatta-Kassinos, D. Life Cycle Assessment of Solar-driven Oxidation as a Polishing Step of Secondary-treated Urban Effluents. *J. Chem. Technol. Biotechnol.* **2017**, *92*, 1315–1327. [CrossRef]
319. Costamagna, M.; Arques, A.; Lo-Iacono-Ferreira, V.G.; Bianco Prevot, A. Environmental Assessment of Solar Photo-Fenton Processes at Mild Condition in the Presence of Waste-Derived Bio-Based Substances. *Nanomaterials* **2022**, *12*, 2781. [CrossRef]
320. Raj, R.; Tripathi, A.; Das, S.; Ghangrekar, M.M. Is Waste-Derived Catalyst Mediated Electro-Fenton a Sustainable Option for Mitigating Emerging Contaminants from Wastewater? *Curr. Opin. Environ. Sci. Health* **2024**, *37*, 100523. [CrossRef]
321. Feijoo, S.; González-Rodríguez, J.; Fernández, L.; Vázquez-Vázquez, C.; Feijoo, G.; Moreira, M.T. Fenton and Photo-Fenton Nanocatalysts Revisited from the Perspective of Life Cycle Assessment. *Catalysts* **2019**, *10*, 23. [CrossRef]
322. Rodríguez, R.; Espada, J.J.; Pariente, M.I.; Melero, J.A.; Martínez, F.; Molina, R. Comparative Life Cycle Assessment (LCA) Study of Heterogeneous and Homogenous Fenton Processes for the Treatment of Pharmaceutical Wastewater. *J. Clean. Prod.* **2016**, *124*, 21–29. [CrossRef]
323. Fan, Y.; Ai, Z.; Zhang, L. Design of an Electro-Fenton System with a Novel Sandwich Film Cathode for Wastewater Treatment. *J. Hazard. Mater.* **2010**, *176*, 678–684. [CrossRef] [PubMed]
324. Ting, W.-P.; Lu, M.-C.; Huang, Y.-H. The Reactor Design and Comparison of Fenton, Electro-Fenton and Photoelectro-Fenton Processes for Mineralization of Benzene Sulfonic Acid (BSA). *J. Hazard. Mater.* **2008**, *156*, 421–427. [CrossRef] [PubMed]
325. Hussain, S.; Aneggi, E.; Goi, D. Catalytic Activity of Metals in Heterogeneous Fenton-like Oxidation of Wastewater Contaminants: A Review. *Environ. Chem. Lett.* **2021**, *19*, 2405–2424. [CrossRef]
326. Salmerón, I.; Plakas, K.V.; Sirés, I.; Oller, I.; Maldonado, M.I.; Karabelas, A.J.; Malato, S. Optimization of Electrocatalytic H_2O_2 Production at Pilot Plant Scale for Solar-Assisted Water Treatment. *Appl. Catal. B Environ.* **2019**, *242*, 327–336. [CrossRef]
327. Bourgin, M.; Beck, B.; Boehler, M.; Borowska, E.; Fleiner, J.; Salhi, E.; Teichler, R.; von Gunten, U.; Siegrist, H.; McArdell, C.S. Evaluation of a Full-Scale Wastewater Treatment Plant Upgraded with Ozonation and Biological Post-Treatments: Abatement of Micropollutants, Formation of Transformation Products and Oxidation by-Products. *Water Res.* **2018**, *129*, 486–498. [CrossRef]
328. Iervolino, G.; Vaiano, V.; Pepe, G.; Campiglia, P.; Palma, V. Degradation of Acid Orange 7 Azo Dye in Aqueous Solution by a Catalytic-Assisted, Non-Thermal Plasma Process. *Catalysts* **2020**, *10*, 888. [CrossRef]